CONTRACTOR REPORT

EFFECTS OF VIBRATION AND SHOCK
ON THE PERFORMANCE OF GAS - BEARING
SPACE-POWER BRAYTON CYCLE TURBOMACHINERY

PART 4: SUPPRESSION OF ROTOR-BEARING SYSTEM VIBRATIONS THROUGH FLEXIBLE BEARING SUPPORT DAMPING

by

J. M. Tessarzik, T. Chiang, and R. H. Badgley

MAY 1974

MECHANICAL TECHNOLOGY INCORPORATED

Latham, New York

Prepared for

NATIONAL AERONAUTICS AND SPACE ADMINISTRATION

NASA—Lewis Research Center

J. DUNN, Project Manager

1. Report No. NASA CR-134697	2. Government Accession No.	3. Recipient's Catalog No.
4. Title and Subtitle EFFECTS OF VIBRATION AND SHOCK ON THE PERFORMANCE OF GAS-BEARING SPACE-POWER BRAYTON CYCLE TURBOMACHINERY		5. Report Date May 1974
		6. Performing Organization Code
7. Author(s) J. M. Tessarzik, T. Chiang, and R. H. Badgley		8. Performing Organization Report No. MTI 74TR30
		10. Work Unit No.
9. Performing Organization Name and Address Mechanical Technology Incorporated 968 Albany-Shaker Road, Latham, New York 12110		
		11. Contract or Grant No. NAS 3-15709
		13. Type of Report and Period Covered Contractor Report
12. Sponsoring Agency Name and Address National Aeronautics and Space Administration Washington, D.C. 20546		
		14. Sponsoring Agency Code

15. Supplementary Notes

Project Manager, James H. Dunn, Brayton Cycle Branch, NASA Lewis Research Center, Cleveland, Ohio

16. Abstract

A bearing damper, operating on the support flexure of a pivoted pad in a tilting-pad type gas-lubricated journal bearing, has been designed, built, and tested under externally-applied random vibrations.

The NASA Brayton Rotating Unit (BRU), a 36,000 rpm, 10-Kwe turbogenerator had previously been subjected in the MTI Vibration Test Laboratory to external random vibrations, and vibration response data had been recorded and analyzed for amplitude distribution and frequency content at a number of locations in the machine. Based upon data from that evaluation, a piston-type damper was designed and developed for each of the two flexibly-supported journal bearing pads (one in each of the two three-pad bearings). A modified BRU, with dampers installed, has been re-tested under random vibration conditions. Root-mean-square vibration amplitudes were determined from the test data, and displacement power spectral density analyses have been performed. Results of these data reduction efforts have been compared with vibration tolerance limits.

Results of the tests indicate significant reductions in vibration levels in the bearing gas-lubricant films, particularly in the rigidly-mounted pads. The utility of the gas-lubricated damper for limiting rotor-bearing system vibrations in high-speed turbomachinery has thus been demonstrated.

17. Key Words (Suggested by Author(s))	18. Distribution Statement Unclassified - unlimited

19. Security Classif. (of this report) Unclassified	20. Security Classif. (of this page) Unclassified	21. No. of Pages 95	22. Price* $3.00

FOREWORD

This report describes the results of work performed by Mechanical Technology
Incorporated (MTI), Latham, New York, under Contract NAS3-15709.

The NASA Project Manager for this investigation was Mr. James Dunn of the
Brayton Cycle Branch - Lewis Research Center, Cleveland, Ohio. The MTI
Project Manager was Dr. Robert H. Badgley. Mr. Juergen M. Tessarzik was
responsible for the experimental portion of the investigation, and was
assisted in that effort by Mr. Walter Spodnewski. The system response
analysis was the responsibility of Dr. Thomas Chiang. The dynamic analysis
of the damper was performed by Mr. Harlan White and the dampers were de-
signed by Mr. John L. Dunne.

ABSTRACT

A bearing damper, operating on the support flexure of a pivoted pad in a tilting-pad type gas-lubricated journal bearing, has been designed, built, and tested under externally-applied random vibrations.

The NASA Brayton Rotating Unit (BRU), a 36,000 rpm, 10 Kwe turbogenerator had previously been subjected in the MTI Vibration Test Laboratory to external random vibrations, and vibration response data had been recorded and analyzed for amplitude distribution and frequency content at a number of locations in the machine. Based upon data from that evaluation, a piston-type damper was designed and developed for each of the two flexibly-supported journal bearing pads (one in each of the two three-pad bearings). A modified BRU, with dampers installed, has been re-tested under random vibration conditions. Root-mean-square vibration amplitudes were determined from the test data, and displacement power spectral density analyses have been performed. Results of these data reduction efforts have been compared with vibration tolerance limits.

Results of the tests indicate significant reductions in vibration levels in the bearing gas-lubricant films, particularly in the rigidly-mounted pads. The utility of the gas-lubricated damper for limiting rotor-bearing system vibrations in high-speed turbomachinery has thus been demonstrated.

TABLE OF CONTENTS

LIST OF FIGURES

SUMMARY

High-speed rotating machinery, such as turboalternators, gas turbine engines and the like, can be particularly susceptible to externally-applied vibrations. Such vibrations can be due to vehicle operational mode changes (e.g., the landing of an aircraft or the restart of a rocket engine), to vehicle buffeting by air or water, and to normal operating events (e.g., rotor-induced vibration in helicopters). These external vibrations, depending upon their frequency content, duration, and severity, can cause significant internal vibration amplitudes within the exposed turbomachinery, with attendant over-stresses, contacts between closely-spaced rotating components, and fatigue of structural members. The NASA Brayton Rotating Unit (BRU) is an example of a turbomachine which must be protected from such effects.

In the case where the external vibration causes high vibration amplitudes because of coincidences with one or more resonance frequencies, it is possible to detune the machinery system through changes to system mass and stiffness elements. When such detuning is not possible (and in most cases where the external vibration is broad-band in nature, detuning is not practical), vibration energy must be extracted from the system through the use of damping. This latter situation exists in the case of the BRU, an inherently low-damping system which must tolerate exposure to broad-band random vibration.

The program described herein included the design, fabrication, installation, and testing of ambient gas-lubricated piston dampers in a modified BRU. The dampers were designed to be exposed to the radial motion of one of the three bearing pads in each of the BRU's journal bearings. This pad, which was flexure-mounted, was found to follow the motion of the rotor quite closely in earlier BRU vibration-mapping studies. Contacts between the rotor and the remaining (rigidly-mounted) pads, were found to limit the externally-applied vibration levels which could be tolerated by the bearings.

Comparisons between "before" and "after" test data indicate that significant vibration reductions have been attained with the dampers installed.

INTRODUCTION

Externally-imposed vibrations can seriously endanger the integrity and operating performance of rotating machinery. The severity of the threat is largely dependent upon the response level of internal machine components relative to the level of the externally-applied vibrations. Vibration-induced contacts between rotating components or fatigue or overstress cracking of flexing parts are the more typical modes of observed failures. In a fluid-film or gas bearing supported rotor system, intermittent contacts between rotor and bearings may be an early indicator of distress, while severe structural vibrations may be more typical for a lightweight, highly-flexible gas turbine type of machine. In either case, the addition of internal vibration damping elements to the structure may be a viable and effective alternative to the more traditional approach of external structural vibration isolation.

This report presents a case study, which draws upon a previously conducted analytical and experimental analysis of the responses of many internal components of the Brayton Rotating Unit, a gas turbine-driven alternator of approximately 10 Kwe maximum output. Based upon the finding that the flexures supporting the flexibly-mounted pivoted pad in each of the journal bearings exhibit some of the largest vibration levels observed, remedial bearing support dampers have been designed, built, and tested in the machine. The design effort utilized the systematic mapping of component responses to external sinusoidal and random vibrations, obtained before bearing support dampers were installed in the BRU. It was aided by a number of analytical response programs developed for that purpose and reported in References 1, 2, and 3. A specific analysis directed towards a reduction in the vibration response of the flexure supports for the journal bearing pads under the influence of external random vibrations has been developed and is presented in this report.

JOURNAL BEARING FLEXURE REDESIGN FOR
VIBRATION ATTENUATION IN THE BRAYTON ROTATING UNIT

During portions of the Brayton Rotating Unit (BRU) vibration tests conducted
under Contract NASw-1713, as reported in Reference 1, inputs were applied
laterally (horizontal direction) to the BRU with its spin axis vertical. The
resulting test data, portions of which are shown in Figures 118 and 120 in
Reference 1, indicate that the gas-lubricant films of the solid-mounted
journal bearing pads have a vibration amplitude approximately 7.5 times
larger than that of the gas film of the flexure-mounted pad. The efforts
described herein are directed at a redesign of the pad-support elements to
reduce the gas-film vibration levels caused by both random and sinusoidal
vibration inputs.

Vibration Response Evaluation of Journal Bearing Support System for Different
Values of Flexure Stiffness and Damping

The BRU journal bearing pad-flexure system was modeled analytically as shown
in Figure 1. In this model, the rotor is allowed to move in both the x- and
y-directions. The pads, however, are assumed to move only in the radial
directions. The vibration input is assumed to be transmitted to the pads and
the rotor through the casing. This vibration input can be at an arbitrary
orientation, specified by the proper phase relationship between the peak
amplitudes x_B and y_B.

The model shown in Figure 1 has five degrees of freedom; the rotor has two
degrees of freedom, and each of the three pads has one. Based on this model,
an analysis was conducted to predict the forced vibration amplitudes of the
rotor, the three pads, and the pads relative to the casing, and the amplitudes
of the gas-film variations. All of the above amplitudes are divided by the
input vibration amplitude in the calculations to obtain amplitude ratios.

To illustrate the results obtained from the analysis, we consider as an example
the flexure-mounted pad-rotor system of the present BRU design. Let the system
be forced by a unit amplitude vibration input in the "12 o'clock" direction
(i.e., $x_B = 1$ and $y_B = 0$). The weight of the rotor is 21 pounds (9.5 Kg).

Since there are two tilting-pad journal bearings, one at the turbine end and one at the compressor end, the effective mass of the rotor at either end is $21/2 = 10.5$ lb (4.3 Kg). Thus, $m_2 = 10.5$ lb (4.3 Kg). The lumped mass of the pad is estimated at 0.22 lb (0.1 Kg) ($m_1 = m_3 = m_4 = 0.22$ lb). The stiffness and damping coefficients of the gas films of the pad are taken at their respective nominal values, $k_2 = k_2' = k_3 = 53, 800$ lb/in. ($9.28 \times 10^6 \frac{N}{m}$) and $c_2 = c_2' = c_3 = 3.42$ lb-sec/in. ($598.9 \frac{N-sec}{m}$). The flexure in the "12 o'clock" direction has a stiffness $k_4 = 2000$ lb/in. ($0.35 \times 10^6 \frac{N}{m}$), whereas the flexures in the "8 o'clock" and "4 o'clock" directions have a stiffness of $k_1 = k_1' = 250,000$ lb/in. ($43.78 \times 10^6 \frac{N}{m}$). (These are the "solid" mounts.) All the flexures are assumed to have a damping coefficient of $c_1 = c_1' = c_4 = 0.1$ lb-sec/in. ($17.5 \frac{N-sec}{m}$), which is representative of the typically low levels of damping found in "undamped" structures.

For a unit amplitude sinusoidal vibration input in the "12 o'clock" direction, responses in terms of gas-film thickness variation and pad vibration amplitude (relative to casing) were calculated and are plotted against frequency in Figures 2 to 5; they are, respectively, amplitude ratio of the gas-film thickness variation of the pad in the "12 o'clock" direction, amplitude ratio of the gas-film thickness variation of the pad in the "8 o'clock" direction, amplitude ratio of the "12 o'clock" pad vibration relative to casing, and amplitude ratio of the "8 o'clock" pad vibration relative to casing. When the input excitation is in the "12 o'clock" direction, the gas film thickness variation and the pad vibration of the "4 o'clock" pad are identical to those of the "8 o'clock" pad because of symmetry. The results for the "4 o'clock" pad are thus not shown.

It is seen from Figures 2 to 5 that the lowest natural frequency of the system is approximately 148 Hz, at which all amplitudes (and thus the amplitude ratios) have peak values. The amplitude ratios with a larger flexure damping coefficient of 1 lb-sec/sec ($175 \frac{N-sec}{m}$), are also indicated at the peaks. These are, as may be expected, somewhat smaller than those with a flexure damping coefficient of 0.1 lb-sec/in. ($17.5 \frac{N-sec}{m}$). Note that in this configuration, the "8 o'clock" gas film has a larger peak amplitude ratio than the "12 o'clock"

gas film as shown in Figures 2 and 3. Later, when different configurations and flexure stiffness combinations are evaluated for their performances, this larger peak amplitude ratio (in this case, 8.4 as shown in Figure 3) becomes the quantity against which comparisons are made.

The amplitude ratio can be interpreted as the amplitude of vibration resulting from and corresponding to an input vibration amplitude of unity. Therefore, if the specification calls for different input amplitudes at different frequencies, a factor which is called the "input weighting factor" should be included to obtain meaningful results.

The specification for sinusoidal vibration input calls for a constant g-level at 0.25 g over the frequency range of 5-35 Hz. The rotor support hardware at each end of the existing BRU includes one soft flexure having a stiffness of 2000 lb/in. ($0.35 \times 10^6 \frac{N}{m}$) and two hard flexures each having a stiffness of 250,000 lb/in. ($43.78 \times 10^6 \frac{N}{m}$). The lowest natural frequency of this system is calculated to be 148 Hz as indicated before. With the two hard flexures replaced by two 2000 lb/in. ($0.35 \times 10^6 \frac{N}{m}$) flexures, the lowest natural frequency would be 51 Hz, which is still considerably above the 5-35 Hz range. The existing BRU thus has no resonant peak in the 5-35 Hz range, and therefore has no difficulty meeting the specification for sinusoidal vibration input.

The specification for random vibration input shown in Figure 10 in Reference 1 is acceleration power spectral density (PSD). The same specification expressed in terms of displacement PSD is shown in Figure 6 herein. Note that for frequencies greater than 100 Hz the acceleration PSD is constant, but the displacement PSD varies as $(Freq.)^{-4}$. In the response analysis the input forcing function is expressed in terms of displacement excitation. And from Figure 6, it is clear that the displacement input is not constant throughout the frequency spectrum. To take this factor into consideration, we take the area under the PSD curve in Figure 6, at a frequency f, over a bandwidth of say, 1 Hz. This area is, by definition, the mean square value of the displacement input at the corresponding frequency f; and the square root of it is the RMS (root mean

square) value of the displacement input at frequency f. Now we divide the RMS value of the displacement input by the RMS value at 100 Hz. The ratio is called the "input weighting factor" which is plotted versus frequency in Figure 7. It is convenient to define

$$
\begin{aligned}
\text{Weighted Variation} &= \text{Amplitude Ratio x Input Weighting Factor} \\
&= \frac{\text{Response Amplitude}}{\text{Input Amplitude at } f} \text{ x } \frac{\text{RMS Input Amplitude at } f}{\text{RMS Input Amplitude at } f = 100 \text{ Hz}} \\
&= \frac{\text{Response Amplitude}}{\text{RMS Input Amplitude at } f = 100 \text{ Hz}}
\end{aligned}
\tag{1}
$$

In the example in Figures 2 to 5, a resonance occurred at a frequency of 148 Hz. From Figure 7, the input weighting factor can be read as 0.44 at 148 Hz. The amplitude ratio of the gas-film thickness variation of the "12 o'clock" pad at resonance is 0.56, and the corresponding quantity for the "8 o'clock" pad is 8.3 as shown in Figures 2 and 3. From the definition in (1):

Weighted Gas-Film Variation of the "12 o'clock" Pad = 0.56 x 0.44 = 0.246
Weighted Gas-Film Variation of the "8 o'clock" Pad = 8.4 x 0.44 = 3.7.

For design calculation, only the maximum weighted gas-film variation is of importance. Thus, with input in the "12 o'clock" direction,

Maximum Weighted Gas-Film Variation = 3.7.

Similarly, from Figures 4, 5, and 7

Maximum Weighted Pad Vibration Relative to Casing = 8.8.

In order to make a meaningful design comparison, the maximum weighted gas-film variation and the maximum weighted pad vibration relative to casing are presented in Figures 8 and 9, respectively, for various flexure stiffness combinations. Note that at least two of the three flexures are assumed to have the same stiffness, and all three flexures are assumed to have the same damping coefficients. Thus,

$$k_1 = k_1'$$

$$c = c_1 = c_1' = c_4.$$

The present BRU with $k_1 = k_1' = 250,000$ lb/in. and $k_4 = 2000$ lb/in. (43.78×10^6 and $0.35 \times 10^6 \frac{N}{m}$, respectively) is the second one from the left. A value of $c = 0.1$ lb-sec/in. ($17.5 \frac{N\text{-sec}}{m}$) is found to produce results which are quite representative of the experimental data presented in References 1 and 2. Therefore, with $c = 0.1$ lb-sec/in. and with $k_1 = k_1' = 250,000$ lb/in. and $k_4 = 2000$ lb/in., the data points for the present BRU are shown in Figures 8 and 9 and accented by a small circle for easy identification and comparison with other stiffness combinations and different values of the damping coefficient.

As marked on the abscissa of Figure 8, there are five discrete stiffness combinations. The combination of $k_4 = 2000$ lb/in. and $k_1 = k_1' = 250,000$ lb/in. represents the existing BRU with $c = 0.1$ lb-sec/in. The combination of $k_4 = 2000$ lb/in. and $k_1 = k_1' = 250,000$ lb/in. ($43.78 \times 10^6 \frac{N}{m}$) and the combination of $k_4 = k_1 = k_1 = 18,000$ lb/in. ($3.15 \times 10^6 \frac{N}{m}$) are of particular interest because with either of these two stiffness combinations the BRU journal pads could be operated with a zero set up interference (see Reference 4). Such a configuration might, for example, permit the elimination of the need for hydrostatic operation during BRU startup.

For each stiffness combination, the input excitation was first assumed to act in the "12 o'clock" direction. In each case, the gas-film thickness variations of the three pads were calculated. From these calculations, the maximum weighted gas-film variation was obtained. The same computation was then performed for inputs in the "9 o'clock" direction and in the "8 o'clock" direction. It was found that for each of the five different stiffness combinations, the "12 o'clock" direction always yields the highest values of the weighted maximum gas-film variation and weighted maximum pad vibration relative to casing (it is these quantities which are shown in Figures 8 and 9, respectively). The corresponding values for $c = 1$ lb-sec/in. and $c = 5$ lb-sec/in. (175 and 875.6 $\frac{N\text{-sec}}{m}$) are also shown.

Figure 8 indicates that without external damping ($c = 0.1$ lb-sec/in.) the existing design ($k_4 = 2000$ lb/in. and $k_1 = k_1' = 250,000$ lb/in.) is reasonably close to optimum from the standpoint of vibration, although the $k_4 = 6000$ lb/in.

$k_1 = k_1' = 250,000$ lb/in. combination is slightly better. However, with external damping of $c = 1.0$ lb-sec/in. or larger, the $k_4 = k_1 = k_1' = 2000$ lb/in. design is superior. This design may not, however, have sufficient structural rigidity to be practical. Note that if an external damping of $c = 2$ lb-sec/in. $(350 \frac{N\text{-}sec}{m})$ could be achieved through design, then the maximum weighted gas-film variation would be 0.75 for the combination of $k_4 = k_1 = k_1' = 6000$ lb/in. Compared to the predicted amplitude ratio of 3.7 for the existing BRU design, this is a reduction of a factor of 5. In References 1 and 2 it was found that the safe RMS g-level (without significant shaft-pad touching) that the present BRU can sustain is only 20-25 percent of the RMS g-level of the specification. It appears, therefore, that one or more of the configurations considered, together with an appropriate level of flexure damping, would permit the BRU to be operated at the full specification level in the transverse direction. Should flexure damping of $c = 5$ lb-sec/in. be attainable, the maximum weighted gas-film variation would be reduced further. The addition of this higher level of damping to the existing design also appears to be a viable alternative, in view of the fact that reductions of a factor of about 4.5 to 5 appear possible for such a configuration.

In summary, it appears that the key to a satisfactory flexure design for the BRU gas bearing pads is the amount of damping that can be realistically added to the flexure.

Design and Component Test of Flexure Dampers for Journal Bearings

Based upon the preceding analysis of the BRU journal bearing support system, a significant reduction in lateral rotor vibration may be achieved from the addition of damping to the 2000 lb/in. $(0.35 \times 10^6 \frac{N}{m})$ pad flexure. A flexure damping level of about 1 to 2 lb-sec/in. $(175 \text{ to } 350 \frac{N\text{-}sec}{m})$ was predicted to yield measurable pad vibration attenuation (a factor of about 2), while damping levels of from 5 to 8 lb-sec/in. $(875 \text{ to } 1401 \frac{N\text{-}sec}{m})$ were predicted to yield very significant attenuations (a factor of 5 or more).

The search for a suitable damper necessarily had to recognize the space limitation arising from the need to fit the damper into the existing machine, and the requirement that the added dampers would not compromise the life expectancy or functional performance of the BRU.

Several damper configurations were considered in light of the foregoing requirements:

a) Oil or other liquid dampers were immediately eliminated from consideration because of the obvious sealing problems which would accompany the introduction of a new fluid.

b) Dampers employing one or more elastomer elements were eliminated because of temperature and lifetime considerations.

c) Coulomb-type dampers were eliminated because of their nonlinearities and because of potential problems with wear of contacting surfaces.

d) Electromagnetic-type dampers were considered to be feasible, but were eventually eliminated in favor of the gas-piston type, primarily because of design uncertainties accompanying such short stroke lengths (about 0.002 in. (0.05 mm) or less).

e) A gas-piston-type damper, utilizing bearing cavity gas at cavity ambient conditions, was selected as being most practical and simplest to implement. No fluids or temperature-sensitive elements are involved. No rubbing occurs between adjacent elements, and perhaps most important, design procedures for this type of device have become well established through MTI's development of resonant piston compressor technology.

The available space envelope for the damper, located immediately outboard of the 2000 lb/in. (0.35 $\frac{N}{m}$) flexure, permitted the addition of a rectangular piston-in-cavity design of approximately 3 in.^{2} (20 cm^2) area. The 2-1/4 by 1-1/4 in. (57 x 32 mm) piston was securely pinned to the flexible element of the flexure assembly. The rectangular cavity was assembled with clearance

(0.0011 in. (0.028 mm) on all four sides) over the piston and rigidly attached
to the rigid part of the original BRU flexure. In the undeflected position,
the clearance between the top of the piston and the bottom of the cavity was
0.018 in. (0.46 mm). When assembled in the BRU simulator, this clearance
decreased to 0.011 in. (0.28 mm) due to flexure deflection under preloading
and operating conditions. Both sides of the original flexure assembly and
the disassembled damper are shown in Figure 10, a composite photograph. Side
2 clearly shows the flexible element in the flexure assembly, which in the
assembled state is gripped at the center location (above the pivot) by two
ears on the underside of the piston. The rectangular cavity of the damper is
visible in Side 1 in the same photograph. A drawing of the complete flexure-
damper assembly is shown in Figure 11.

The clearance dimensions between damper piston and cavity were derived from
an optimization analysis in which the gaseous medium was nitrogen at 10 psia
(6.9×10^4 N/m^2) and 800 F (425 C). The piston (and thus the bearing pad
pivot and flexure) were assumed to vibrate predominantly at 100 Hz with an
amplitude of 0.001 in. (0.025 mm). The vibration values had been found in
a previous experimental analysis to be representative for the high-response
range (References 2 and 3). The optimum predicted performance of the damper
is shown graphically in Figure 12. Under nominal gap conditions between
piston and cavity, a damping factor in excess of 3 lb-sec/in. ($52.5 \frac{N\text{-}sec}{m}$)
may be expected, and even for a completely de-centered piston (which would,
of course, rub on the cavity walls), a damping factor of better than 2 lb-
sec/in ($350 \frac{N\text{-}sec}{m}$) is predicted.

The completed damper-flexure assemblies were subjected to preliminary perform-
ance testing prior to installation in the BRU simulator.

Each assembly was mounted on a shake table and vibrated at constant table dis-
placement amplitude through the frequency range in which the natural frequency
of the movable mass of the flexure-damper assembly occurred. Measurement of
damper piston amplitude relative to the piston cavity, together with absolute

motion of the table, provided data from which relative transmissibility values
and the damping in the vibrating system may be calculated. Figure 13(a) shows
the results obtained for 0.0005 in. (0.013 mm) peak-to-peak table vibration
with the flexure-damper assembly in the "as-delivered" condition. The damping
obtained in this assembly is relatively low, as evidenced by the Relative
Transmissibility ratio of 8, and as predicted by prior analysis. Examination
of the analytically-obtained performance trends for the flexure-damper assembly
reveals two reasons for these results:

1. The designed piston-cylinder clearance (above the top of the piston)
    was a nominal value of 0.011 in. (0.28 mm). This clearance will
    exist after assembly of the flexure-damper assembly into the BRU
    (flexure preload) and the lift-off of the bearing pad from the
    shaft during operation. The flexure-damper assembly in its 'free'
    state (as it existed during preliminary testing) has a top
    clearance of 0.018 in. (0.46 mm), a clearance which is predicted
    to produce a large reduction in damping.

2. The pneumatic damper has been designed for an operating frequency
    of 100 Hz because previously obtained vibration data for the BRU
    simulator had indicated maximum vibration responses to occur around
    that frequency. However, damping of the flexure-damper assembly
    decreases inversely with frequency, resulting in considerably lower
    values at those frequencies (around 600 Hz, the damper resonant
    frequency) at which the damper assembly was tested.

To achieve better assurance that the damper assembly would meet design specifi-
cations, a temporary plastic shim was attached to the face of the piston, re-
ducing the clearance above the piston to 0.011 in. (0.28 mm). The vibration
tests were then repeated with this configuration. The resultant transmissi-
bility curve in Figure 13(b) clearly shows a significant increase in system
damping, an increase which was predicted within satisfactory limits by analysis.
(The accompanying increase in the system critical frequency is due to the in-
crease in the gas volume stiffness in the damper cavity, which accounts for more

than half of the total system spring stiffness. The other half is accounted for by the mechanical spring stiffness of the flexure.)

Additional temporary modifications of the flexure-damper for further preliminary tests were not made due to their complexity and potential risks to the mechanical integrity of the flexure assembly. For instance, if it has been feasible to attach approximately five (5) pounds (2 Kg) of mass to the flexure (through the pivot), the system natural frequency could have been decreased to approximately 100 Hz. Tests under those conditions would have been expected to indicate the higher level of damping that exists for this device at 100 Hz as compared to what is shown in Figure 13(b) for 600 Hz.

A final preliminary experimental verification of the damping characteristics of the flexure-damper assembly was made through temporary increase of the gas escape path from the piston cavity. Normally (when installed in the BRU simulator), the only gas escape path exists at the clearance between piston and cavity. During the final preliminary tests, an additional escape path was provided around the capacitance probe which was mounted in the cavity housing for measurement of piston motion relative to the cavity. The results, shown in Figure 13(c), demonstrated a further increase in damping. Evaluation of the significance of this increase showed clearly that a corresponding increase in piston clearance would be desirable for a design which was optimized at a frequency of 600 Hz. Excellent correlation of all preliminary test results with predictions, however, indicated that the hardware as originally designed was optimum for provision of damping at 100 Hz.

EXPERIMENTAL SETUP FOR EVALUATION OF
FLEXURE DAMPERS IN THE BRAYTON ROTATING UNIT

Introduction

In Reference 1, the BRU simulator without flexure dampers had been subjected
to external sinusoidal and random vibrations which were applied in the rotor
axial direction and in a direction perpendicular to the rotor axis. The re-
sponse of the rotor and of many bearing system components was recorded on
magnetic tape for later analysis. In References 2 and 3, an experimental
analysis was presented which drew upon the data obtained and cataloged in
Reference 1. Descriptions of the Test Apparatus (BRU simulator), the test
instrumentation and a description of vibration tests performed may also be
found in Reference 1, and in abbreviated form in References 2 and 3.

Since it is the objective of this report to describe a program aimed at a
reduction of the vibration response of the previously examined BRU, pertinent
base line information from Reference 1 through 3 is repeated here for con-
venience. The following section furnishes a brief description of the in-
strumented basic test apparatus as it was used for the tests described in
References 1 - 3, and also for the tests described in this report.

Test Apparatus

A schematic of the BRU simulator with the rotor in the vertical orientation is
shown in Figure 14. The rotor, from the top down, consists of the following
components:

1. The (simulated) compressor wheel, containing the cold gas simulator
   drive turbine.
2. The thrust runner.
3. The compressor end journal.
4. A center section (homopolar generator rotor).
5. The turbine end journal
6. The (simulated) gas turbine wheel.

The three-pad configuration of the gas film journal bearings is shown in cross-
section in Figure 14. The pads are individually supported by pivots, with one

of the pivots in each bearing assembly mounted on a mechanical flexure. The flexure, which has a radial stiffness of approximately 2000 pounds per inch $(0.35 \times 10^6 \frac{N}{m})$, permits the bearing to accommodate radial centrifugal growth of the journal and differential, radial, thermal expansion between the various bearing parts.

The double-acting thrust bearing is supported by a gimbal assembly with two sets of gimbals 90° apart. These permit the thrust bearing to align itself with the thrust runner of the rotor. The surface geometry of the thrust plates consists of nine equal sectors of 39° each with narrow radial grooves separating the sectors. Each sector in turn consists of a slightly depressed sector of 15° arc followed by the raised part in the direction of rotor rotation. Design details for the complete journal and thrust bearing assemblies are given in Reference 5.

The journal bearings, as well as both thrust bearing plates, have hydrodynamic and hydrostatic operating capabilities. For hydrostatic operation, each journal bearing pad and each raised thrust plate sector is equipped with a small gas supply hole, connected to an outside gas source. Hydrostatic bearing operation is normally employed to separate the bearing and rotor surfaces at startup until rotor speed is high enough to produce a sufficiently large gas film for safe bearing operation. At the design speed of 36,000 rpm and above, the rotor operates hydrodynamically. The BRU design also requires hydrostatic bearing operation at shutdown to prevent rubbing contact between the rotor and the bearing surfaces at speeds too low to provide hydrodynamic film separation of the bearing surfaces. Prior to the vibration tests described in this report, all bearing and corresponding rotor surfaces had been coated by MTI with chrome oxide and refinished to the original dimentional specifications. This was done to imporve the tolerance of the bearing surfaces against accidental rubs which might occur in the course of the vibration tests.

When mounted in a support fixture for vibration testing, the simulator is held without isolators by three mounting brackets extending radially outward from the simulator casing and resting on the rim of the support fixture. Flexible

air hoses served to pressurize separately each of the journal bearings, the thrust bearing plates, the bearing cavity, the thrust loader chamber and the cold gas drive turbine. Nitrogen at room temperature was used for hydrostatic bearing operation and to provide the ambient gas atmosphere during all hydrodynamic tests.

Test Instrumentation

The dynamic response measurements on the rotor-bearing system were made with capacitance probes. These probes may be divided for convenience into two categories: those measuring displacements of the rotor or some bearing component relative to the simulator casing, and those measuring gas-film thickness variations between the rotor and the thrust bearing or between the rotor and any of the journal bearing pads.

Gas-film thickness variations between the rotor and individual journal bearing pads were measured with capacitance probes built into each pad. These probes, which were installed by MTI prior to tests, were located next to the pivot on the inboard side of each bearing pad (a total of six).

Two sets of two probes were used to measure rotor displacement relative to the simulator casing at two locations inboard of the journal bearings. (The angular orientation of these capacitance probes is indicated in Figure 15.) The radial motions of the two flexures supporting each one of the three pads of each journal bearing were measured near the pivot location relative to the casing. Pad motions at the pad leading edge were recorded for one solid-mounted and one flexure-mounted pad. The probe locations in relation to the rotor are shown in Figure 15. The probes are identified in Figure 16.

Temperatures from nine locations, including both flexure-mounted journal pads, one solid-mounted pad at the compressor-end journal, and one thrust plate were recorded by automatic printout throughout the tests.

The root-mean-square values of the random displacement signals were extracted through application of a true-rms-reading voltmeter, and the tape recorded BRU random data was further analyzed with the aid of a real-time frequency analyzer to obtain displacement power spectral density plots.

VIBRATION TEST RESULTS FOR
BRAYTON ROTATING UNIT WITH JOURNAL BEARING FLEXURE DAMPERS

Test Conditions and Specifications

The BRU simulator was tested under random vibration input conditions with the shaft in the vertical position (compressor end up). Tests were conducted with the direction of applied vibrations perpendicular to the rotor axis (transverse vibration tests) and then repeated with vibrations applied in a direction along the rotor axis (vertical vibration tests). For the former tests, the shake table was turned by 90° into the horizontal position and the simulator was mounted in a different support fixture. During the lateral vibration tests, the simulator was so oriented that the direction of vibration passed through the pivot of the flexure-supported journal pad in each journal bearing. Small-scale schematics of the BRU simulator in either the transverse or vertical test fixture are shown in all data graphs.

All vibration tests were conducted according to NASA Spec 417-2-C*, which calls for random vibration input levels (with shaft rotation) of the following description:

    20 - 100 Hz . . . 3 db/octave increase
    100 - 2000 Hz. . . 0.015 g^2/Hz

A graphic representation of the random specification is shown in Figure 17.

Since these tests were not intended as qualification tests, input vibration levels were raised gradually in small steps until intermittent contacts between rotor and bearing surfaces were indicated by rapidly rising bearing temperatures and a steady slowdown in rotor speed. This criterion was used as the prime indicator for the maximum permissible vibration levels identified in Figure 17 (for transverse tests only) and in Table I (transverse and axial tests). The values shown in Figure 17 and in Table I

*Environmental Specification of SNAP-8 Electrical Generating System, dated March 31, 1967.

TABLE I.   BRU RANDOM VIBRATION TOLERANCE LIMITS, g rms*

Direction of Applied Vibration	Operating Mode of Gas Bearings	BRU With Journal Bearing Flexure Dampers	BRU Without Journal Bearing Flexure Dampers
Transverse	All Hydrodynamic	2.80	N.A.
	Turbine Journal Brg ⎤Hydro- Thrust Bearing ⎦dynamic Compressor Jnl Brg-150**psia	2.90	1.70
	All Hydrostatic - 150 psia	4.55	N.A.
Axial	All Hydrodynamic	2.15	N.A.
	Turbine Journal Brg⎤Hydro- Thrust Bearing ⎦dynamic Compressor Jnl Brg-55***psia	2.15	2.15
	Turbine Journal Brg⎤Hydro Thrust Bearing ⎦dynamic Compressor Jnl Brg-150 psia	2.30	N.A.
	Journal Brgs-Hydrodynamic Thrust Bearing - 150 psia	2.90	N.A.

*Shaped Random Vibrations According to NASA Specifications 417-2-C-3.5.
**150 psia = 10^6 N/m^2
***55 psia = 0.38 x 10^6 N/m^2

are slightly lower (by approximately 0.2 g rms) than those at which rotor slowdown was observed, and may therefore be considered the maximum levels at which BRU operation could be maintained.

BRU simulator rotor speed was 36,000 rpm for all tests. Normally, both journal bearings and the thrust bearing operate hydrodynamically. However, as a result of a partial structural failure in the compressor end journal bearing, the previous random vibration tests (BRU without dampers) were

conducted with the turbine journal bearing and the thrust bearing operating hydrodynamically and the compressor end journal bearing pressurized from an outside gas supply. During these tests, the gas supply pressure to the compresor end journal bearing was 150 psia (10^6 N/m^2) when the vibrations were applied in the transverse direction and 55 psia (0.38×10^6 N/m^2) when applied along the rotor axis (axial vibration tests).

Random Vibration Tolerance Limits

The above referenced bearing operating conditions were exactly duplicated for the tests recorded here, because these tests were intended to establish the difference in vibration tolerance limits of the BRU as a result of the bearing damper addition. As indicated in Table I and Figure 17, with random vibrations applied in the transverse direction, the BRU vibration tolerance limit increased from 1.70 g rms to 2.90 g rms. This increase of about 70 percent represents a definite improvement as a result of flexure damper addition, but it falls short of the goal of an improvement of more than 300 percent which would be necessary to meet the BRU random vibration specification limits. With all bearings operating hydrodynamically, the improvement was slightly less, with 2.60 g rms recorded for a maximum level.

The addition of flexure dampers did not improve the vibration tolerance of the simulator when vibrations were applied along the shaft axis. This agrees perfectly with expectations, and lends credence to the previously-advanced deduction, based upon examination of experimental data, that the thrust bearing alone determines simulator vibration tolerance for the axial direction (Reference 2). For axially-applied vibrations, tolerance limits were identical when all journal bearings operated fully hydrodynamically and when the compressor end journal bearing was pressurized to 55 psia. This result again confirms the secondary role of the journal bearings as a limiting factor in the axial vibrational mode, at least at vibration levels which constitute the tolerance limits for the thrust bearings when axial vibrations are applied.

External pressurization of the thrust bearing (to 150 psia) raised the vibration tolerance of the simulator in the vertical mode to 2.90 g rms. This

value does not represent a large increase and it does not compare favorably with the 4.55 g rms level achieved in the transverse mode with all bearings externally pressurized to 150 psia. The latter results may reflect the reduction of journal bearing pad-to-shaft contacts due to the combined effect of larger gas film clearances obtained by external pressurization and the improvement in journal bearing flexure vibration due to the addition of dampers.

The corroborating evidence that confirms the occurrence of intermittent contacts between rotor and bearing surfaces during the final stages of random vibration testing is supplied by the temperature recordings of the various bearing elements. Two examples of temperature records are given in Figures 18 and 19. The temperature recording shown in Figure 18 was obtained for the random test case where vibrations were applied in a transverse direction and all bearings were operating hydrodynamically. It clearly indicates a steep temperature rise for both solid and flex-mounted journal bearing pads, in both bearings.

External pressurization of the compressor end journal bearing for the next test case had a double effect upon the temperature history of the pads of that bearing (Figure 19). During the noncontacting phase of the random tests, the compressor journal bearing pads remained at a temperature of $20^{\circ}F$ ($11^{\circ}C$) below that of the turbine end journal bearing pads. During the final phase of the test, only the turbine-end journal bearing pads indicate a sharp temperature rise, with the flexure-mounted pad beginning to show the temperature rise earlier than the solid-mounted pad.

Examination of the temperature records for the vertical random vibration tests indicates that all tests were terminated due to contacts between the thrust rotor and the thrust plates.

Amplitude Analysis: Root-Mean-Square (rms) Values

An analysis of all individual displacement signals from the BRU simulator, as they were recorded on magnetic tape during the vibration tests, can be very

helpful in identifying the rotating-stationary interface of the bearing system at which rubbing first begins. Unfortunately, two test-hardware-connected circumstances have introduced some difficulties and complications to this analysis. The failure of some of the internal probes in the simulator during the early phases of the test limits the amount of information available for exact comparisons. The partial structural failure in the compressor-end journal bearing during the previous test series (without flexure dampers) introduced the need to operate that journal bearing in the hydrostatic mode. When operating hydrostatically, the journal bearing has a much larger gas film of appreciably lower stiffness than under hydrodynamic operating conditions. Consequently, larger film thickness variations may be observed in the compressor-end journal bearing than in the turbine-end bearing without being indicative of greater distress under external vibration. It must also be remembered that the associated sets of casing-to-shaft sensors may be accordingly affected by the greater gas-film clearance in their neighboring journal bearings. The third, and quite separate, element in the rotor-bearing system is the thrust bearing. The two masses of the thrust bearing gimbal support, with their different sets of pivots, may be expected to show quite different characteristics about their two perpendicular axes. Finally, the flexure-mounted pad in each journal bearing will show very different responses than the solid-mounted pads in the respective bearings. Due to the different modes of journal bearing operation in some tests, these responses will also be different from each other. (The physical relationships and locations of the various bearings and displacement sensors is shown in Figure 15.)

The root-mean-square values of all recorded random displacement and acceleration signals obtained during tests of the BRU simulator with bearing flexure dampers installed, have been plotted for comparison. Figures 20 through 22 provide three typical examples, taken from the transverse test series, where the compressor journal had been externally pressurized to 150 psia (10^6 N/m^2). Figure 20 depicts the stepped increases of input acceleration (in g rms) applied to the mounting fixture of the BRU simulator on the shake table.

The time base indicates that the dwell time at each of the vibration input

levels was approximately one minute. (Tests were generally repeated a second time for complete taping of all signals.) A typical step-for-step response pattern in displacement amplitude (rms value), as it was obtained for casing-to-shaft probes, is shown in Figure 21. This response is also typical for the gas-film thickness variations of the solid-mounted pads. The thrust bearing generally exhibited quite a different response (Figure 22). After about three step increases in shake table input acceleration, the thrust bearing rotor response amplitude has reached values close to the possible maximum, which corresponds to the full clearance between thrust plates. Further increases in the shake table vibration input level produce only very small increases in the response amplitude of the thrust runner. A third amplitude response plot, shown in Figure 23, is for the film thickness variation of the flexure-mounted, damped pad in the compressor-end journal bearing under hydrodynamic operating conditions. The increase in response amplitude with increasing input level is the smallest observed during the current test series, as well as in all previous tests without the flexure dampers installed (Reference 1).

The rms amplitude response values from all functioning displacement probes, obtained at the 1.5 g rms vibration input level, are given in the first two columns in Table II. These two columns contain values obtained in the current test series, which was conducted with bearing flexure dampers installed in the BRU simulator. The third column in Table II has been taken from previously-obtained data, where the BRU simulator had been tested under identical conditions, but without the newly designed bearing flexure dampers (Reference 1).

Part (a) of Table II refers to data from random vibration tests with the direction of applied vibrations perpendicular to the rotor axis (transverse tests). Part (b) refers to tests where the direction of applied vibrations was along the rotor axis (axial tests).

The second and third column in Part (a) of Table II are of prime interest in the evaluation of the effectiveness of the newly installed bearing flexure dampers, because they afford a direct comparison of bearing component responses

TABLE II(a).   DISPLACEMENT ROOT-MEAN-SQUARE AMPLITUDES (in. x 10^4)***

FOR RANDOM VIBRATION INPUT LEVEL OF 1.5 g rms*

Transverse Direction of Applied Random Vibration

Probe Ident.	Probe Designation	With Journal Bearing Flexure Dampers		Without Journal Bearing Flexure Dampers**
		All Bearings Hydrodynamic	Turbine Jnl. Brg and Thrust Brg: Hydrodynamic Compressor Jnl. Brg: Externally-Pressurized 150 psia	
A	Pivot film thickness probe, flex-mounted pad, compressor end	0.5	1.9	2.8
B	Pivot film thickness probe, solid-mounted pad, compressor end	6.5	N.A.	N.A.
C	Pivot film thickness probe, solid-mounted pad, compressor end	1.9	2.5	2.5
D	Pivot film thickness probe, flex-mounted pad, turbine end	0.55	N.A.	0.9
E	Pivot film thickness probe, solid-mounted pad, turbine end	2.5	2.25	N.A.
F	Pivot film thickness probe, solid-mounted pad, turbine end	4.0	N.A.	5.0
21	Turbine journal flex-mounted pad load probe	11.0	8.5	8.5
22	Compressor journal flex-mounted pad load probe	4.5	6.8	10.0
1	Compressor journal orthogonal probe	3.5	4.5	N.A.
2	Compressor journal orthogonal probe	4.0	N.A.	9.0
3	Turbine journal orthogonal probe	5.5	5.8	N.A.
4	Turbine journal orthogonal probe	5.0	5.5	13.0
19	Turbine thrust plate film thickness probe	5.5	5.5	4.7
20	Turbine thrust plate film thickness probe	6.5	5.1	6.5
23	Thrust bearing gimbal probe to casing	3.7	3.0	3.9
24	Thrust bearing gimbal probe to casing	3.3	2.0	3.5

*Shaped Random Vibrations According to NASA Specification 417-2-C-3.5.

**From Reference 1.

***Multiply by 0.00254 to

TABLE II(b).   DISPLACEMENT ROOT-MEAN-SQUARE AMPLITUDES (in. x 10^4)[***]

FOR RANDOM VIBRATION INPUT LEVEL OF 1.5 g rms[*]

Axial Direction of Applied Random Vibration

Probe Ident.	Probe Designation	With Journal Bearing Flexure Dampers		Without Journal Bearing Flexure Dampers[**]
		All Bearings Hydrodynamic	Turbine Journal Brg and Thrust Brg: Hydrodynamic Compressor Jnl. Brg: Externally-Pressurized 150 psia	
C	Pivot film thickness probe, solid-mounted pad, compressor end	1.8	1.8	2.5
E	Pivot film thickness probe, flex-mounted pad, turbine end	2.5	2.5	N.A.
F	Pivot film thickness probe, solid-mounted pad, turbine end	N.A.	N.A.	3.0
21	Turbine journal flex-mounted pad load probe	2.3	2.5	3.1
22	Compressor journal flex-mounted pad load probe	1.6	2.2	3.0
1	Compressor journal orthogonal probe	1.7	N.A.	N.A.
2	Compressor journal orthogonal probe	N.A.	N.A.	2.6
3	Turbine journal orthogonal probe	2.4	2.5	N.A.
4	Turbine journal orthogonal probe	N.A.	N.A.	3.2
20	Turbine thrust plate film thickness probe	7.5	7.7	7.0
23	Thrust bearing gimbal probe to casing	6.0	6.7	6.6
24	Thrust bearing gimbal probe to casing	4.2	4.5	6.3

[*]Shaped Random Vibrations According to NASA Specification 417-2-C-3.5
[**]From Reference 1.
[***]Multiply by 0.00254 to obtain mm.

under identical test conditions. The film thickness variations of the flexure-mounted pad in the (hydrostatically pressurized) compressor end journal bearing show a definite decrease (by about 30 percent) as the result of damper addition. A similar reduction is observed for the hydrodynamically operating flexure-supported turbine-end journal bearing pad. The solid-mounted pad in the hydrostatically operating compressor-end journal bearing shows no change in response amplitudes, and a similar conclusion is reached for the solid-mounted pads in the hydrodynamically operating turbine-end journal bearing. The casing-to-shaft probes show a very significant reduction (over 50 percent) in amplitude variation under all bearing operating conditions. As anticipated, the thrust bearing probes show little change for all tests.

The second half of Table II gives a similar listing of all rms amplitude values obtained under axial random vibration input conditions. Except for a reduction in flexure amplitudes for both test cases where dampers had been installed, there appear to be no significant amplitude differences between tests at the vibration input level of 1.5 g rms. The very nearly equal performance at less than maximum vibration input level points to the possibility that nearly identical maximum levels might be reached in all three test cases. This agrees well with the final test results (vibration tolerance limits) given in Table I. It may be also noted from Table II that thrust bearing amplitudes are very nearly equal in all three test cases and generally higher than those observed for transverse vibration applications.

The data presented in Table III give some indication of the maximum displacement rms amplitudes the BRU simulator can tolerate before rotor-to-bearing contacts occur. The data in Table III was obtained from the same plots of rms values used for the extracting of values shown in Table II. However, the values in Table III represent the displacements obtained for maximum vibration input levels in each of the six individual vibration tests. (Three transverse and three axial tests.) The maximum vibration input levels associated with these displacements are those listed in Table I.

Inspection of Table III reveals certain regularities which may indicate the

TABLE III(a).   DISPLACEMENT ROOT-MEAN-SQUARE AMPLITUDES (in. x 10^4)**

FOR MAXIMUM VIBRATION INPUT TEST LEVELS

Transverse Direction of Applied Random Vibration

Probe Ident.	Probe Designation	With Journal Bearing Flexure Dampers		Without Journal Bearing Flexure Dampers (Ref. 1)
		All Bearings Hydrodynamic (Vibr Input Level 2.8 g rms)	Turbine Jnl. Brg and Thrust Brg: Hydrodynamic Compressor Jnl. Brg: Externally-Pressurized 150 psia (Vibration Input Level 2.9 g rms*)	(Vibration Input Level 1.7 g rms*)
A	Pivot film thickness probe, flex-mounted pad, compressor end	0.43	N.A.	3.4
B	Pivot film thickness probe, solid-mounted pad, compressor end	10.0	N.A.	N.A.
C	Pivot film thickness probe, solid-mounted pad, compressor end	3.0	4.7	3.3
D	Pivot film thickness probe, flex-mounted pad, turbine end	0.62	N.A.	0.9
E	Pivot film thickness probe, solid-mounted pad, turbine end	5.0	4.7	N.A.
F	Pivot film thickness probe, solid-mounted pad, turbine end	7.0	N.A.	N.A.
21	Turbine journal flex-mounted pad load probe	16.0	14.0	9.6
22	Compressor journal flex-mounted pad load probe	6.5	15.0	14.0
1	Compressor journal orthogonal probe	4.5	10.0	N.A.
2	Compressor journal orthogonal probe	5.0	N.A.	10.0
3	Turbine journal orthogonal probe	6.0	10.0	N.A.
4	Turbine journal orthogonal probe	6.5	11.0	13.0
19	Turbine thrust plate film thickness probe	6.0	5.8	N.A.
20	Turbine thrust plate film thickness probe	7.0	6.3	6.5
23	Thrust bearing gimbal probe to casing	9.0	9.0	3.9
24	Thrust bearing gimbal probe to casing	4.2	3.8	3.5

*Shaped Random Vibrations According to NASA Specification 417-2-C-3.5.   **Multiply by 0.00254 to obtain mm.

TABLE III(b). DISPLACEMENT ROOT-MEAN-SQUARE AMPLITUDES (in. x 10^4)***

FOR MAXIMUM VIBRATION INPUT TEST LEVEL OF 2.15 g rms*

Axial Direction of Applied Random Vibration

Probe Ident.	Probe Designation	With Journal Bearing Flexure Dampers		Without Journal Bearing Flexure Dampers**
		All Bearings Hydrodynamic	Turbine Journal Bearing and Thrust Brg: Hydrodynamic Compressor Jnl. Brg: Externally-Pressurized 150 psia	
C	Pivot film thickness probe, solid-mounted pad, compressor end	2.7	2.8	N.A.
E	Pivot film thickness probe, flex-mounted pad, turbine end	4.5	4.5	N.A.
F	Pivot film thickness probe, solid-mounted pad, turbine end	N.A.	N.A.	4.0
21	Turbine journal flex-mounted pad load probe	6.0	5.0	N.A.
22	Compressor journal flex-mounted pad load probe	2.5	4.2	N.A.
1	Compressor journal orthogonal probe	3.0	N.A.	N.A.
2	Compressor journal orthogonal probe	N.A.	N.A.	N.A.
3	Turbine journal orthogonal probe	4.5	5.0	N.A.
4	Turbine journal orthogonal probe	N.A.	N.A.	5.3
20	Turbine thrust plate film thickness probe	8.5	8.5	7.0
23	Thrust bearing gimbal probe to casing	12.0	9.8	9.5
24	Thrust bearing gimbal probe to casing	9.0	7.3	10.5

*Shaped Random Vibrations According to NASA Specification 417-2-C-3.5.
**From Reference 1.
***Multiply by 0.00254 to obtain mm.

vibration tolerance limits of individual bearing system components. For
example, with transverse vibrations, the maximum rms casing-to-shaft (probes
1 through 4) amplitudes are between 10 and 13 x 10^{-4} in. (0.025 to 0.032 mm),*
both with and without bearing flexure dampers, but only when the compressor-
end journal bearing was pressurized to 150 psia (10^6 N/m^2). Without external
pressurization of the compressor-end journal bearing (all bearings operating
hydrodynamically), the maximum observed casing-to-shaft displacement rms
amplitudes are only 6.5 x 10^{-4} in. (0.017 mm). The pad-to-shaft film thick-
ness variations of the solid-mounted pads under externally-pressurized con-
ditions may possibly have reached their maximum operating limits with
recorded maximum values of 7 to 10 x 10^{-4} in. (0.018 to 0.025 mm). Inspection
of the axial vibration data table shows clearly the noncritical aspects of all
journal bearing displacements in this mode. Solid-mounted pad-to-shaft,
casing-to-shaft, and flexure amplitudes are all much lower than those obtained
under transverse vibration. The thrust bearing and the thrust bearing gimbal
probes indicate, however, the expected maximum values.

Frequency Analysis: Displacement Power Spectral Density

When random vibration data is put through a narrow frequency band pass filter,
all random amplitude signals that occur in that particular frequency band are
permitted to pass. As the center frequency of the filter is moved through
the frequency range of interest, an amplitude density spectrum is obtained.
Since the units of amplitude densities are those of the data squared, per unit
frequency, they are usually referred to as power spectral density (PSD) values.
When the frequency is given in Hz, and when the data is displacement amplitude,
(instead of for example acceleration), the units of this analysis are in.^{2}/Hz.

The significance of the frequency analysis for the BRU simulator is in the
determination of resonant frequencies for the hardware components whose dis-
placement signals were analyzed, and in the concurrent determination of the

*Displacement rms values of the BRU simulator cannot readily be converted to
peak-to-peak values due to the non-Gaussian character of most of the observed
amplitude distributuons. For a detailed analysis of BRU amplitude probability
distributions see References 2 and 3.

relative severity of the resonances (amplitude density). When the external vibration input acceleration (or input displacement) is used as a base line for comparison, the relative gain or attenuation of the vibrating part may be determined at each particular frequency. Comparison of the new frequency spectra obtained from the damper-equipped BRU, with similar data previously obtained from the simulator without dampers (References 2, and 3), can also be expected to reveal the effectiveness of the frequency-tuned dampers in suppressing the most substantial resonances in the 100 to 400 Hz region.

Most of the previously-obtained displacement power spectral density plots (BRU without damper) had been obtained at the input level of 1.5 g rms, which represented the maximum value for which data was available from both transverse and axial tests. To facilitate a meaningful comparison, the new data obtained from the evaluation reported here has also predominantly been analyzed at the same input level of 1.5 g rms. For one test series (transverse vibration, compressor end journal bearing externally pressurized), the random response data obtained at the maximum test input level (3 g rms) has been analyzed for the purpose of providing an indication of the amount of increases at specific resonance frequencies that might be expected from a known amount of input level increase (from 1.5 g rms to 3 g rms). The displacement PSD plots obtained from the experimental data for the BRU with bearing flexure dampers may be directly compared with the previously presented data for the BRU without dampers, as given in References 2 and 3. Some of the PDS analysis plots from the data in Reference 2 have been re-run from magnetic tape as part of the instrumentation repeatability assurance process. Some are presented here for comparison, although any PSD plot from Reference 2 or 3 representing the appropriate vibration input level may be used for the same purpose.

The comparative evaluation of the displacement power spectral density plots has to take into consideration the inherent difficulty that arises from the attempt to compare peak values of relatively undamped resonances. Although the evaluation of the total area under a resonance peak that exceeds the vibration input level might perhaps be a better method, the comparison of peak values has been chosen for this study. Attention is focused for the most part on the frequency range between 100 and 400 Hz, which had already

previously been identified as the frequency band in which the most severe and significant journal bearing resonances occur. (The thrust bearing gas-film resonance which occurs at about 60 Hz, and the once-per-revolution runout and/or lateral dynamic unbalance response of the rotor occurring at the rotational frequency of 600 Hz may be clearly observed in all appropriate power spectral density plots, but are of no real concern or interest in this evaluation.)

Before examining the detailed test results which illustrate the effects of the dampers, it is instructive to return briefly to the earlier work reported in Reference 2 to understand the behavior of the BRU without the dampers.

Comparison of Figures 24 and 25, taken from Reference 2, illustrates the relative vibration levels between the solid-mounted pads and journals in the damper-less BRU, for the compressor-end and turbine-end bearings, respectively. (Note that the former was operated hydrostatically and the latter hydrodynamically.) These figures show clearly the predominant vibration peaks in the region of 100-150 Hz which the dampers were subsequently designed to suppress. Comparison of these peaks, and also the peaks at higher frequencies, relative to the dashed input line, shows that the amplitudes are generally less severe (lower relative vibration) in the hydrostatically-operating compressor-end bearing than in the hydrodynamically-operating turbine-end bearing. The peak values are 5×10^{-9} in.^{2}/Hz (3.2×10^{-12} m^2/Hz) in Figure 25 for the turbine-end, and 8×10^{-10} in.^{2}/Hz (5.2×10^{-13} m^2/Hz) in Figure 24 for the compressor-end, a ratio of about 6.3 to 1 in displacement power spectral density. This is equivalent to a ratio of about 2.5 to 1 in rms displacement terms. The above results indicate that the solid-mounted (hydrostatic) compressor-end bearing pads track the journal better (less relative motion) than do the solid-mounted (hydrodynamic) turbine-end bearing pads.

Comparison of Figures 26 and 27, also taken from Reference 2, illustrates the relative vibration levels between the flexure-mounted pads and journals in

the damper-less BRU for the compressor-end and turbine-end bearings, respectively. Again, these figures show the major peaks in the 100 Hz region, as well as a significant peak in the 300-500 Hz region. The peaks in the hydrostatically-operating compressor-end bearing flexure-mounted pad are slightly higher, generally, than those in the hydrodynamic turbine-end bearing. The peak values (of the 100 Hz peak) are 4×10^{-11} in.^{2}/Hz (2.5 x 10^{-14} m^2/Hz) in Figure 27 for the turbine-end and 7×10^{-11} in.^{2}/Hz (4.5 x 10^{-14} m^2/Hz) in Figure 26 for the compressor-end, or a ratio of about 1 to 1.75 in displacement power spectral density. This is equivalent to a ratio of about 1 to 1.3 in rms displacement terms. These results indicate that the flexure-mounted (hydrostatic) compressor-end bearing pad tracks the journal somewhat less accurately than does the flexure-mounted (hydrodynamic) turbine-end bearing pad.

Comparison of the magnitudes of the 100 Hz peaks in Figures 24 and 26 for the compressor-end bearing, and Figures 25 and 27 for the turbine-end bearing shows the ability of the flexure-mounted pads to track the journal under different operating conditions:

	Solid-Mounted Pad	Flexure-Mounted Pad
Compressor-End Bearing (Hydrostatic)	8×10^{-10} in.^{2}/Hz (5.2×10^{-13} m^2/Hz)	7×10^{-11} in.^{2}/Hz (4.5×10^{-14} m^2/Hz)
Turbine-End Bearing (Hydrodynamic)	5×10^{-9} in.^{2}/Hz (3.2×10^{-12} m^2/Hz)	4×10^{-11} in.^{2}/Hz (2.6×10^{-14} m^2/Hz)

From these PSD values, the peak amplitudes of the 100 Hz peaks may be determined, if desired, by the equation:

$$A(rms) = \sqrt{PSD \times Filter\ Width}$$

where Filter Width = 6 Hz.

Comparisons of square roots of ratios of the above PSD values show that in the hydrostatic compressor-end bearing, the flexure-mounted pad-to-journal relative motion is lower by about a factor of three than that of the solid-mounted pad. The difference in the turbine-end bearing, on the other hand, is about a factor of 10.

Having examined the dynamic behavior of the BRU without dampers, we turn next to a comparison of the relative pad-to-journal motions resulting from introduction of the dampers, with the foregoing data. This comparison may be made between Figures 25 and 28 for the solid-mounted turbine-end pad (hydrodynamic operation). Additional data may be obtained through a comparison between Figures 24 and 29 for one solid-mounted compressor-end pad (hydrostatic operation), and between Figures 26 and 30 for the flexure-mounted compressor-end pad (hydrostatic operation). However, in the latter two cases it should be noted that the dampers have not been designed for the hydrostatic condition of the compressor-end bearing. The additional stiffnexx and damping provided by the damper may hot be optimum for that condition, and may even increase the amplitude of the pad-to-journal relative motion.

Examination of Figures 25 and 28 discloses clearly the beneficial result of the damper upon the BRU in its hydrodynamic design condition. The 100 Hz peak in the displacement PSD plot has a magnitude of about 5×10^{-9} in.^{2}/Hz $(3.2 \times 10^{-12}$ m^2/Hz) in Figure 25, while in Figure 28 the peak has an amplitude of only about 8×10^{-10} in.^{2}/Hz $(5.2 \times 10^{-13}$ m^2/Hz). This amounts to a reduction by about a factor of 6 in the PSD level, or about a factor of 2.5 in displacement. Note that this comparison is made through the use of probes E and F, which were located in different solid-mounted pads in the turbine-end bearing. Vibrations in these pads are essentially identical because of symmetry in the externally-applied vibration relative to the pad axes.

Examination of Figures 24 and 29, and Figures 26 and 30 discloses that the presence of the damper during hydrostatic operation causes increased relative

vibration levels in both the solid-mounted and the flexure-mounted pads. In Figures 24 and 29 it is observed that the amplitude of the 100 Hz peak increases from about 8×10^{-10} in.^{2}/Hz to about 1.5×10^{-9} in.^{2}/Hz (5.2×10^{-13} to 2.2×10^{-12} m^2/Hz). In Figures 26 and 30, the amplitude of the 100 Hz peak increases from about 7×10^{-11} in.^{2}/Hz to about 4×10^{-10} in.^{2}/Hz (4.5×10^{-14} to 2.6×10^{-13} m^2/Hz). While these increases are not excessive in terms of amplitudes in a hydrostatic bearing (with its larger operating films) it is essential to note that off-design operation of a gas-lubricated rotor-bearing system equipped with dampers may result in increased vibration levels in the lubricating films. Nevertheless, the damper can be very beneficial during design-condition operation.

It is worth noting in passing the relative vibration levels between the solid-mounted and flexure-mounted pads in the compressor-end bearing, with that bearing operating hydrostatically after addition of the dampers. This comparison may be made through Figures 29 and 30 and subsequent comparison with Figures 24 and 26:

	Solid-Mounted Pad	Flexure-Mounted Pad
Without Damper	8×10^{-10} in.^{2}/Hz	7×10^{-11} in.^{2}/Hz
	(5.2×10^{-13} m^2/Hz)	(4.5×10^{-14} m^2/Hz)
With Damper	1.5×10^{-9} in.^{2}/Hz	4×10^{-10} in.^{2}/Hz
	(2.2×10^{-12} m^2/Hz)	(2.6×10^{-14} m^2/Hz)

From this data, it may be observed that the effect of the damper is to reduce the difference between the solid-mounted and flexure-mounted pad relative vibration levels. In effect, proportionally larger changes occur in the flexure-mounted pad vibration levels than occur in the vibration levels of the solid-mounted pads.

The foregoing completes the before-after comparisons of damper effectiveness under the precise conditions for which the damper-less BRU was tested (e.g.,

compressor-end bearing hydrostatic, turbine-end bearing hydrodynamic). We turn now to an examination of the vibration behavior of the BRU at its design condition (all bearings hydrodynamic) with the dampers installed.

The compressor-end bearing probes are expected to display the most significant changes with changeover of that bearing's operation from hydrostatic to hydrodynamic. Examination of Figures 29 and 31 shows the effect of this changeover in the solid-mounted pad. In those Figures it may be seen that the 100 Hz peak drops from about 1.5×10^{-9} in.^{2}/Hz (2.2×10^{-12} m^2/Hz) to about 8×10^{-10} in.^{2}/Hz (5.2×10^{-13} m^2/Hz). A similar trend is seen for the flexure-mounted pad in Figures 30 and 32. There, the 100 Hz peak drops from about 4×10^{-10} in.^{2}/Hz (2.6×10^{-13} m^2/Hz) to about 3×10^{-11} in.^{2}/Hz (1.9×10^{-14} m^2/Hz). It is also worth noting that in both Figures 31 and 32 the 100 Hz peak moves up to about 120 Hz, reflecting an overall increase in bearing stiffness as a result of the changeover from hydrostatic to hydrodynamic operation.

Figures 28 and 33 illustrate the effect of this changeover in the compressor-end bearing on the turbine-end bearing solid-mounted pads. This bearing was operated hydrodynamically in all testing. The net effect on the 100 Hz peak from Figure 28 to Figure 33 is an increase from about 8×10^{-10} in.^{2}/Hz (5.2×10^{-13} m^2/Hz) to about 1.5×10^{-9} in.^{2}/Hz (9.7×10^{-13} m^2/Hz). This increase is attributed to the increased stiffness of the hydrodynamic compressor-end bearing, and the more uniform lateral motion along the rotor axis which accompanies symmetric bearing stiffness in a two-bearing system.

We turn next to an examination of the effect of the damper on the relative vibration in the turbine-end bearing pads. This bearing was operated hydrodynamically during all tests. The solid-mounted pad probe readings are displayed in Figures 33 and 25, which were obtained with and without the dampers, respectively. In Figure 25, the level of the 100 Hz peak is about 5×10^{-9} in.^{2}/Hz (3.2×10^{-12} m^2/Hz), while in Figure 33 the peak drops to about 1.5×10^{-9} in.^{2}/Hz (9.7×10^{-13} m^2/Hz). In light of the fact that

going from hydrostatic to hydrodynamic operation in the compressor-end
bearing increases the vibration level in the solid-mounted turbine-end
bearing pads (compare Figures 28 and 33), the foregoing net decrease in-
dicates considerable positive effect of the damper in vibration reduction.

The turbine-end bearing flexure-mounted pad probe readings are displayed in
Figures 34 and 27, which were obtained with and without the dampers, respec-
tively. In Figure 27 the level of the 100 Hz peak is about 7×10^{-11} in.^{2}/Hz
(4.5×10^{-14} m^2/Hz), while in Figure 34 the peak drops to about 3×10^{-12}
in.^{2}/Hz (1.9×10^{-15} m^2/Hz), a significant reduction.

Finally, we turn to an examination of the effects of increased external
vibration input level on the dynamic behavior of the BRU with dampers. It
is possible to examine this effect most directly in the turbine-end
bearing, through comparison of Figures 28 and 35. In Figure 28, the level
of the 100 Hz peak is about 8×10^{-10} in.^{2}/Hz (5.2×10^{-13} m^2/Hz), while the
input curve is 1×10^{-9} in.^{2}/Hz (6.45×10^{-13} m^2/Hz) at 150 Hz. In Figure
35 the input curve has increased to about 5×10^{-9} in.^{2}/Hz (3.2×10^{-12}
m^2/Hz) at 150 Hz while the level of the 100 Hz peak has increased to $3 \times$
10^{-9} in.^{2}/Hz (1.9×10^{-12} m^2/Hz). While the input level went up by a factor
of 5, the response at the 100 Hz peak increased only by a factor of about
3.7, indicating that more energy absorption was taking place at the higher
input level.

Similar comparisons may be made for the compressor-end bearing, although
these comparisons may only be made with hydrostatic operating conditions.
Figures 29 and 36 may be used for this purpose for the hard-mounted pads,
while Figures 30 and 37 may be used for the flexure-mounted pad. Figures 29
and 36 show that for the same vibration input level increase as quoted above,
a factor of 5, the 100 Hz peak level went from about 1.5×10^{-9} in.^{2}/Hz
(9.7×10^{-13} m^2/Hz) to about 4×10^{-9} in.^{2}/Hz (2.6×10^{-12} m^2/Hz), an in-
crease by a factor of only about 3. Figures 30 and 37 show an increase of
from 4×10^{-10} in.^{2}/Hz (2.6×10^{-13} m^2/Hz) to about 6×10^{-10} in.^{2}/Hz (3.9
$\times 10^{-13}$ m^2/Hz), a factor of only about 1.5.

It is worth noting, for the fully hydrodynamic operating condition with dampers, the degree to which the data from the compressor-end bearing pads matches that from the turbine-end bearing pads. Comparison of Figures 33 and 31 for the solid-mounted pads in the turbine-end and compressor-end bearings, respectively, indicates that both pads are quite similar dynamically. Comparison of Figures 34 and 32 for the flexure-mounted pads in the turbine-end and compressor-end bearings, respectively, however, shows that the flexure-mounted pads are quite different, dynamically. The turbine-end bearing response is lower by 1.5 to 2 orders of magnitude compared to the compressor-end bearing over a wide frequency range, from 50-1000 Hz. No apparent reason exists for this difference.

The PSD plots for the casing-to-shaft sensor (probe No. 1) that was located near the hydrostatically operated compressor-end journal bearing shows (Figure 38) no change when compared with the base line value in Figure 39. The two sensors near the hydrodynamically-operating turbine-end journal bearing (Figures 40 and 41) indicate slightly lower PSD values, and remain unchanged during the test when both journal bearings were operating hydrodynamically (Figures 42 and 43).

When the compressor-end journal bearing was operating hydrodynamically, the PSD values (Figure 44 and 45) were lower than during hydrostatic tests (Figure 38) and also lower than for the turbine end journal bearing (Figures 40 through 43).

The flexure of the compressor-end journal bearing (probe 22) and the leading edge of a solid-mounted pad did not show significant variations between operations with or without dampers. It was noted however that resonances increased much more sharply at the higher input level (3 g rms) for the flexure of the hydrostatically operating compressor journal bearing than for the hydrodynamically operating turbine-end journal bearing. This sharp increase in flexure motion must be seen in conjunction with the decrease in pad-to-rotor film variations, indicating relatively increased "tracking" by the flexure-mounted pad of the rotor as the vibration level increases.

Results for the thrust bearing gas film thickness variation show virtually
no change for the transverse test series, which confirms earlier findings.

The results for the axial vibration tests were similarly examined, but only
minimal changes were found. Consequently, no PSD plots are given in this
report. (The original data is, of course, still available on magnetic tape
for further study.)

CONCLUSIONS

The primary objective of the work reported in this volume was assessment of
the ability of constrained-volume dampers to reduce the vibration levels in
the gas films of the BRU journal bearing pads. This objective was achieved
via the following steps:

1. An experimental analysis of previously-obtained vibration data,
   to identify the frequencies of interest and the relative severity
   of the associated resonances;

2. An analytical study of the lateral vibration characteristics of
   the BRU journal bearing and pads, in order to determine the
   desired levels of pad-mount flexure stiffness and damping, and
   to assess the impact of various design alternatives on the pad
   gas-film vibration levels;

3. An experimental study of the effectiveness of dampers which had
   been built and installed based upon the results of the analytical
   study.

The conclusions drawn from the analytical study may be summarized as follows:

1. For pad support flexure stiffnesses as currently designed (250,000
   lb/in. (43.78 x 10^6 N/m) for the two solid-mounted pads and 2000
   lb/in. (0.35 x 10^6 N/m) for the flexibly-mounted pad), and with
   vibrations in the direction of the flexibly-mounted pad, the solid-
   mounted pad experiences the highest gas-film response amplitudes.

2. If both solid flexures are replaced by "soft" flexures (2000 lb/in.
   (0.35 x 10^6 N/m)), the resulting system lateral natural frequencies
   do not drop below the upper limit of the sinusoidal vibration spec-
   ification of 35 Hz. Thus, the BRU with soft flexures on each pad
   would not be expected to have a resonance within the sinusoidal
   vibration specification limits.

3. For low values of damping in the flexures, the current design

(250,000 lb/in. - 2000 lb/in. (43.78 x 10^6 N/m - 0.35 x 10^6 N/m)) was found to be near optimum in terms of predicted gas-film response amplitudes. The 250,000 lb/in - 6000 lb/in. (43.78 x 10^6 N/m - 1.05 x 10^6 N/m)) combination was found to be slightly better.

4. With increasing values of damping in all flexures, the all-soft-flexure configuration is predicted to be superior.

The conclusions drawn from the experimental damper investigation may be summarized as follows:

1. Temperature recordings from thermocouples located on journal bearing pads and thrust bearing plates indicate that when external vibration is applied to the BRU, contact between rotor and bearings occurs first in the journal bearings with lateral vibration inputs, and first in the thrust bearings with axial vibration inputs.

2. When random vibration was applied laterally to the BRU with one journal bearing externally pressurized, rapid temperature rises due to intermittent contact between journal and pads appeared only in the hydrodynamically-operating bearing.

3. Addition of the two dampers was found to increase by 70 percent the externally-applied lateral vibration levels at which the BRU could be operated without journal-to-pad rubs. As expected, no improvement was noted for externally-applied vibrations in the axial direction.

4. With both journal bearings pressurized (hydrostatic operation) and without dampers, the lateral vibration tolerance limit increases significantly compared to the limit with hydrodynamic operation (from 1.7 g rms to 4.55 g rms, a 265 percent increase). With the thrust bearing pressurized on the other hand, the vibration tolerance limit for axial vibration increases from 2.15 g rms to only 2.9 g rms, a 35 percent increase. Thus, the journal bearings are more vibration resistant than the thrust bearing for hydrostatic operation.

5. The chrome-oxide coated bearing surfaces survived repeated high-speed contacts without apparent ill effect. Rotor speed was reduced by bearing rubbing, at constant turbine inlet pressure, approximately six times with lateral external vibration and approximately six times with axial external vibration.

6. Analysis of vibration measurements shows that addition of the dampers yielded not only reduced pad vibration levels (film thickness variations), but also reduced rotor-to-casing vibration levels as well.

7. When the BRU was operated without the dampers, the solid-mounted pads were found to have lower vibration levels (film thickness variations) under hydrostatic operation than under hydrodynamic operation.

8. When the BRU was operated without dampers, the flexibly-mounted pads were found to have slightly higher vibration levels (film thickness variations) under hydrostatic operation than under hydrodynamic operation.

9. Based upon amplitude power spectral density values, the addition of the dampers reduces peak vibration levels in the solid-mounted, hydrodynamically-operating pad gas films by a factor of six. The dampers were found to produce an increase in pad-to-shaft gas film vibration under hydrostatic conditions for the same vibration input levels.

REFERENCES

1. Tessarzik, J.M., Chiang, T. and Badgley, R.H., "Effects of Vibration and Shock on the Performance of Gas-Bearing Space-Power Brayton Cycle Turbo-machinery, Part 2: Sinusoidal and Random Vibration." Report No. MTI 71TR66, prepared for NASA by Mechanical Technology Incorporated, October 1971.

2. Tessarzik, J.M., Chiang, T. and Badgley, R.H., "Effects of Vibration and Shock on the Performance of Gas-Bearing Space-Power Brayton Cycle Turbo-machinery, Part 3: Sinusoidal and Random Vibration Data Reduction ar Evaluation, and Random Vibration Probability Analysis." Report No. TI 73TR4, prepared for NASA by Mechanical Technology Incorporated, January 1973.

3. Tessarzik, J.M., Chiang, T. and Badgley, R.H., "The Response of Rotating Machinery to External Random Vibration," ASME Paper No. 73-DET-110, Journal of Engineering for Industry (Transactions of the ASME), Vol. 96, Series B, No. 2, pp. 477-489, May, 1974.

4. Waldron, W.D., "Design and Testing of Gas Bearings For Brayton Cycle Rotating Unit," MTI Report No. 72TR34, July 1972.

5. Davis, J.E., "The Design and Fabrication of the Brayton Rotating Unit (BRU)." Report No. APS-5334-R, prepared by AiResearch Manufacturing Company of Arizona for NASA-Lewis Research Center under Contract NAS3-9427, March 15, 1971.
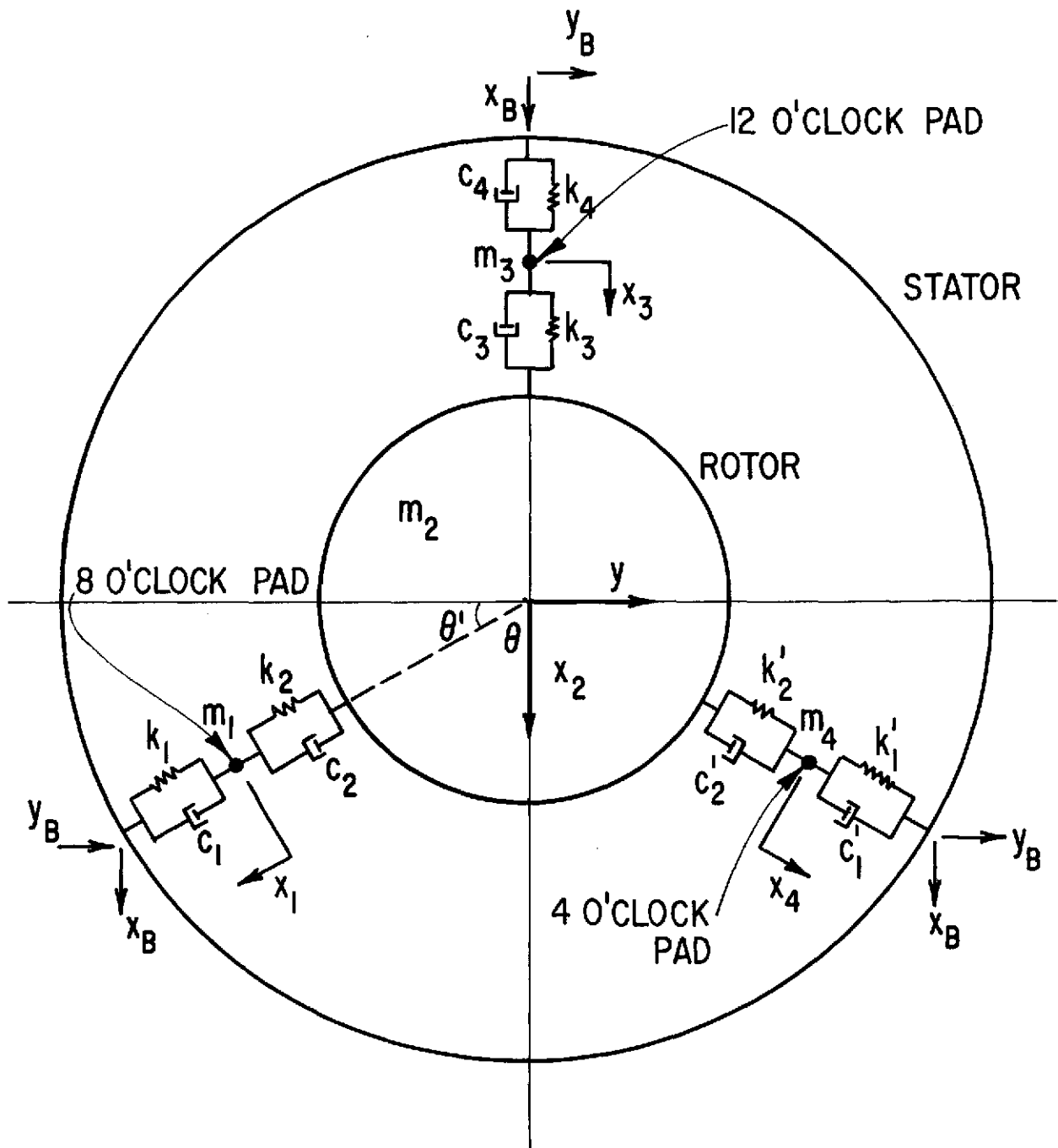
Fig. 1   Analytical Model For BRU Rotor, Pads And Flexures

$K_1 = K_1' = 250,000$ LB/IN. $(43.8 \times 10^6 \frac{N}{m})$

$K_2 = K_2' = K_3 = 53,800$ LB/IN. $(9.3 \times 10^6 N/m)$

$C_2 = C_2' = C_3 = 3.42$ LB-SEC/IN. $(599 \frac{N-SEC}{m})$

$K_4 = 2000$ LB/IN. $(3.5 \times 10^5 \frac{N}{m})$

$C = C_1 = C_1' = C_4$

C=0.1 LB-SEC/IN $(17.5 \frac{N-SEC}{m})$

I.

AMPLITUDE RATIO OF GAS-FILM THICKNESS VARIATION OF THE "12 O'CLOCK" PAD

FREQUENCY - HZ
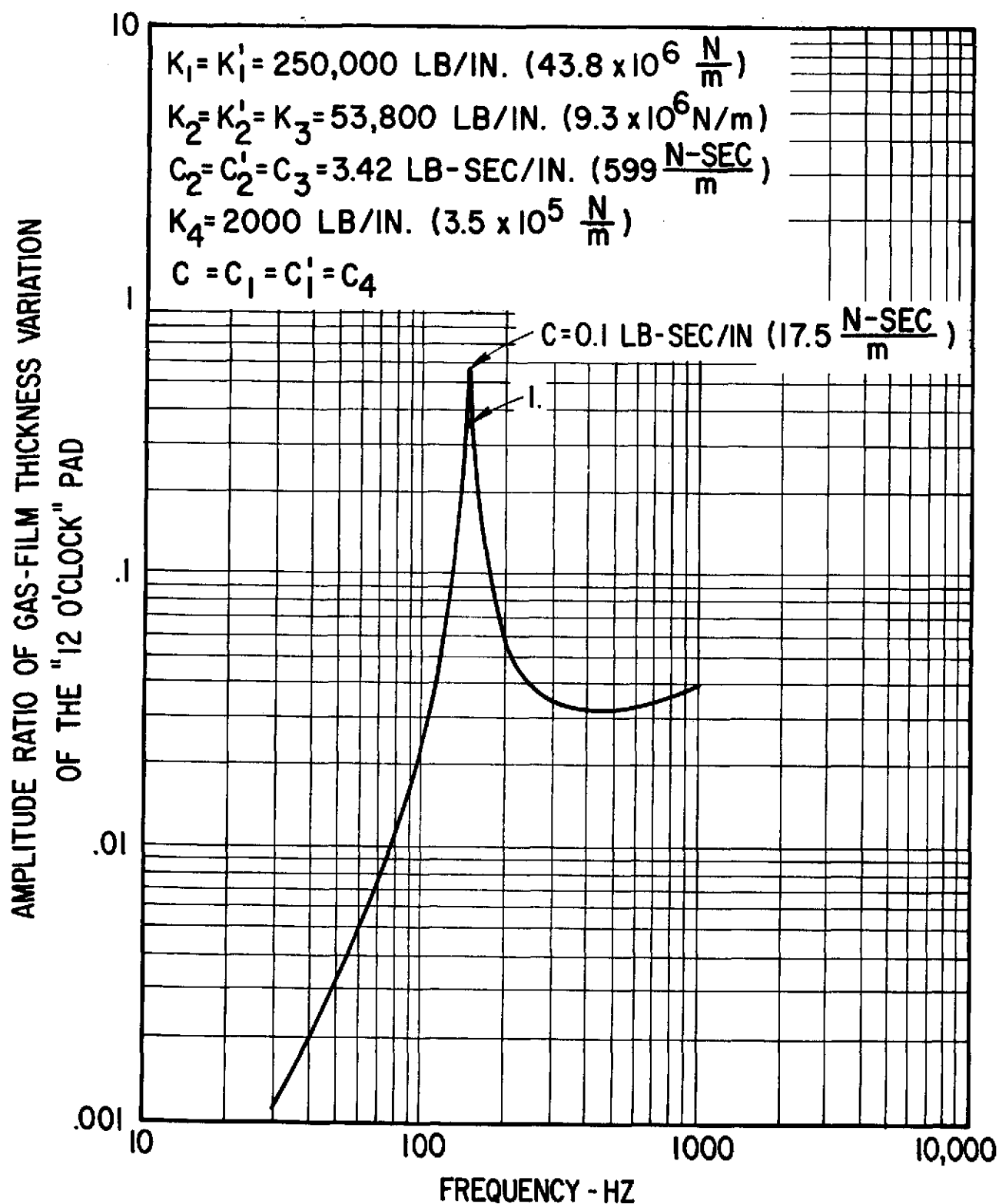
Fig. 2   Amplitude Ratio Of Gas-Film Thickness Variation Of The
"12 O'Clock" Pad With Sinusoidal Vibration Input In
The "12 O'Clock" Direction

The graph shows:

AMPLITUDE RATIO OF GAS-FILM THICKNESS VARIATION OF THE "8 0'CLOCK" PAD (vertical axis)

FREQUENCY - HZ (horizontal axis)

$K_1 = K_1' = 250,000$ LB/IN. $(43.8 \times 10^6 \frac{N}{m})$

$K_2 = K_2' = K_3 = 53,800$ LB/IN. $(9.3 \times 10^6 N/m)$

$C_2 = C_2' = C_3 = 3.42$ LB-SEC/IN. $(599 \frac{N-SEC}{m})$

$K_4 = 2000$ LB/IN. $(3.5 \times 10^5 \frac{N}{m})$

$C = C_1 = C_1' = C_4$

$C = 0.1$ LB-SEC/IN $(17.5 \frac{N-SEC}{m})$

1.
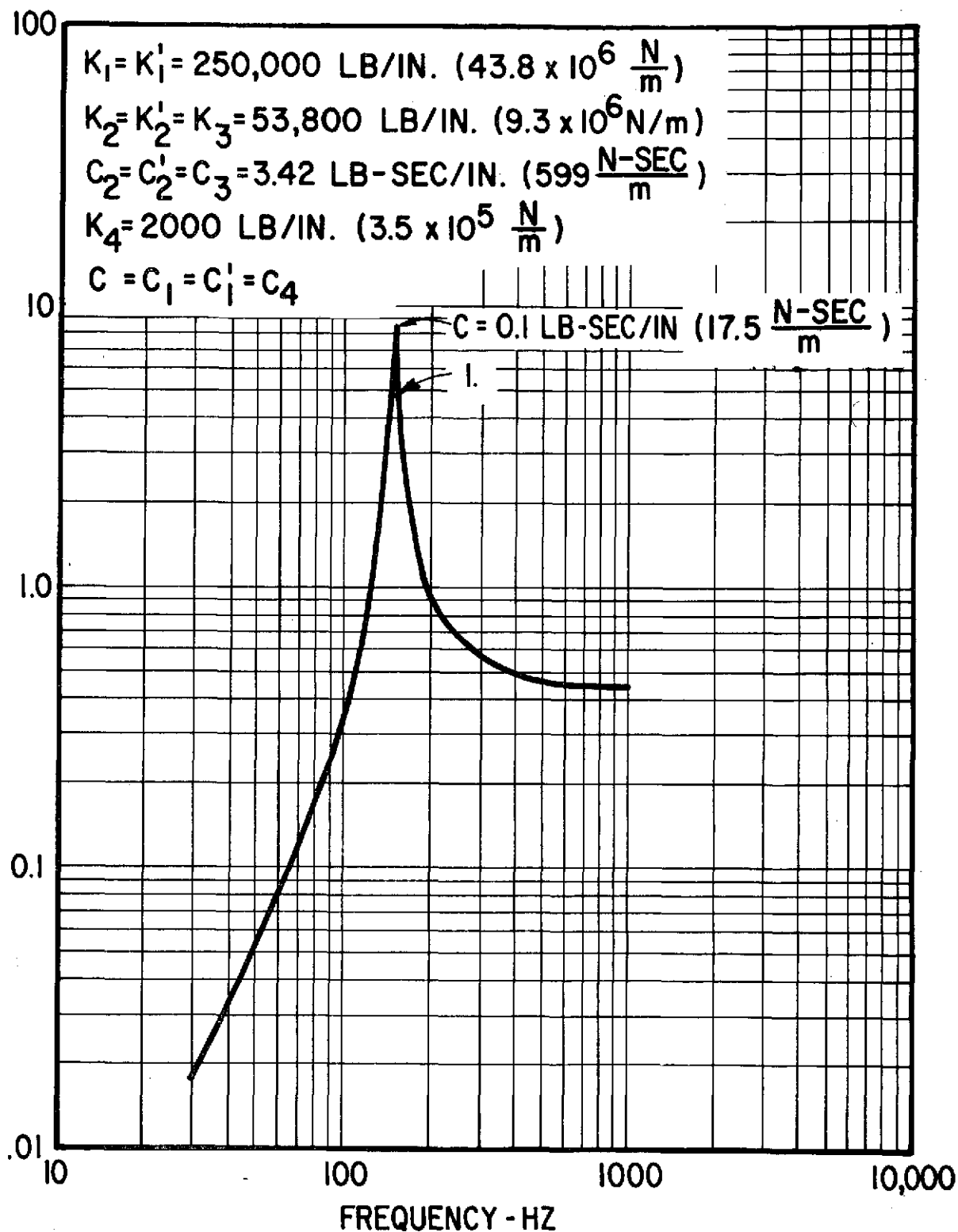
Fig. 3   Amplitude Ratio Of Gas-Film Thickness Variation Of The
          "8 O'Clock" Pad With Sinusoidal Vibration Input In The
          "12 O'Clock" Direction

MTI-16194
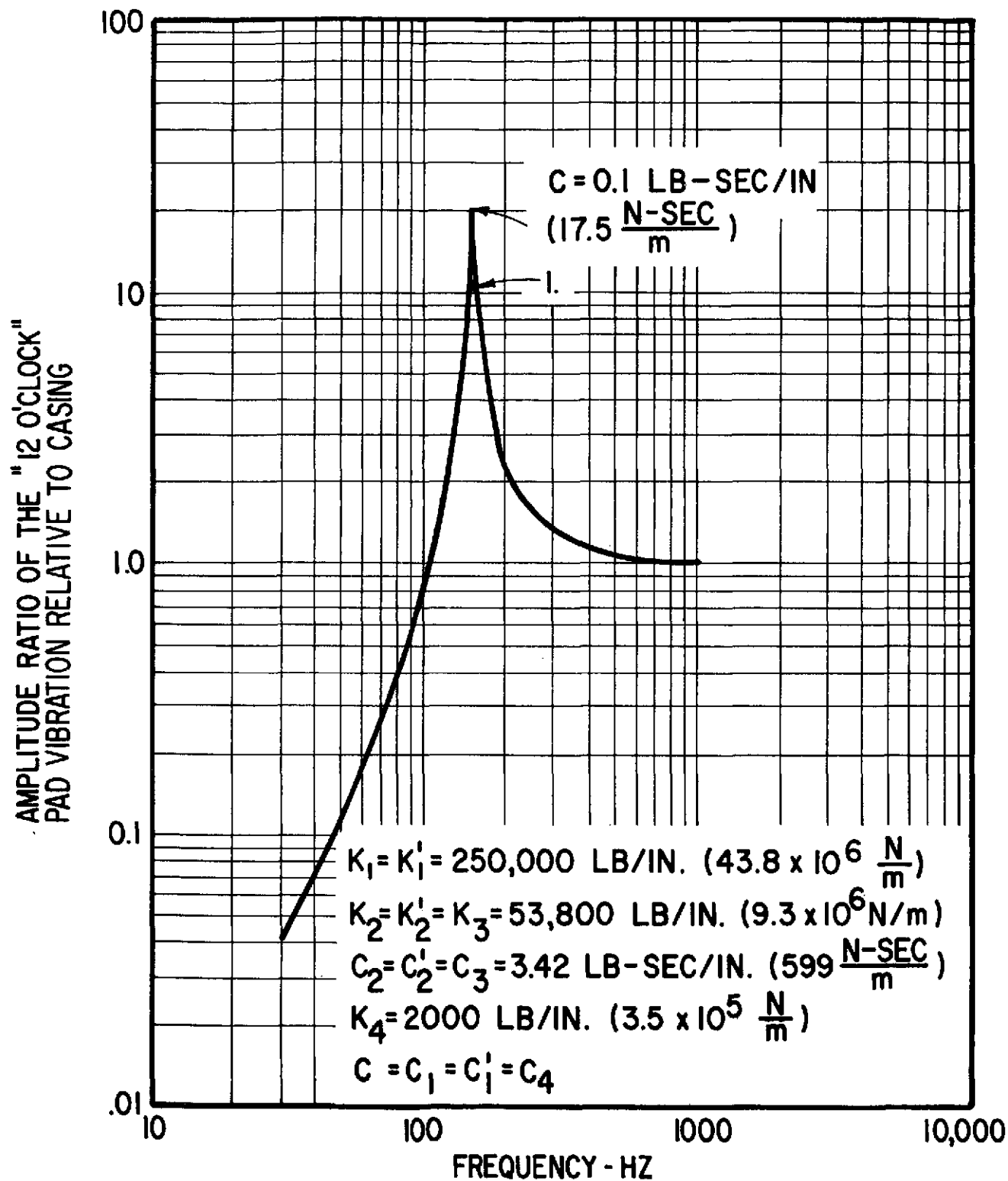
Fig. 4   Amplitude Ratio Of The "12 O'Clock" Pad Vibration With
Sinusoidal Vibration Input In The "12 O'Clock"
Direction
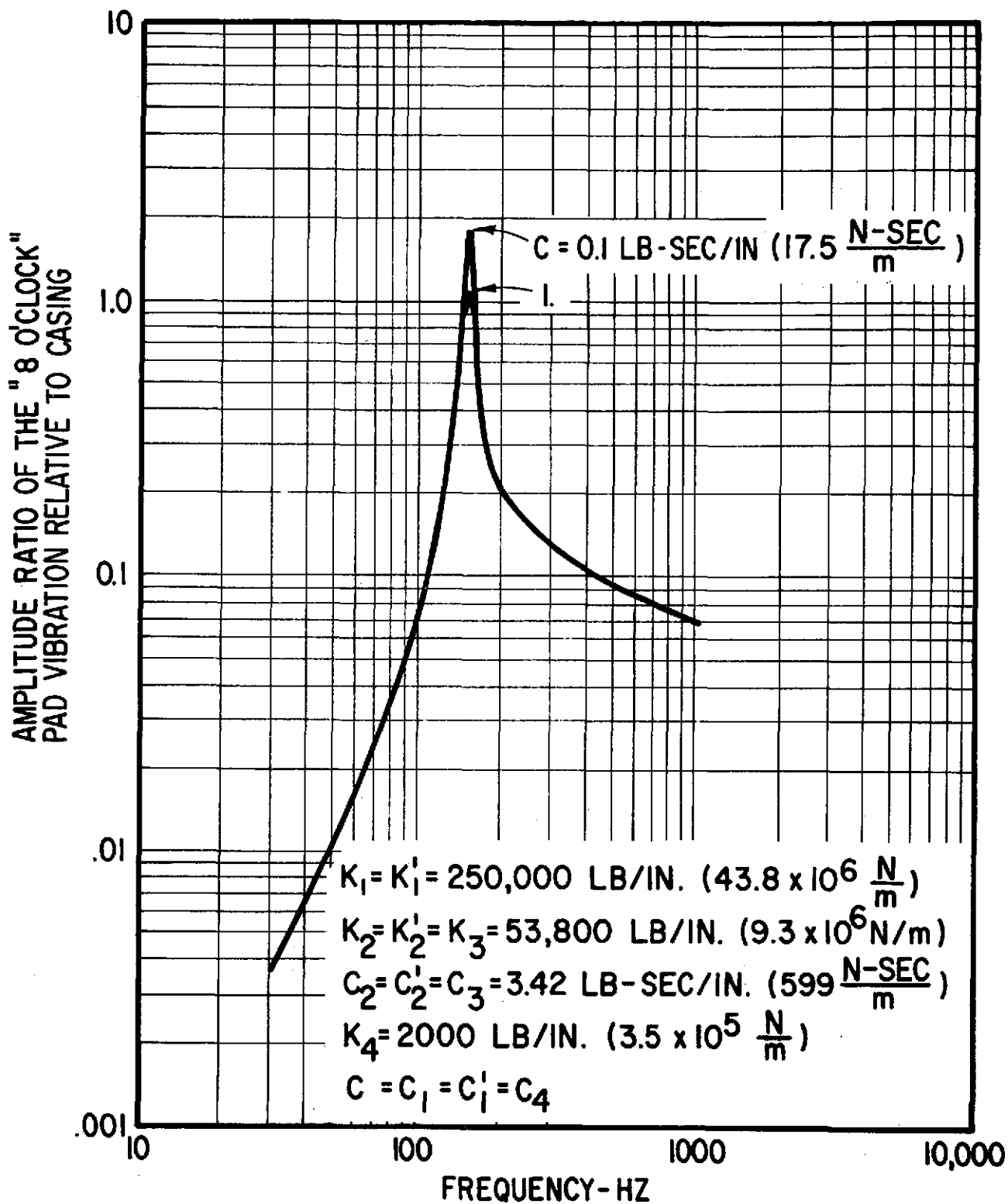
Fig. 5   Amplitude Ratio Of The "8 O'Clock" Pad Vibration With
Sinusoidal Vibration Input In The "12 O'Clock"
Direction

MTI-16191
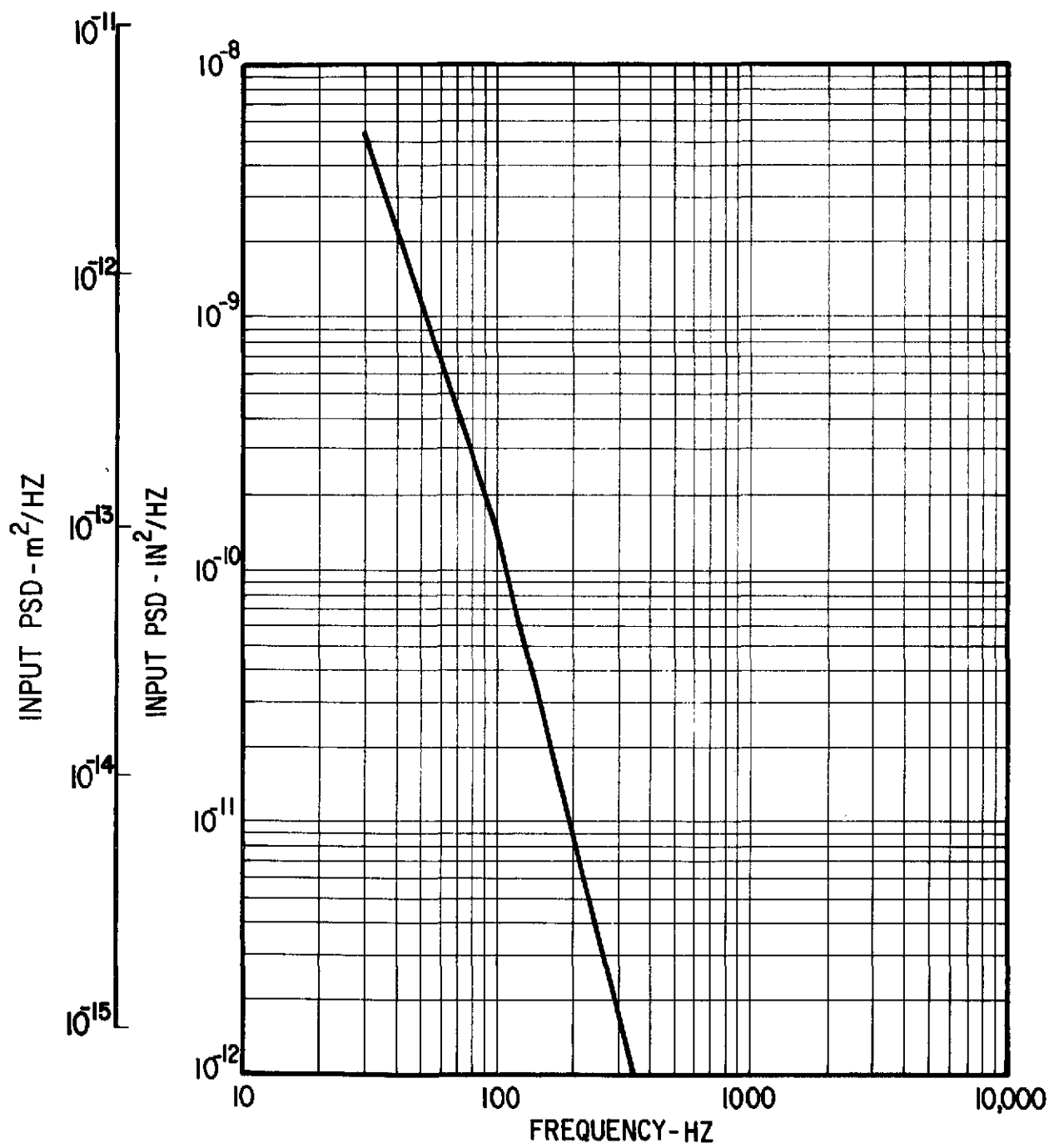
Fig. 6   Input Displacement Power Spectral Density
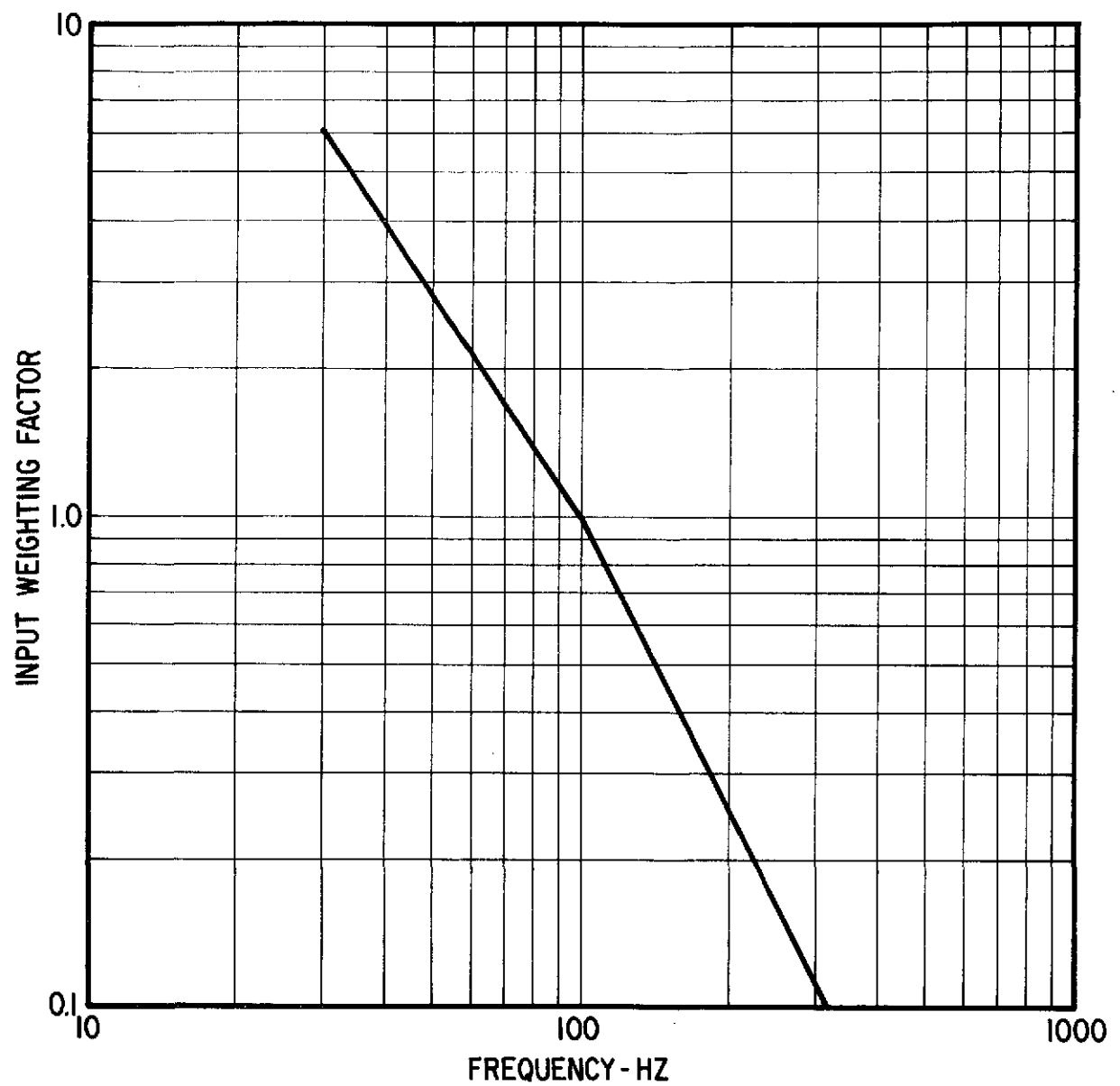
Fig. 7   Input Weighting Factor With Respect To Displacement Input At 100 Hz
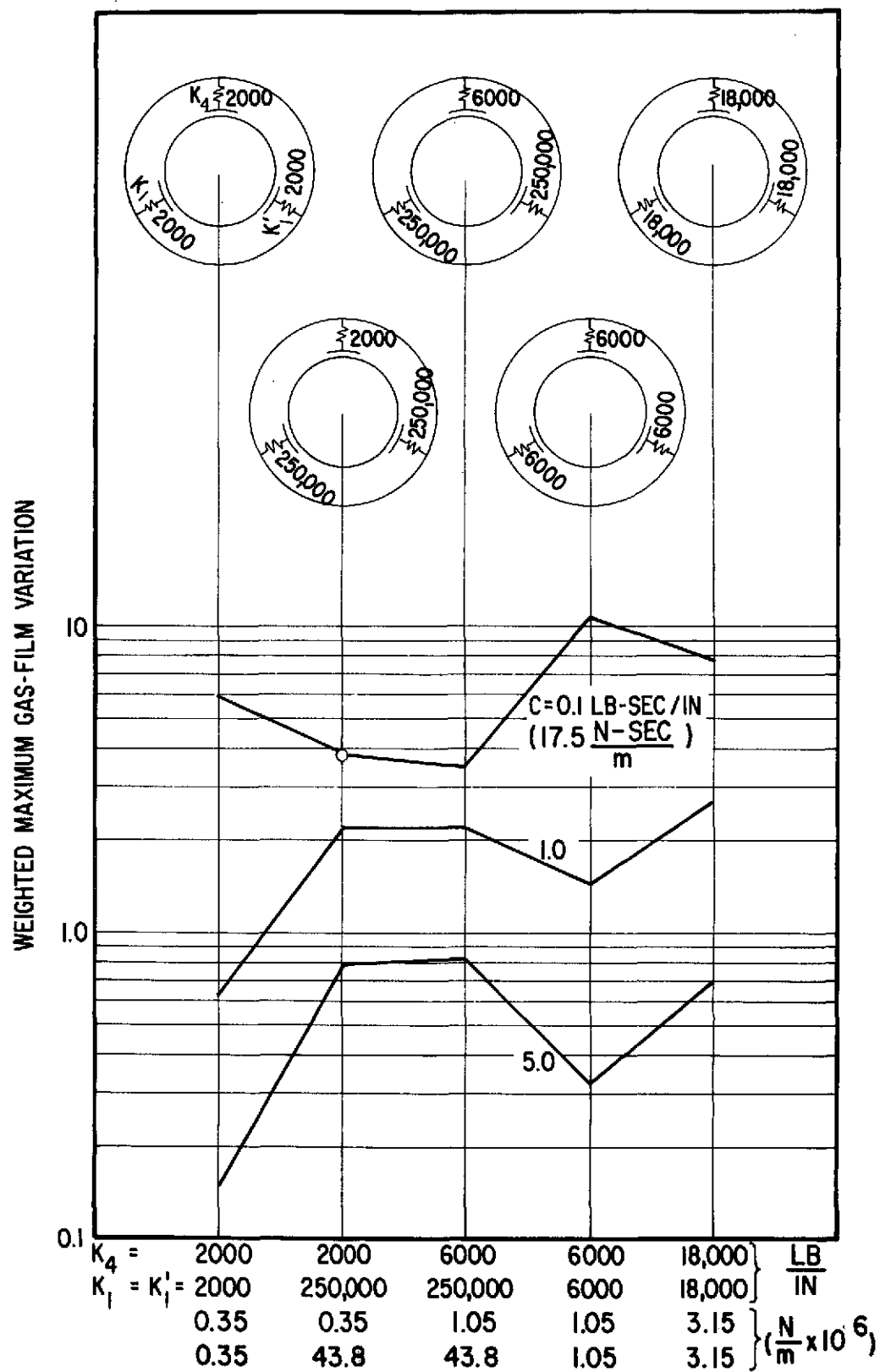
Fig. 8   Weighted Maximum Gas-Film Variation For Various Flexure Stiffness
Combinations
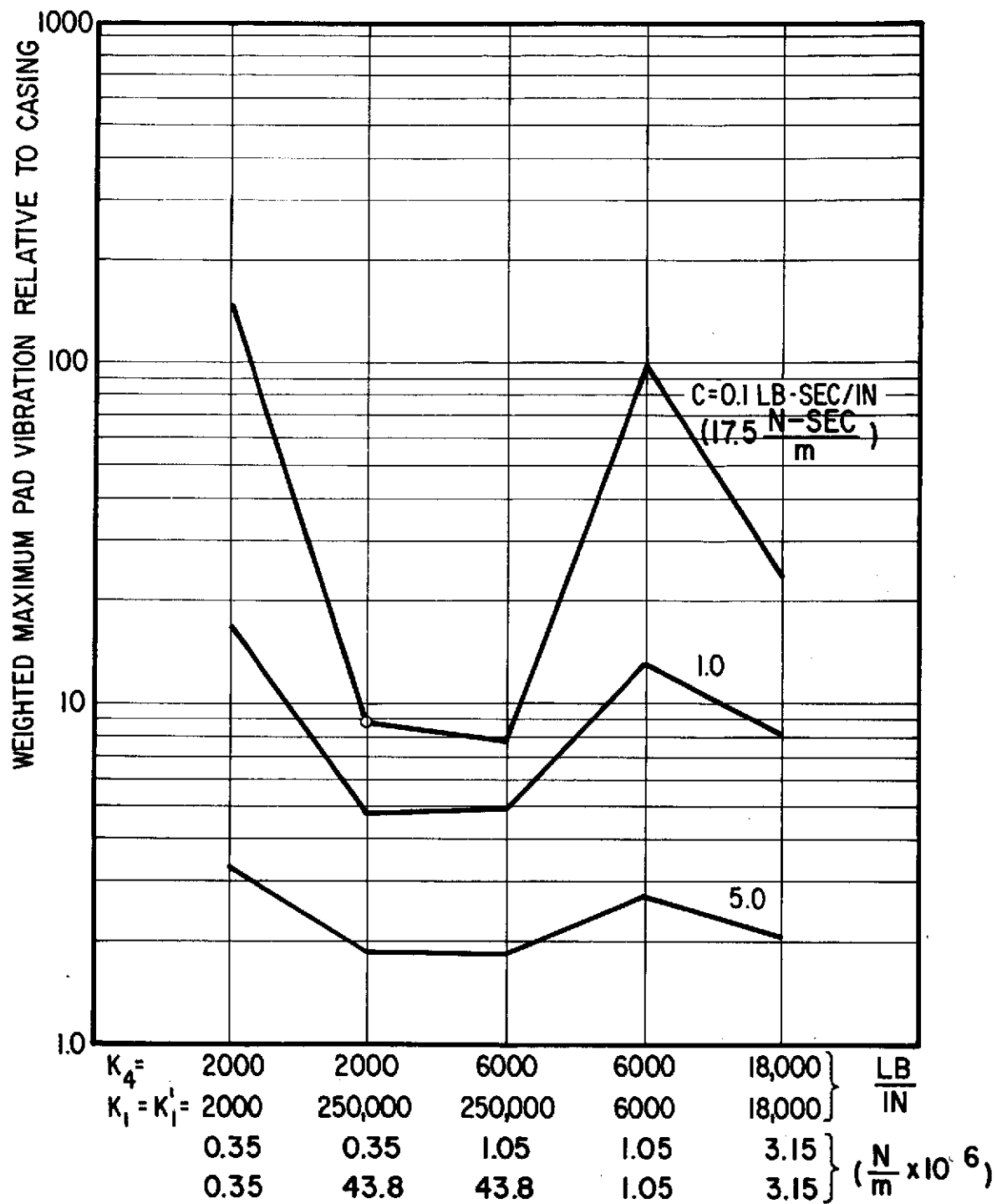
Fig. 9   Weighted Maximum Pad Vibration Relative To Casing For Various
Flexure Stiffness Combinations

CAVITY

RECTANGULAR PISTON

FLEXURE ASSEMBLY

FLEXIBLE ELEMENT

SIDE 1

SIDE 2
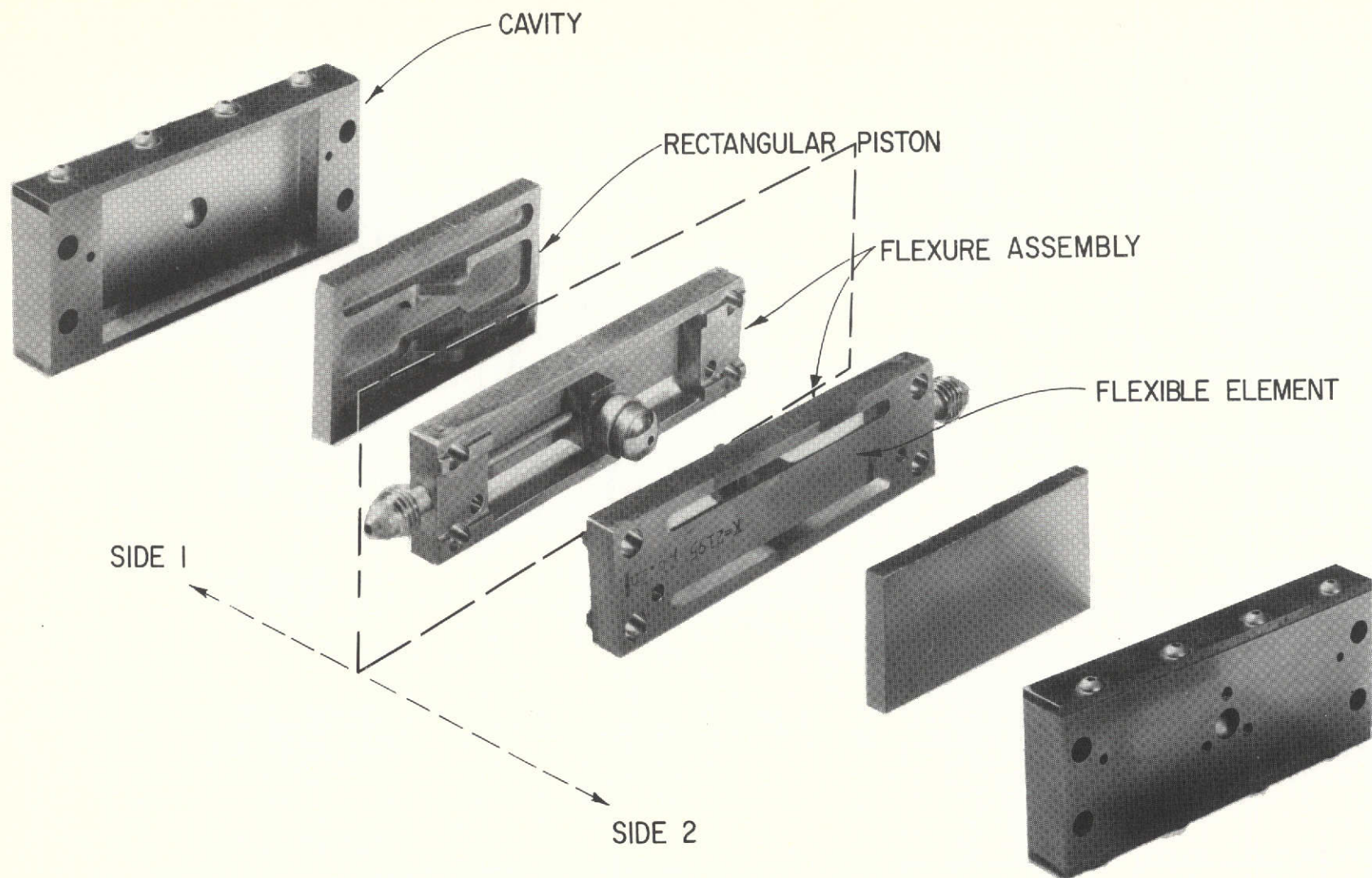
Fig. 10   BRU Journal Bearing Flexure Assembly And Damper Elements

3.25"
(83mm)

A

A

2.25"
(57 mm)

SECTION C-C

1.22"
(31 mm)

C

0.011"
(0.28 mm)

.0011" CLEARANCE ON
FOUR SIDES
(0.028 mm)

C

SECTION A-A
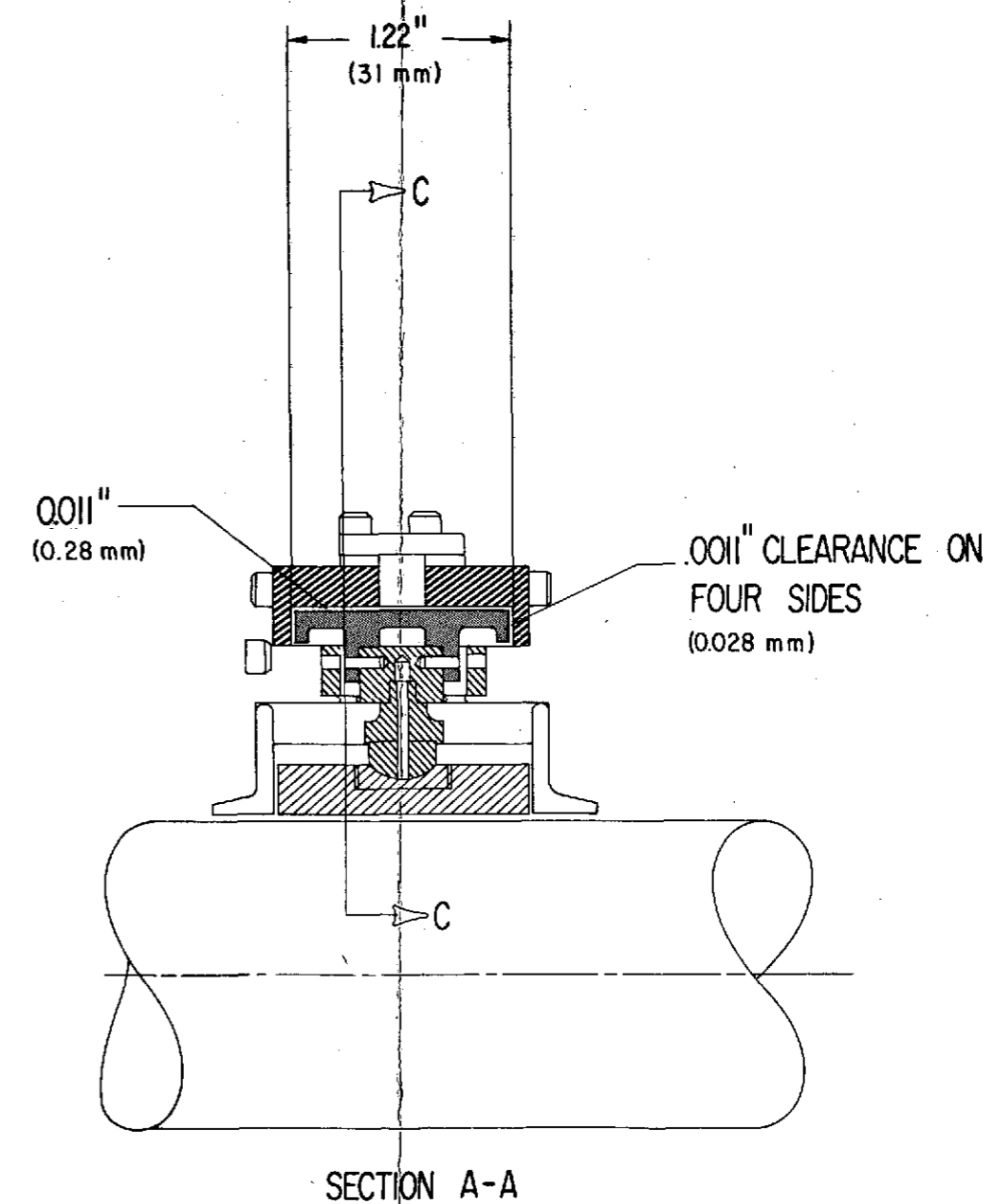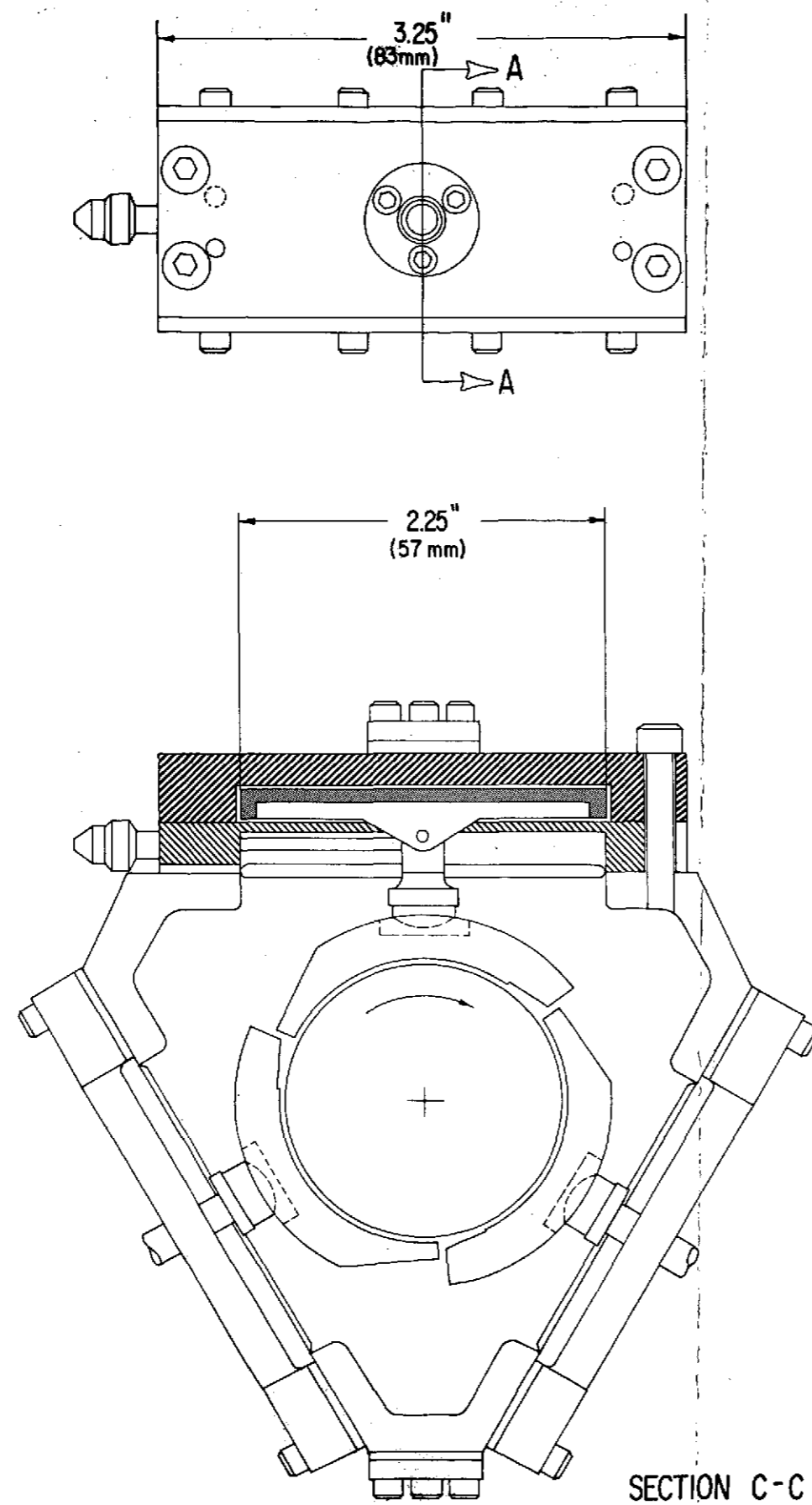
Fig. 11   BRU Journal Bearing Flexure Damper
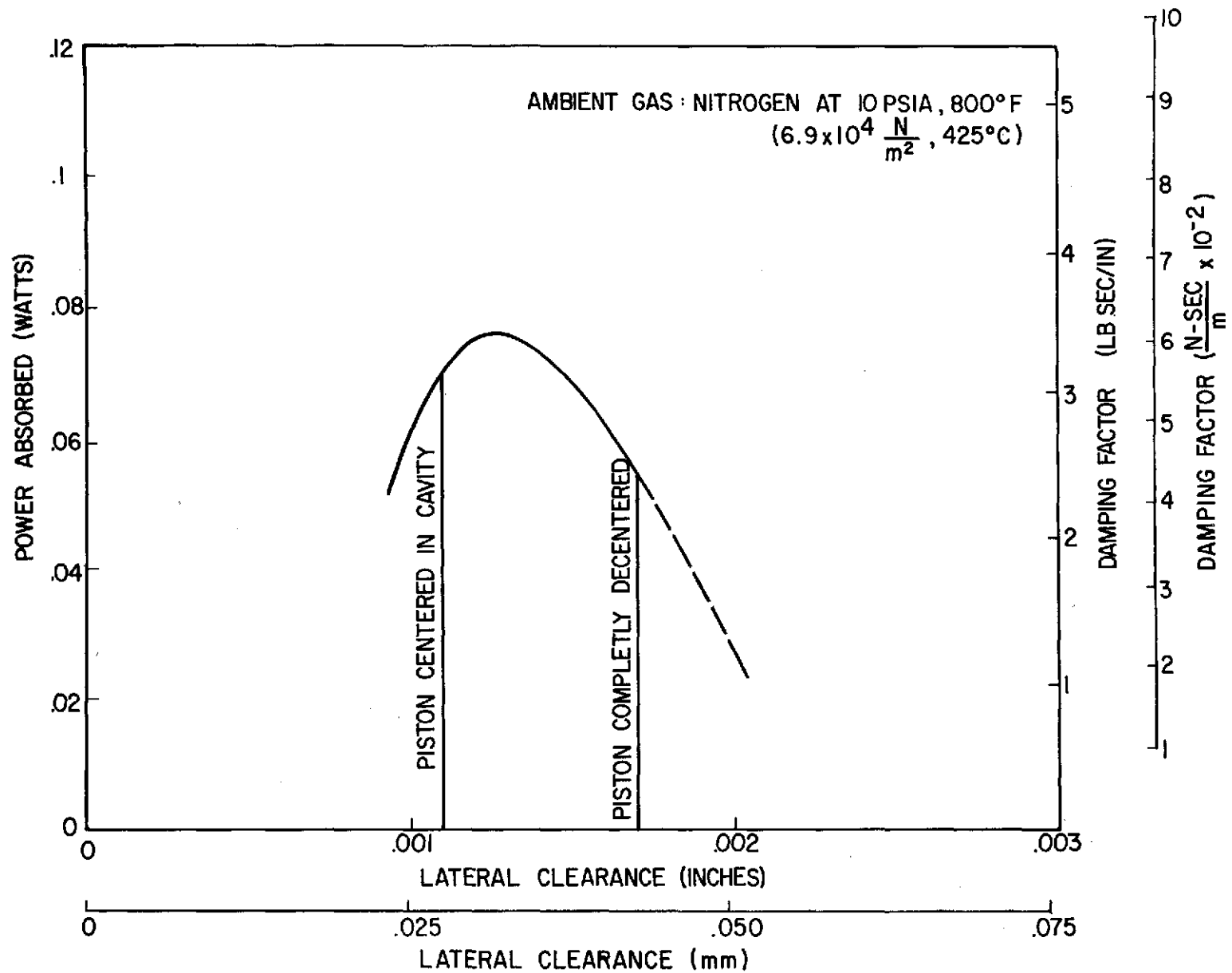
Fig. 12   Predicted Performance Curve For Optimized BRU Damper Assembly At 100 Hz And 0.001 Inch (0.025 mm) Amplitude

Fig. 13(a)

Relative Piston Damper
Amplitude At 0.018 Inch
(0.46 mm) Top Dead
Center Clearance
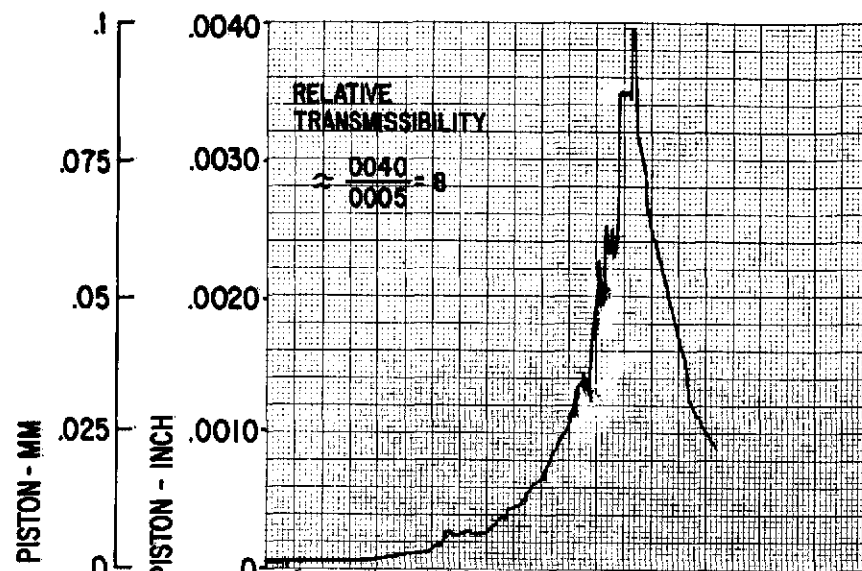
Fig. 13(b)

Relative Piston Damper
Amplitude At 0.011 Inch
(0.28 mm) Top Dead
Center Clearance
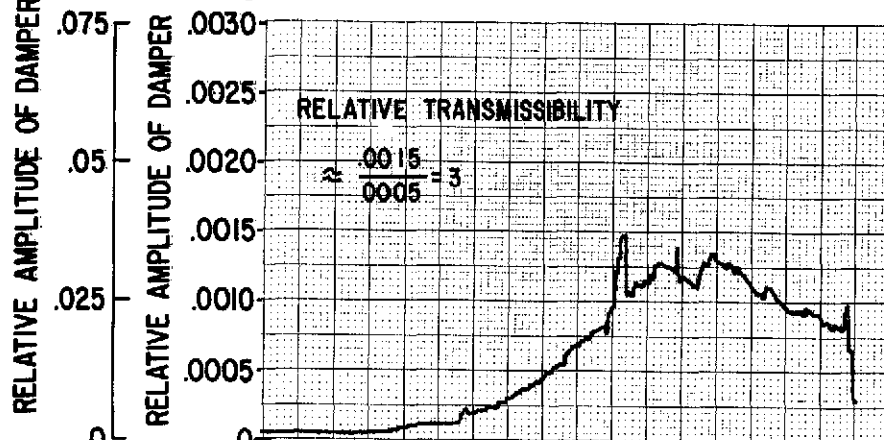
Fig. 13(c)

Relative Piston Damper
Amplitude At 0.011 Inch
(0.28 mm) Top Dead
Center Clearance And
Additional 0.004 Inch
x 0.775 Inch Air Gap
(0.1 x 19.7 mm)
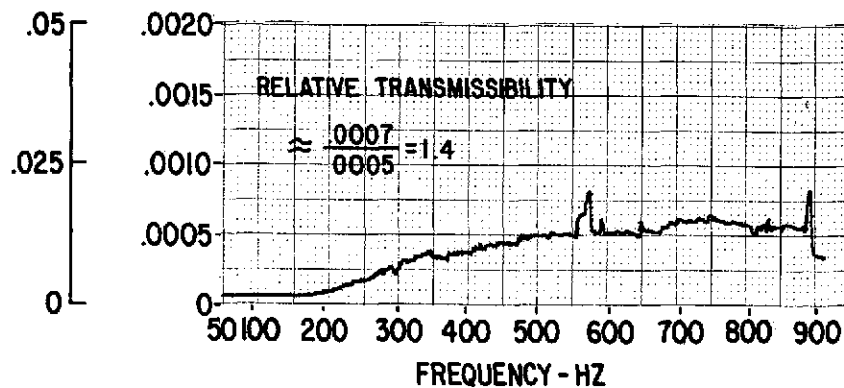
Fig. 13   BRU Journal Bearing Flexure Assembly Vibration Attenuation
Test Results (Component Test)

MTI-13787

COMPRESSOR END

COLD GAS
TURBINE

THRUST RUNNER

COMPRESSOR END
JOURNAL BEARING ASSY

COMPRESSOR JOURNAL
BEARING PIVOT FILM
THICKNESS PROBES

COMPRESSOR JOURNAL
ORTHOGONAL PROBES
(GROUND-TO-SHAFT)

ROTOR

TURBINE JOURNAL
ORTHOGONAL PROBES
(GROUND-TO-SHAFT)

TURBINE JOURNAL
BEARING PIVOT FILM
THICKNESS PROBES

TURBINE END
JOURNAL BEARING ASSY

THRUST BEARING STATOR
AND GIMBAL ASSEMBLY

THRUST BEARING FILM
THICKNESS PROBES

INSTRUMENTATION
TURRET

GRAVITY

TURBINE END

SOLID
MOUNTED TILTING
PADS

LEADING EDGE
JOURNAL BEARING PROBES

FLEX MOUNTED
TILTING PAD

FLEXURE DAMPER

JOURNAL BEARING ASSEMBLY

Fig. 14   Schematic Of BRU Simulator

MTI-16187

COMPRESSOR END UP

TURBINE END DOWN
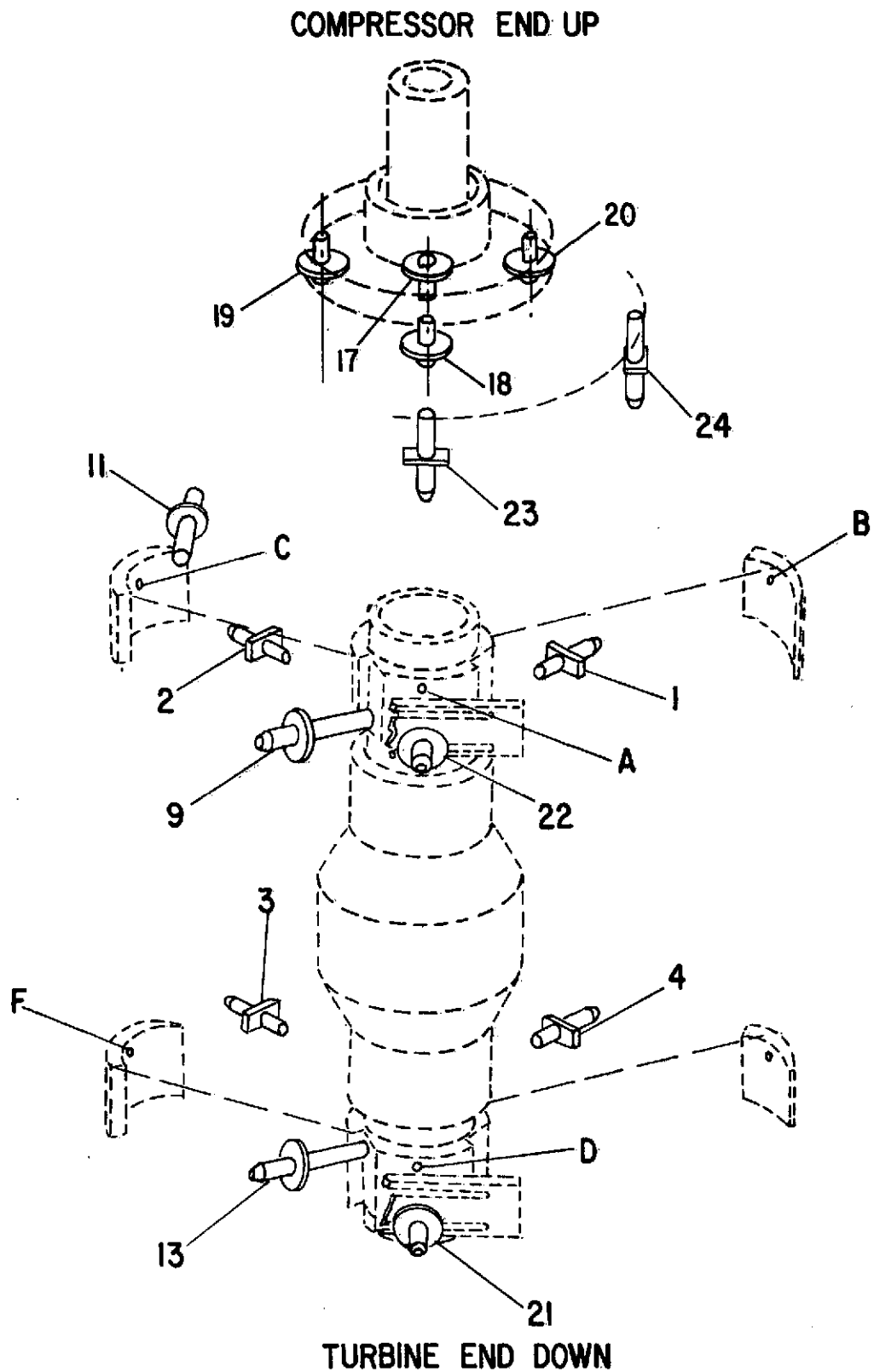
Fig. 15   Proximity Probe Locations On BRU Simulator Rotor And Bearings

Probe Identification	Proximity Probe Designation
PROXIMITY PROBE DESIGNATION ON BRU SIMULATOR	
A	Pivot film thickness probe, flex-mounted pad, compressor end
B	Pivot film thickness probe, solid-mounted pad, compressor end
C	Pivot film thickness probe, solid-mounted pad, compressor end
D	Pivot film thickness probe, flex-mounted pad, turbine end
E	Pivot film thickness probe, solid-mounted pad, turbine end
F	Pivot film thickness probe, solid-mounted pad, turbine end
1	Compressor journal orthogonal probe
2	Compressor journal orthogonal probe
3	Turbine journal orthogonal probe
4	Turbine journal orthogonal probe
9	Flex-mounted pad leading edge probe, compressor end
11	Solid-mounted pad leading edge probe, compressor end
13	Flex-mounted pad leading edge probe, turbine end
17	Compressor thrust plate film thickness probe
19	Turbine thrust plate film thickness probe
20	Turbine thrust plate film thickness probe
21	Turbine journal flex-mounted pad load probe
22	Compressor journal flex-mounted pad load probe
23	Thrust bearing gimbal probe to ground
24	Thrust bearing gimbal probe to ground

Fig. 16   Capacitance Probes Used On BRU Simulator For Vibration Testing
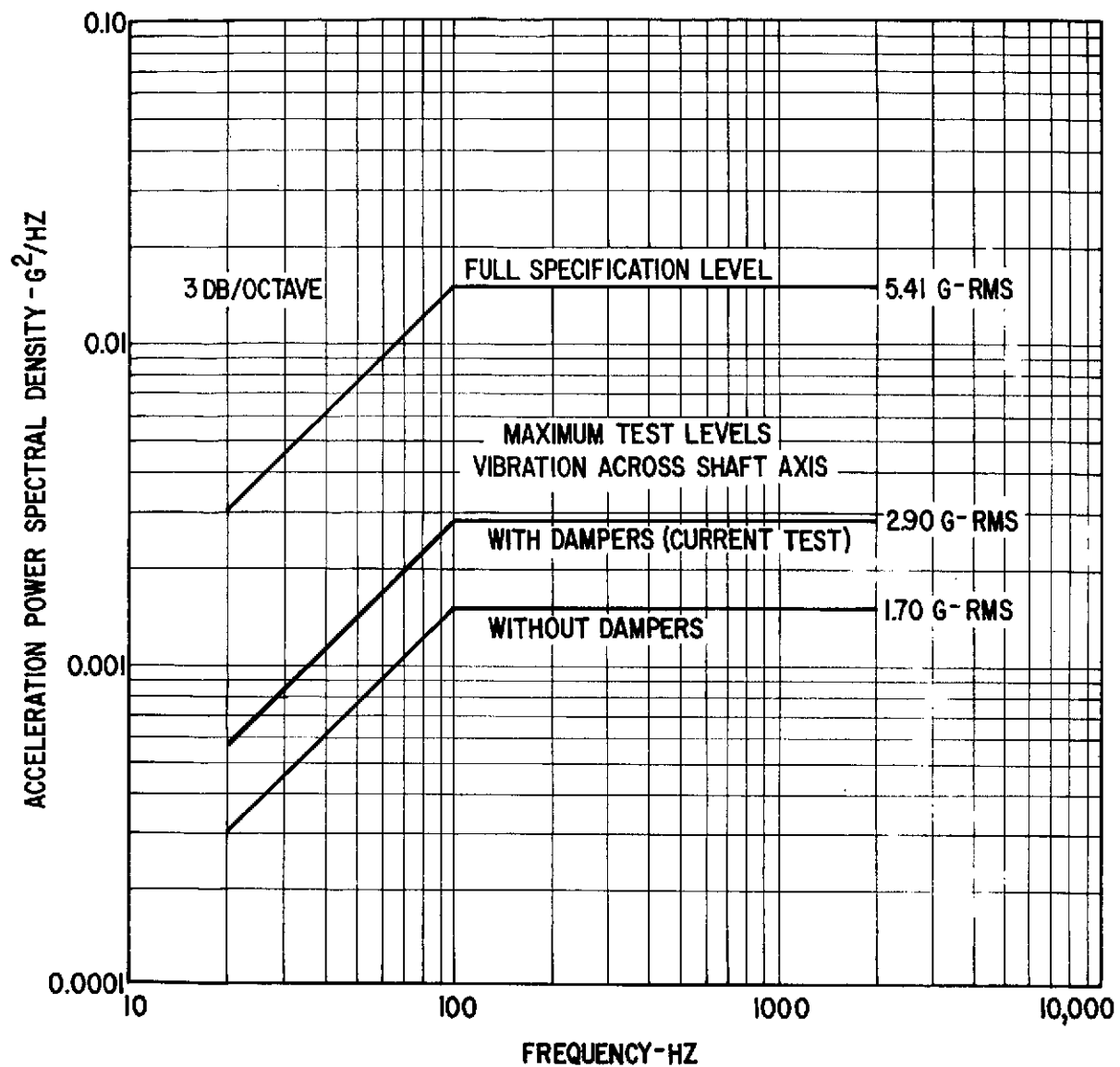
Fig. 17   Random Vibration Power Spectral Density Test Specification
           417-2 (Rev. C) For Electrical Generating System Components
           (Operating) And Simulator Test Levels
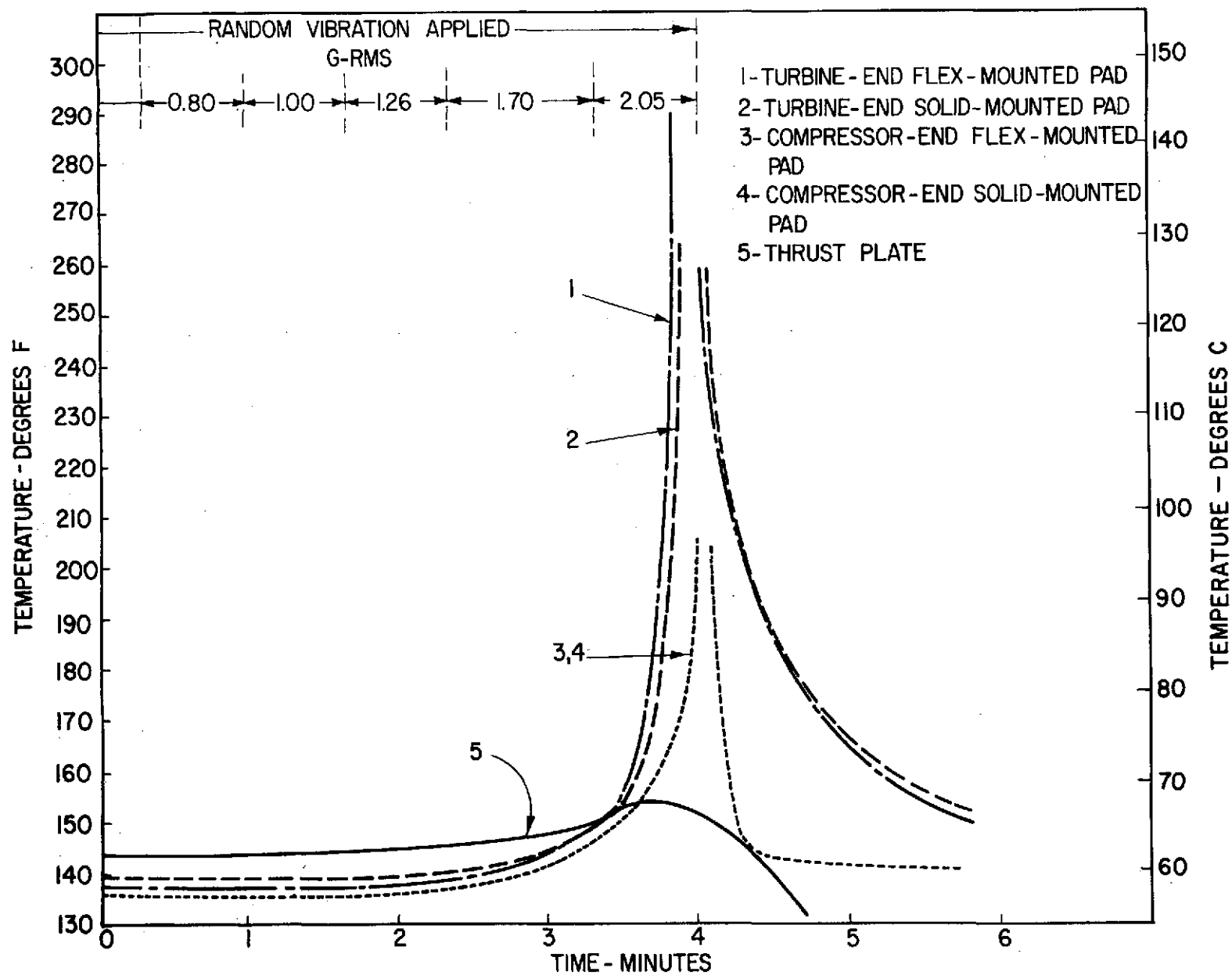
Fig. 18   Measured Temperature In BRU Simulator Components With Transverse Random
Excitation And Fully-Hydrodynamic Journal Bearing Operation
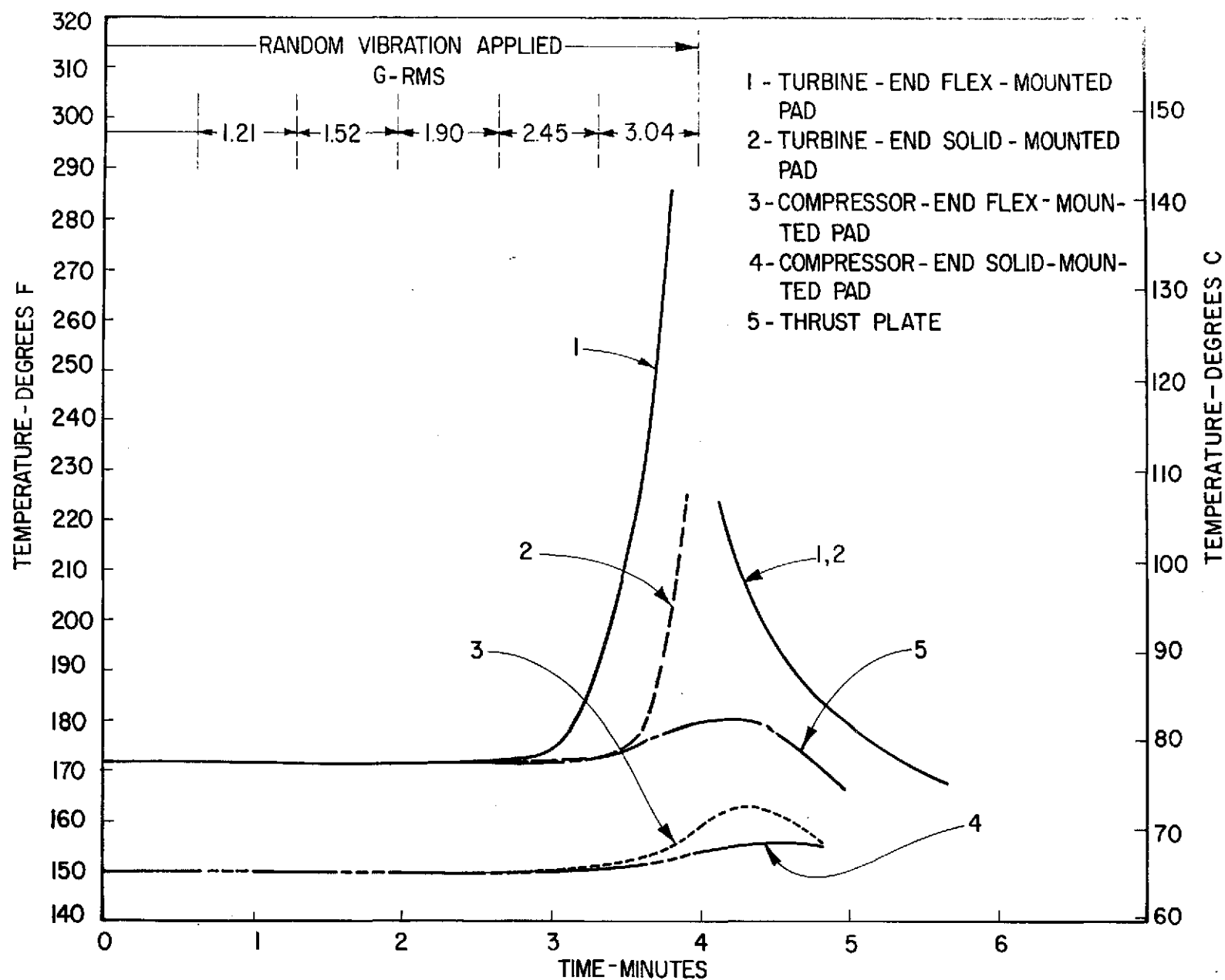
Fig. 19   Measured Temperature In BRU Simulator Components With Transverse Random
Excitation And Hydrostatic Operation Of The Compressor-End Journal
Bearing
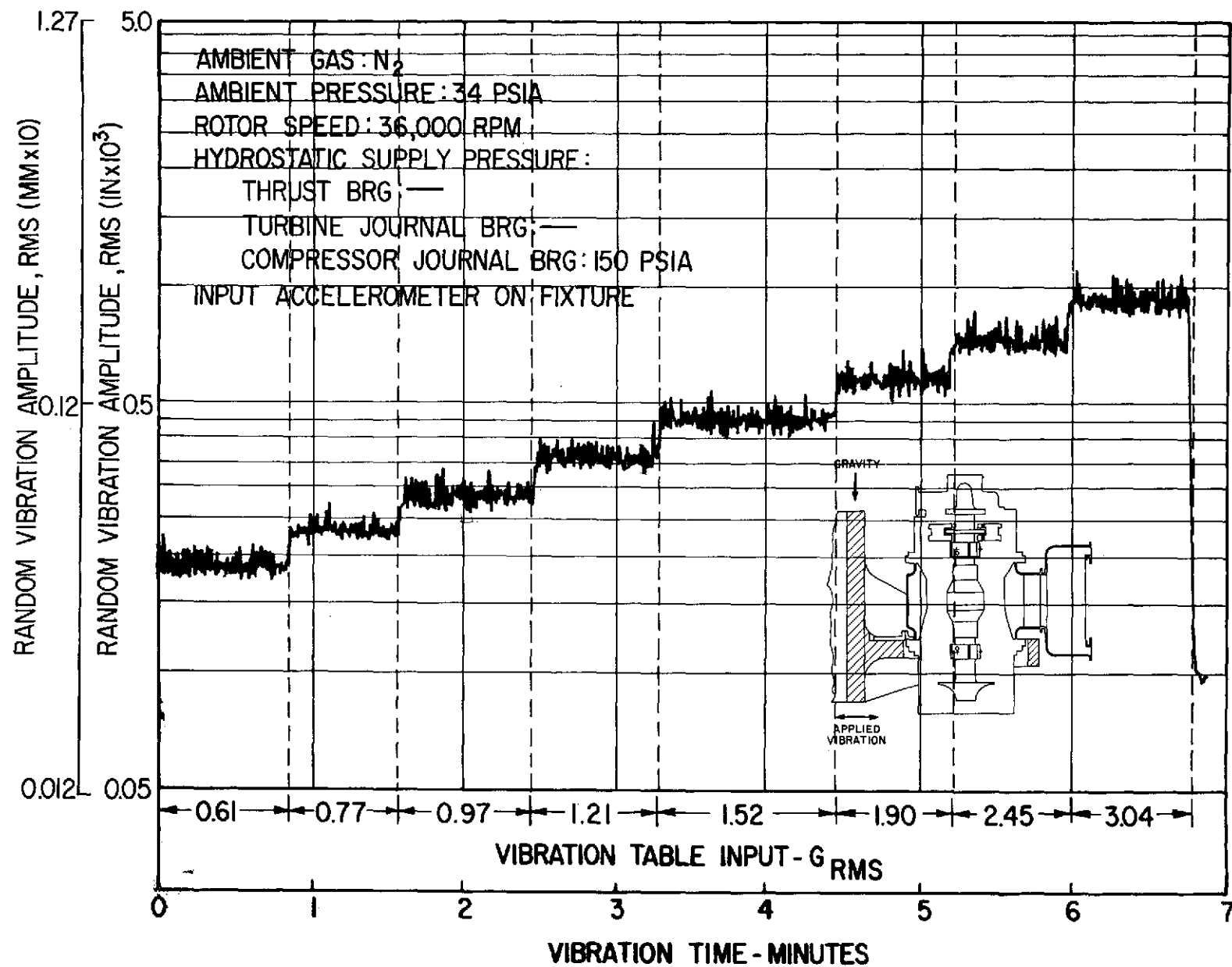
Fig. 20   Random Vibration Input Accelerations (Shaped Spectrum) According To NASA
Spec 417-2-C-3.5
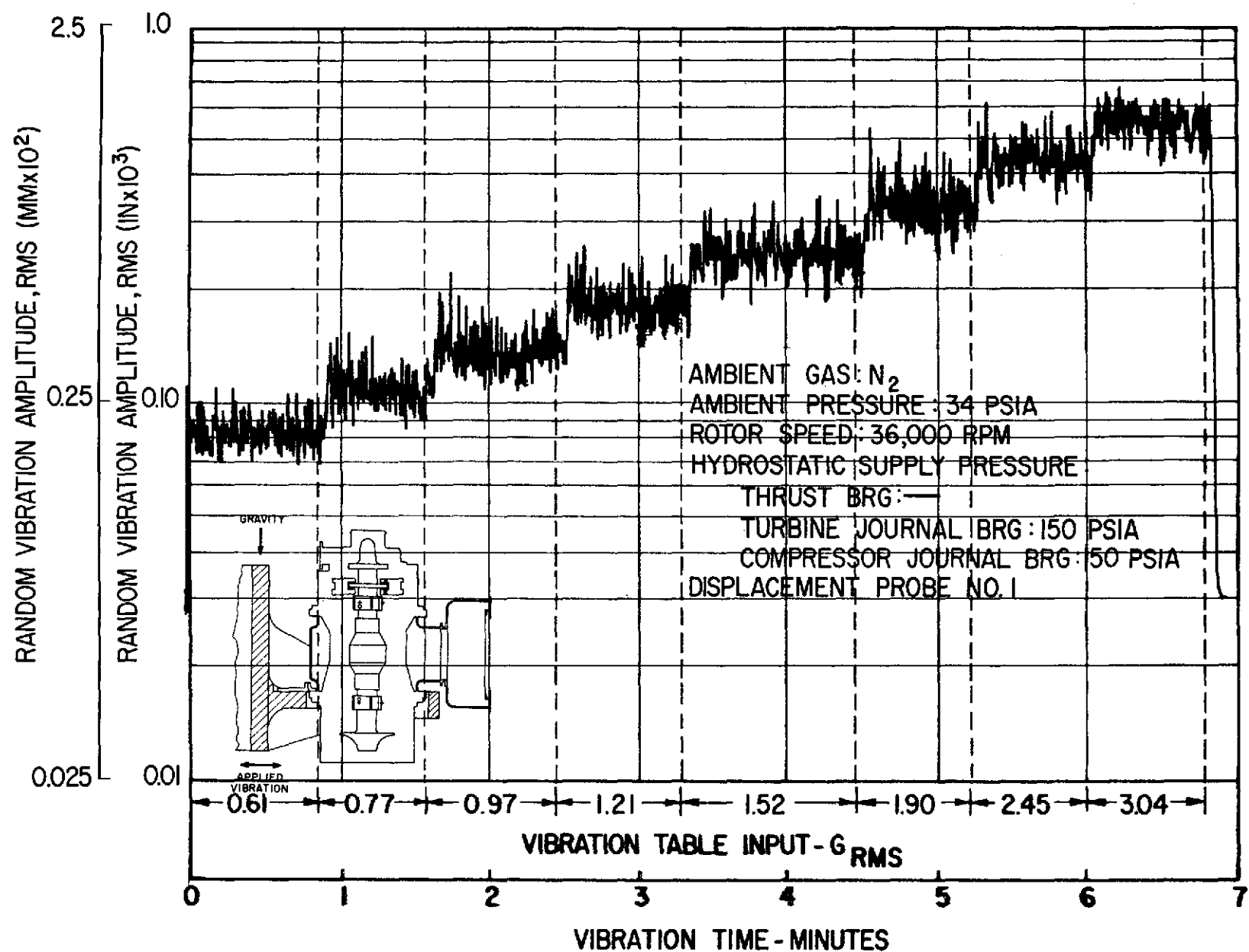
Fig. 21   Compressor Journal Rotor Amplitudes (Casing-To-Shaft, With Journal Bearing
Flexure Dampers) Under Shaped Random Vibrations According To NASA Spec
417-2-C-3.5
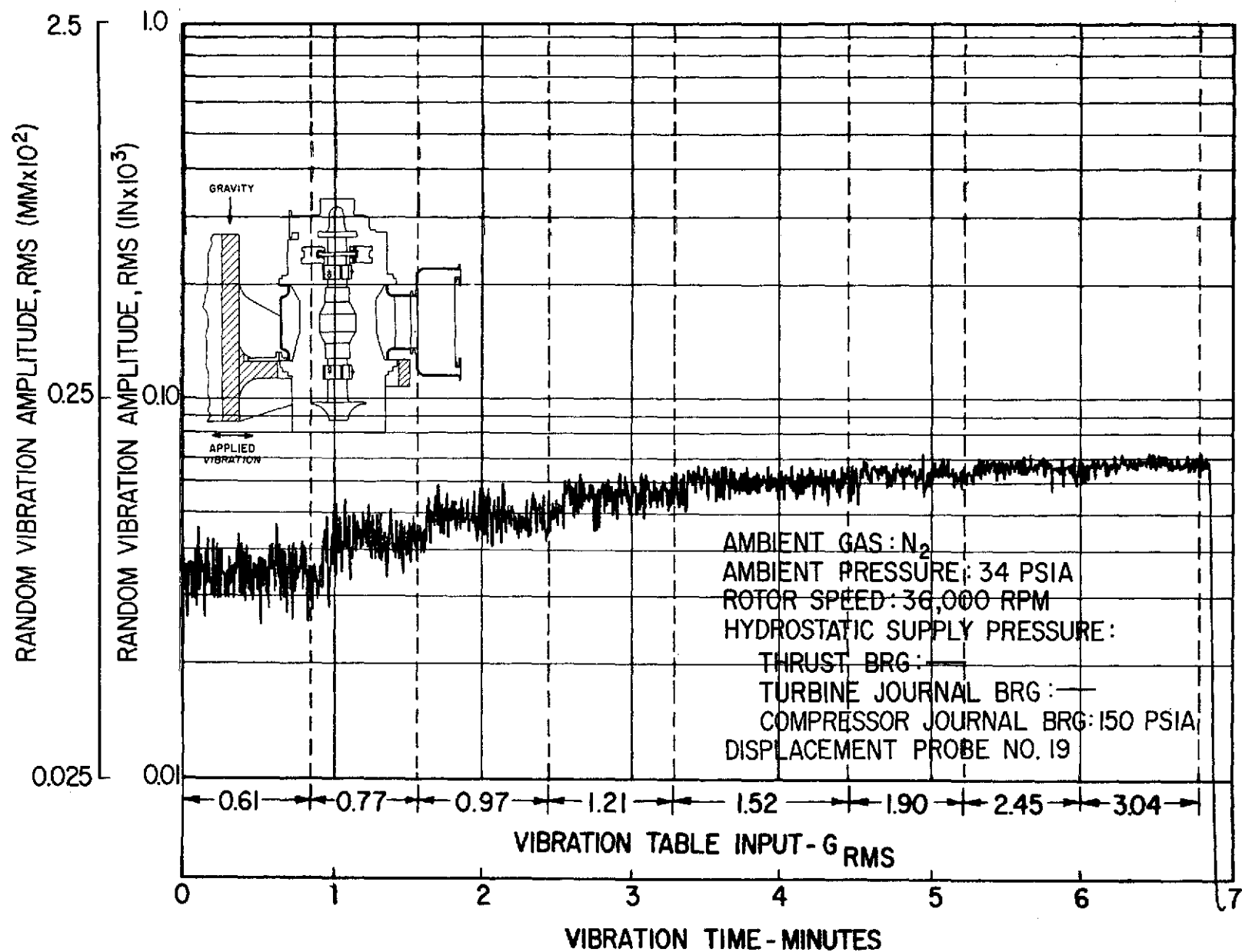
Fig. 22   Thrust Bearing Film Thickness Variation Under Externally-Imposed Shaped
Random Vibrations According To NASA Spec 417-2-C-3.5 (Journal Bearing
Equipped With Flexure Dampers)
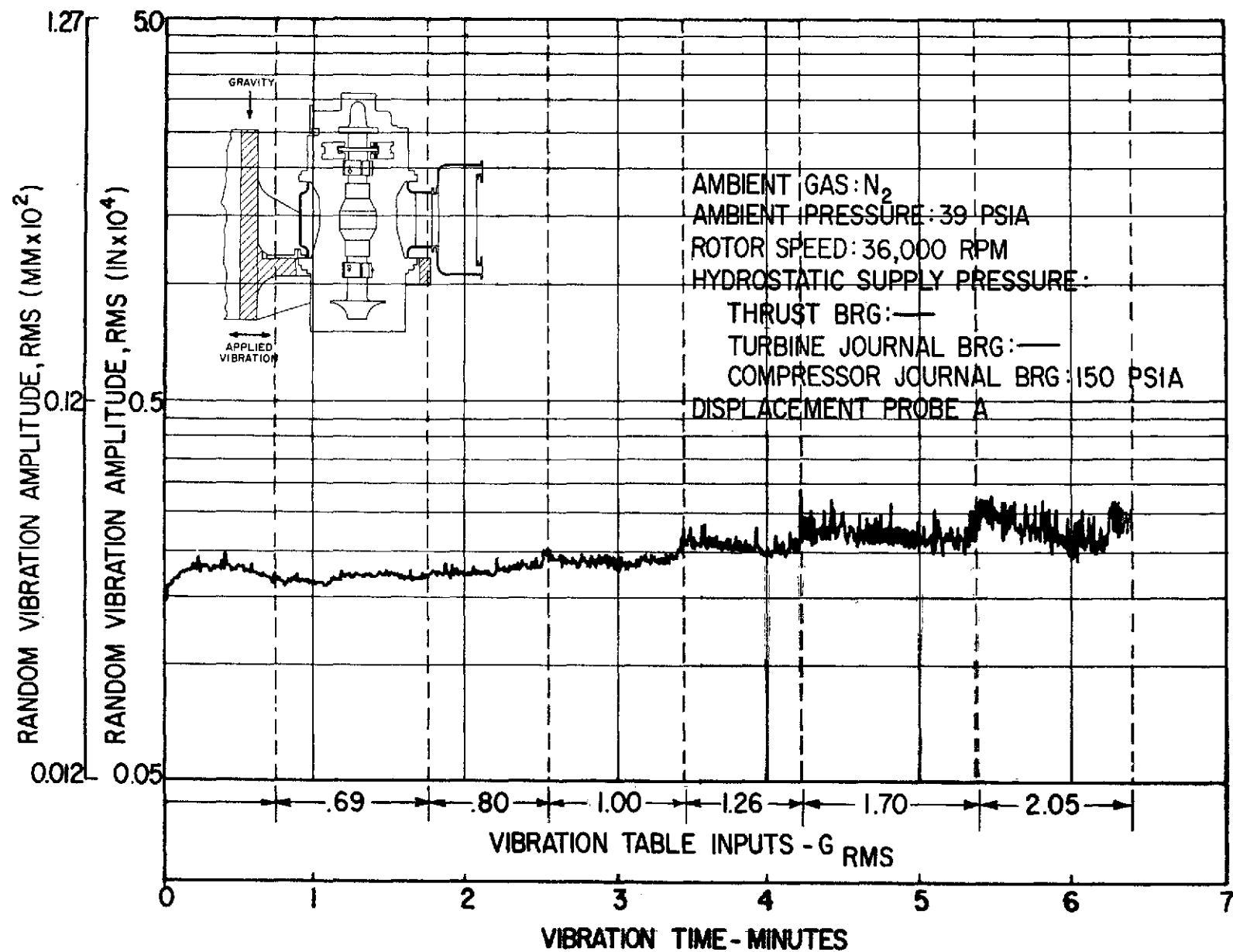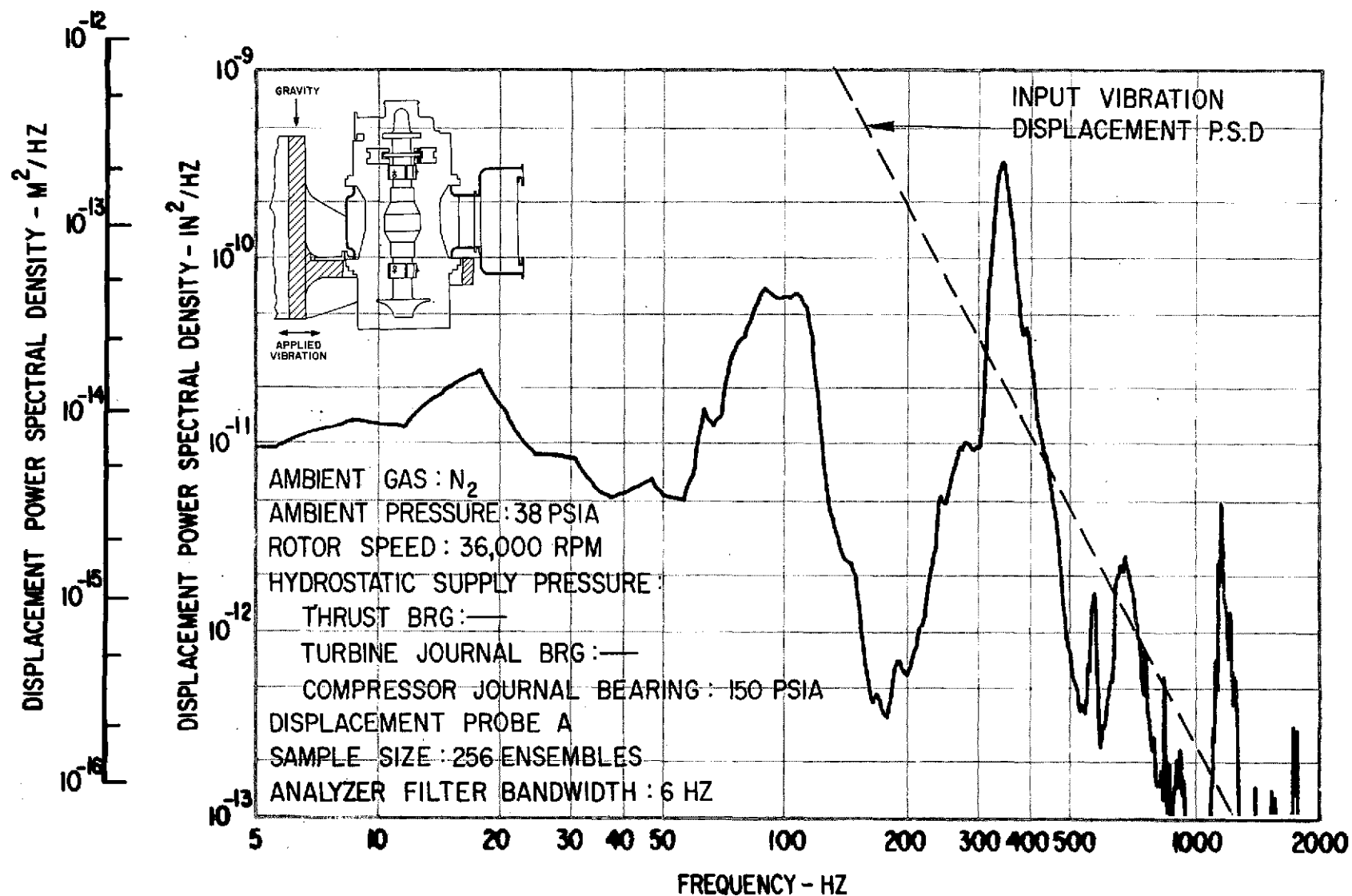
Fig. 23   Pad-To-Shaft Pivot Film Thickness Variation For Flex-Mounted Compressor
Journal Bearing Pad (With Journal Bearing Flexure Dampers) Under
Externally-Imposed Shaped Random Vibrations According To NASA S
Spec 417-2-C-3.5
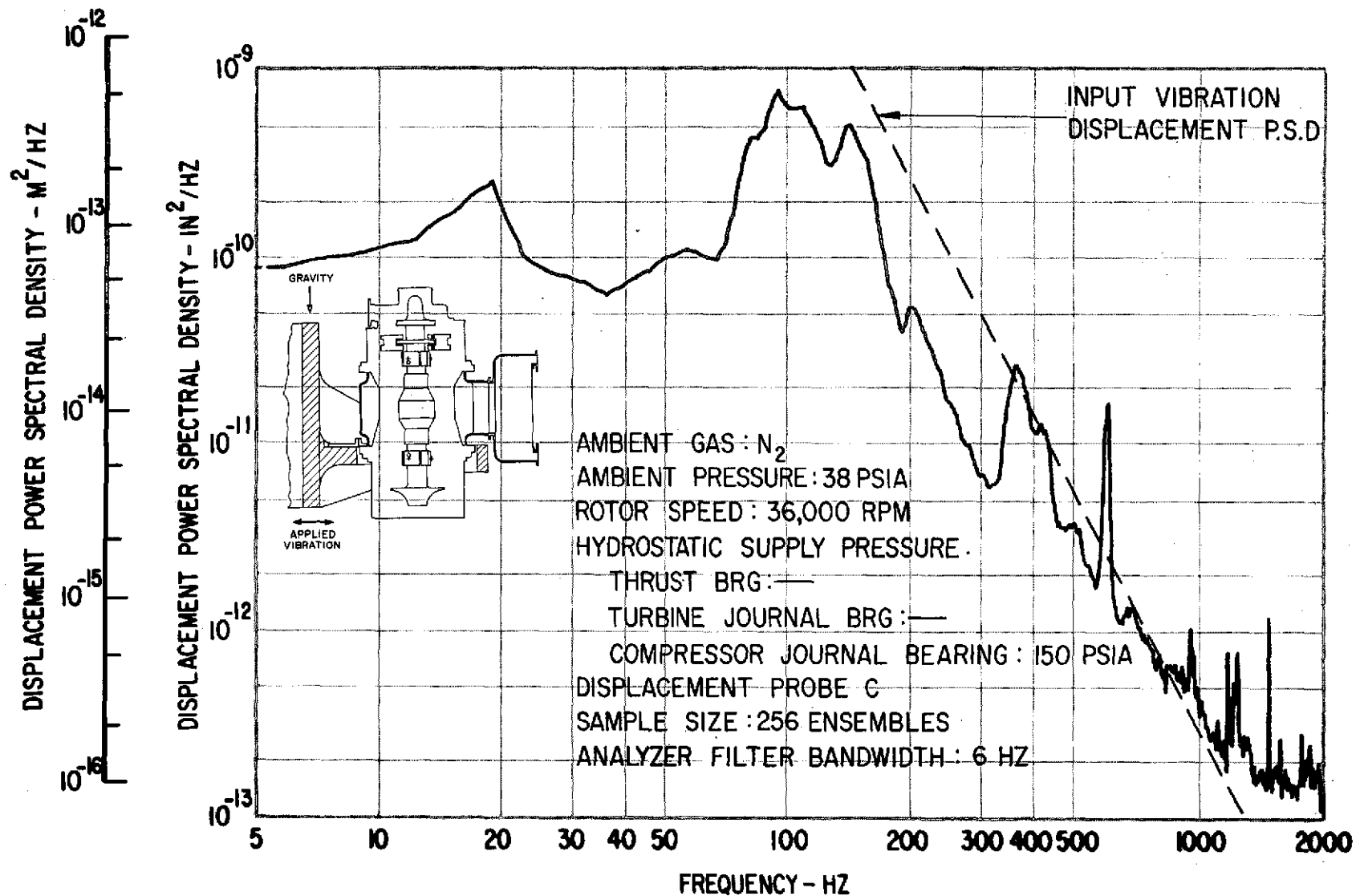
Fig. 24   Frequency Distribution Of Pad-To-Shaft Pivot Film Thickness Variation For
           Solid-Mounted Compressor Journal Bearing Pad Without Journal Bearing
           Flexure Dampers Under Externally-Imposed Shaped Random Vibrations
           (1.52 g rms Input) According To NASA Spec 417-2-C-3.5 (Compressor
   Journal Bearing Externally Pressurized)

DISPLACEMENT POWER SPECTRAL DENSITY – M²/HZ

DISPLACEMENT POWER SPECTRAL DENSITY – IN²/HZ

INPUT VIBRATION
DISPLACEMENT P.S.D

GRAVITY

APPLIED
VIBRATION

AMBIENT GAS : N₂
AMBIENT PRESSURE : 38 PSIA
ROTOR SPEED : 36,000 RPM
HYDROSTATIC SUPPLY PRESSURE :
 THRUST BRG : ——
 TURBINE JOURNAL BRG ——
 COMPRESSOR JOURNAL BEARING : 150 PSIA
DISPLACEMENT PROBE F
SAMPLE SIZE : 128 ENSEMBLES
ANALYZER FILTER BANDWIDTH : 6 HZ

FREQUENCY – HZ

5   10   20   30   40 50   100   200   300 400 500   1000   2000
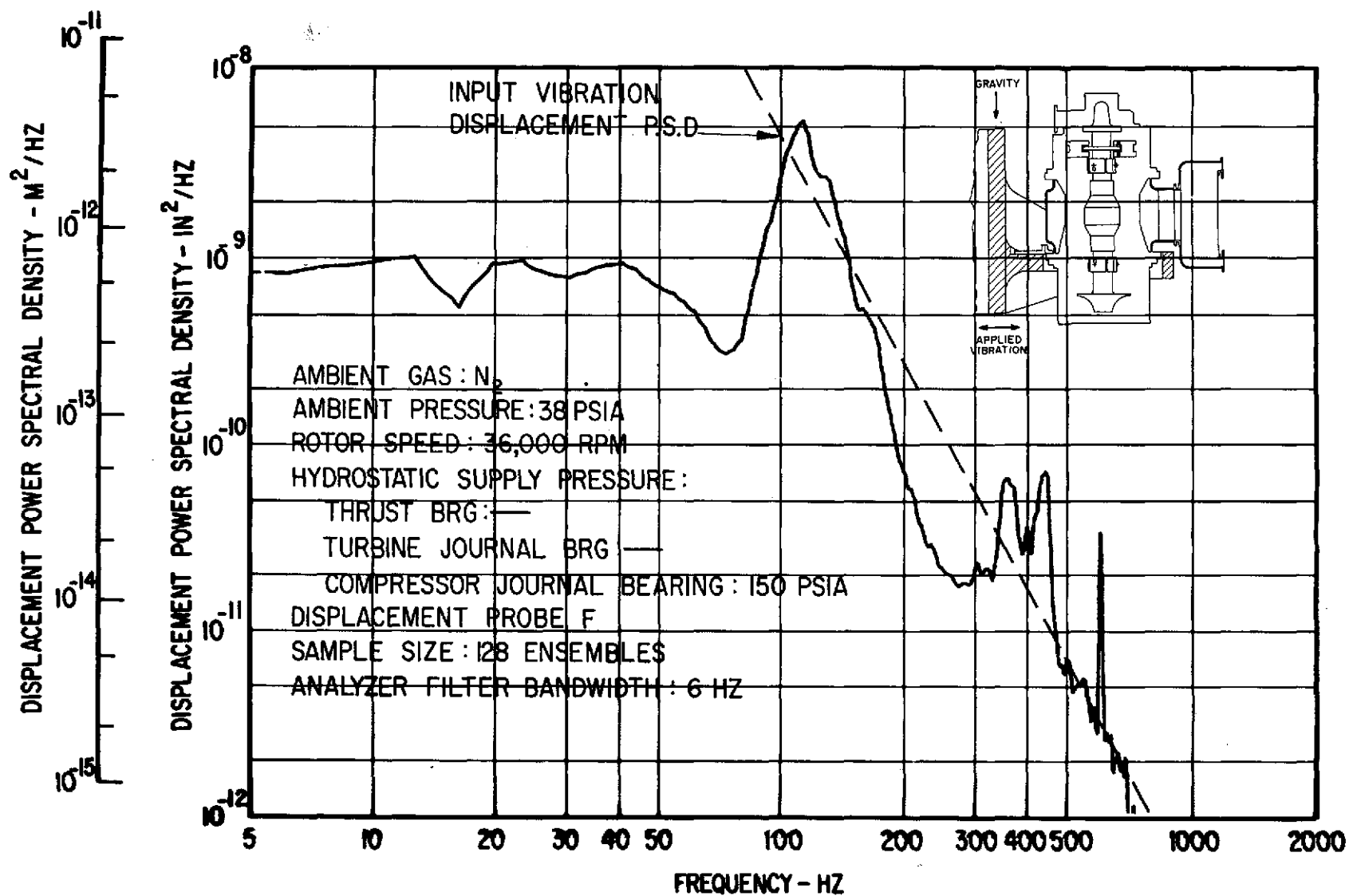
Fig. 25   Frequency Distribution Of Pad-To-Shaft Pivot Film Thickness Variation For
Solid-Mounted Turbine Journal Bearing Pad Without Journal Bearing Flexure
Dampers Under Externally-Imposed Shaped Random Vibrations (1.35 g rms
Input) According To NASA Spec 417-2-C-3.5 (Compressor Journal Bearing
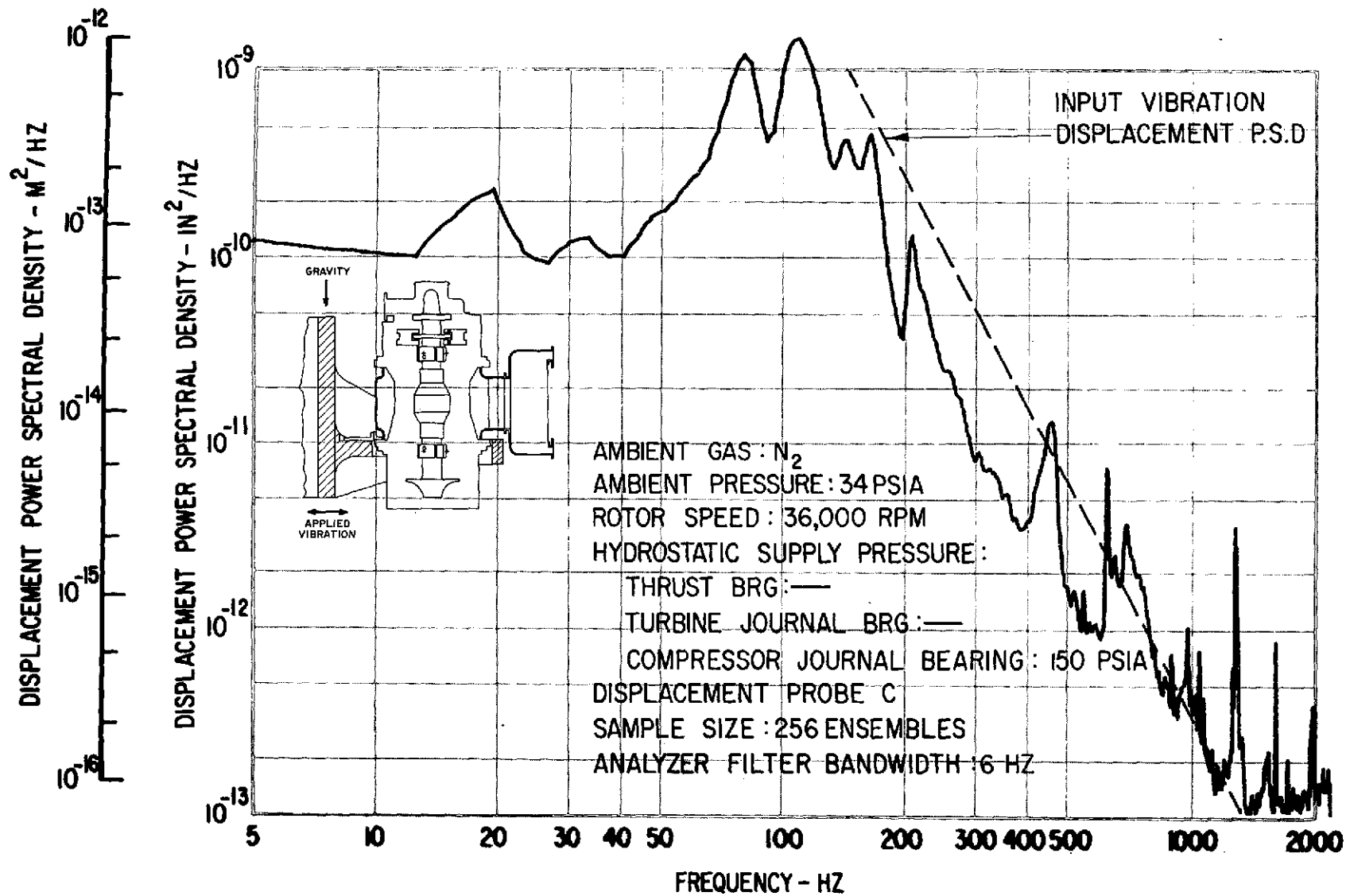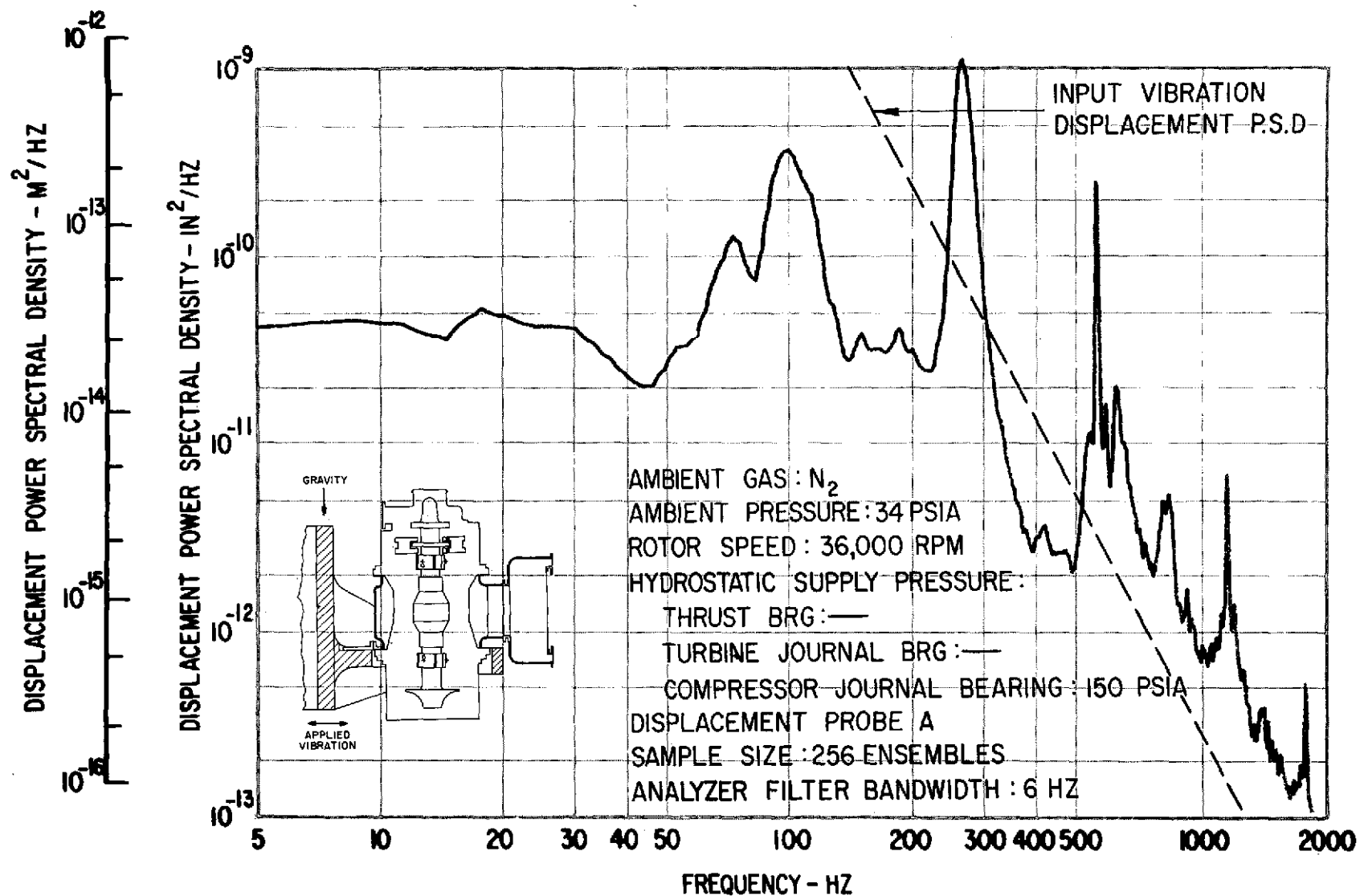Externally Pressurized)

Fig. 26   Frequency Distribution Of Pad-To-Shaft Pivot Film Thickness Variation For
Flex-Mounted Compressor Journal Bearing Pad Without Journal Bearing
Flexure Dampers Under Externally-Imposed Shaped Random Vibrations
(1.52 g rms Input) According To NASA Spec 417-2-C-3.5 (Compressor
Journal Bearing Externally Pressurized)
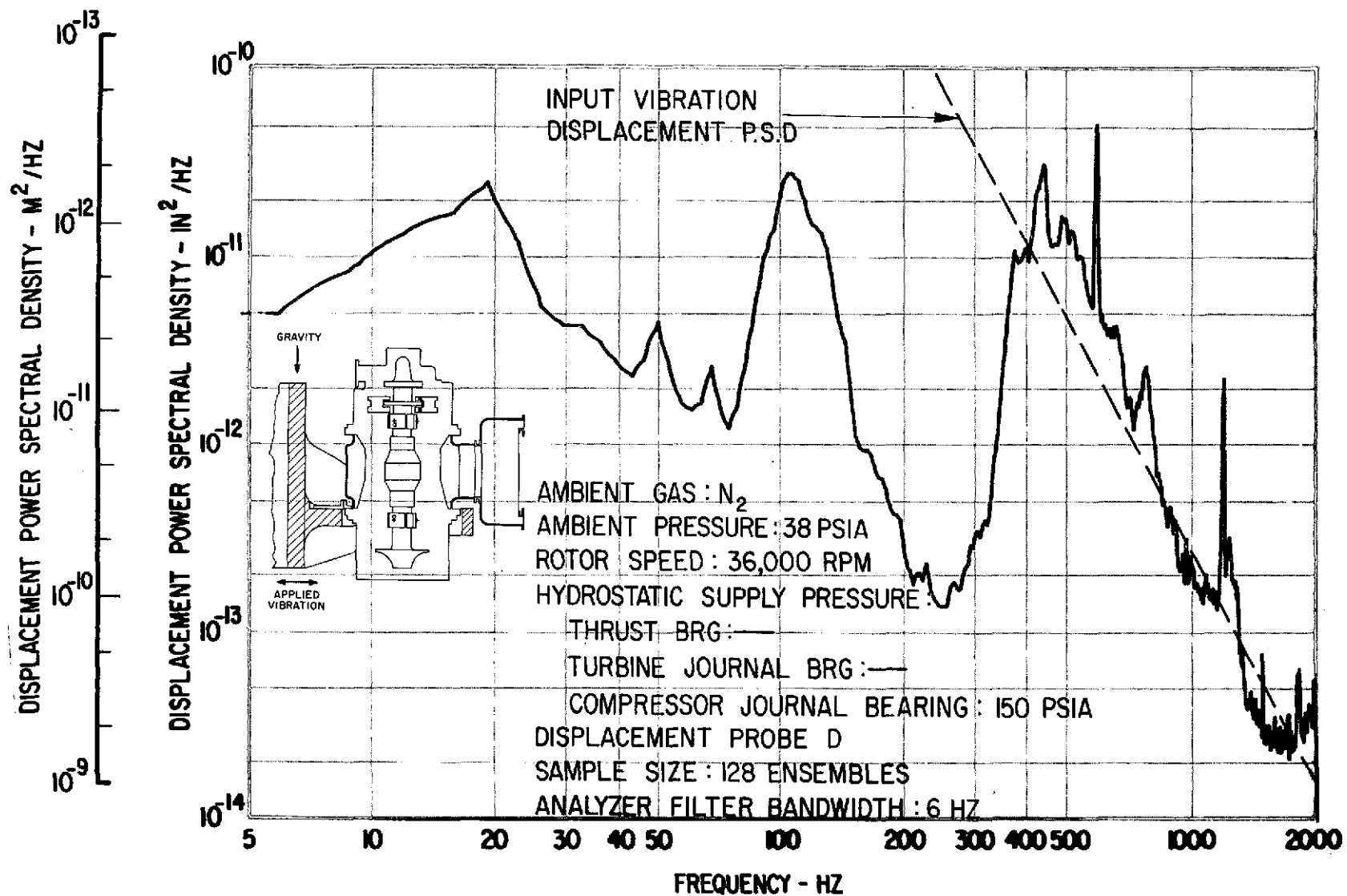
Fig. 27   Frequency Distribution Of Pad-To-Shaft Pivot Film Thickness Variation For
Flex-Mounted Turbine Journal Bearing Pad Without Journal Bearing Flexure
Dampers Under Externally-Imposed Shaped Random Vibrations (1.35 g rms
Input) According To NASA Spec 417-2-C-3.5 (Compressor Journal Bearing
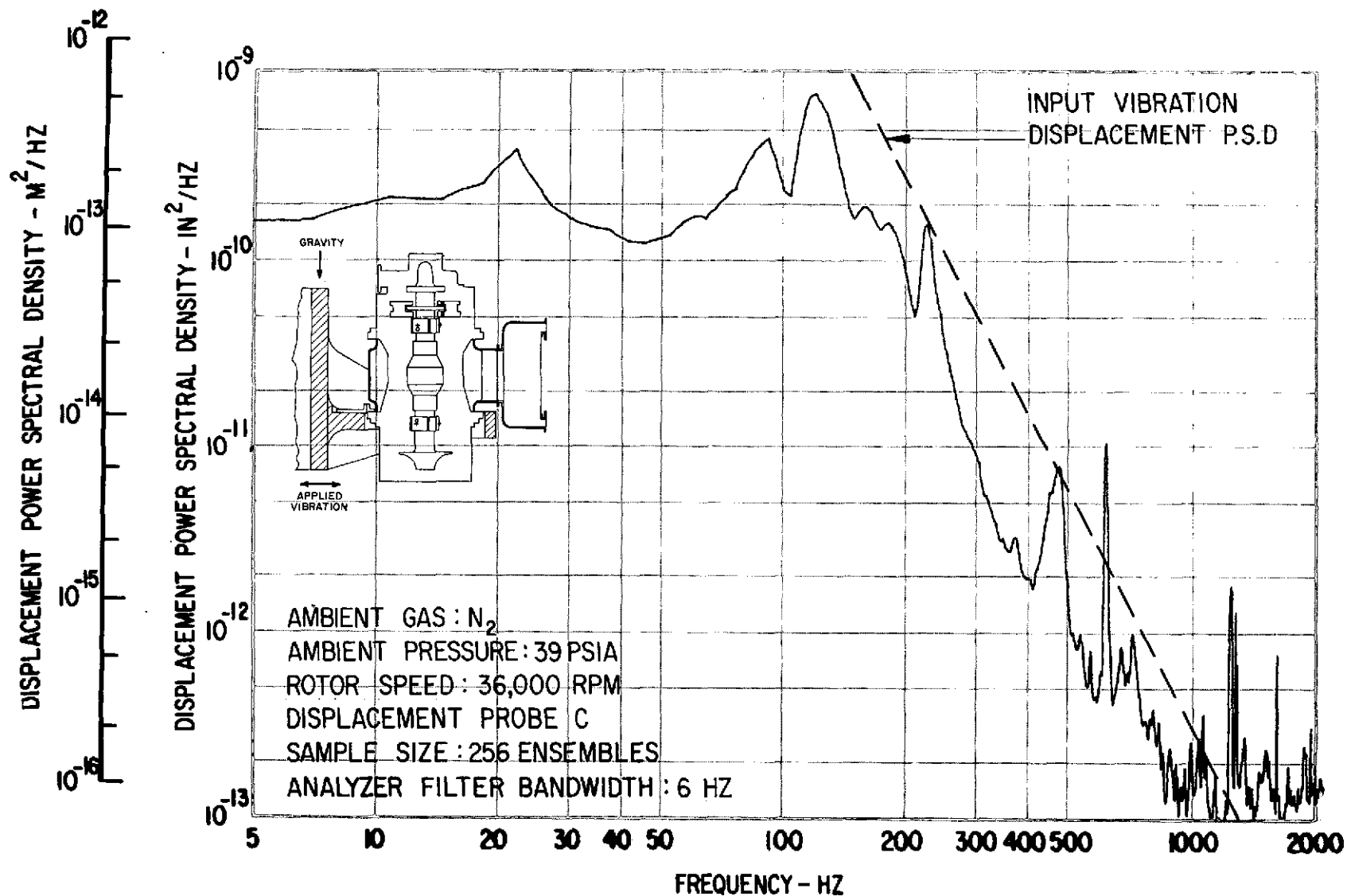Externally Pressurized)
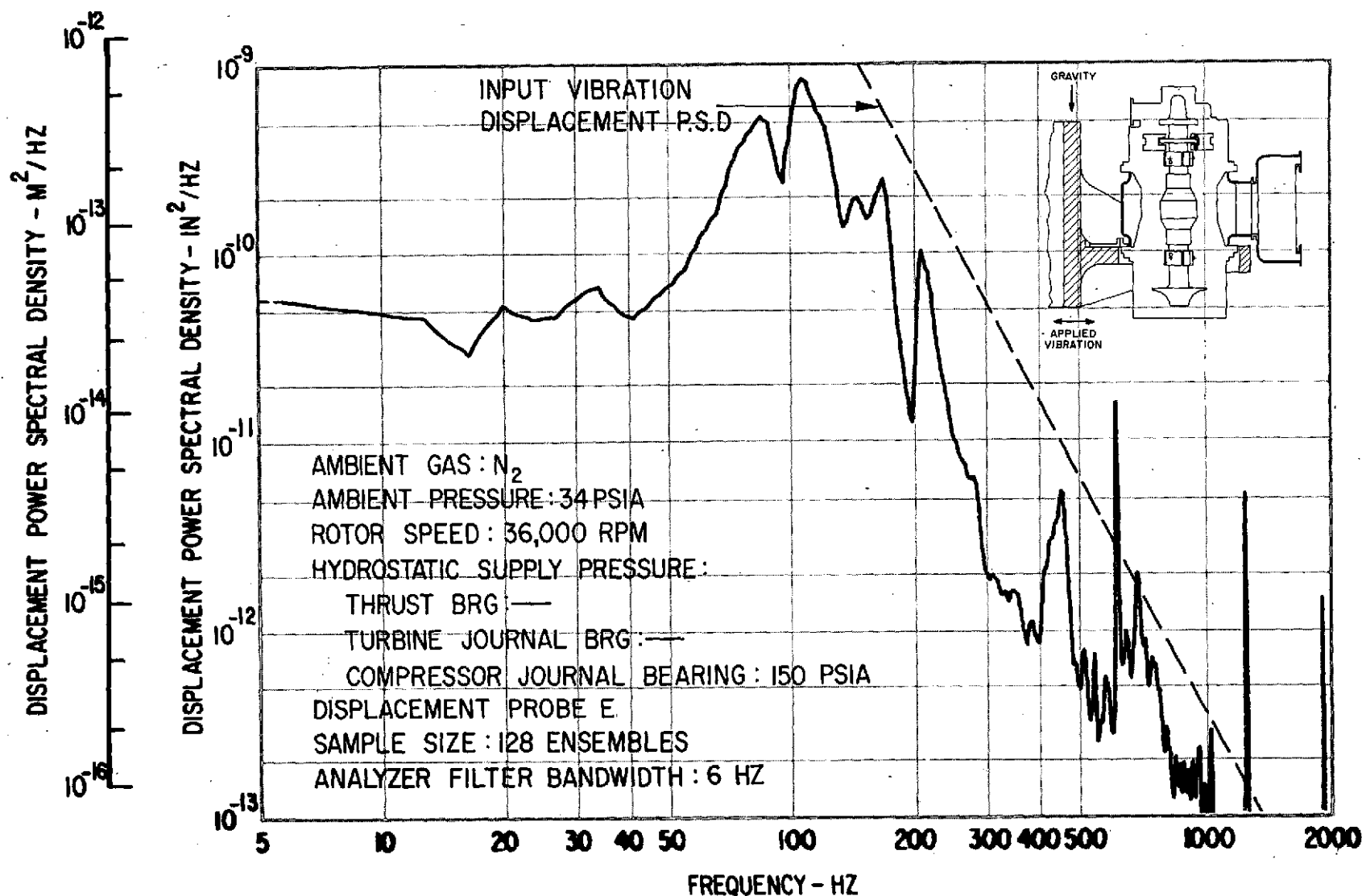
Fig. 28   Frequency Distribution Of Pad-To-Shaft Pivot Film Thickness Variation For
Solid-Mounted Turbine Journal Bearing Pad With Journal Bearing Flexure
Dampers Under Externally-Imposed Shaped Random Vibrations (1.35 g rms
Input) According To NASA Spec 417-2-C-3.5 (Compressor Journal Bearing
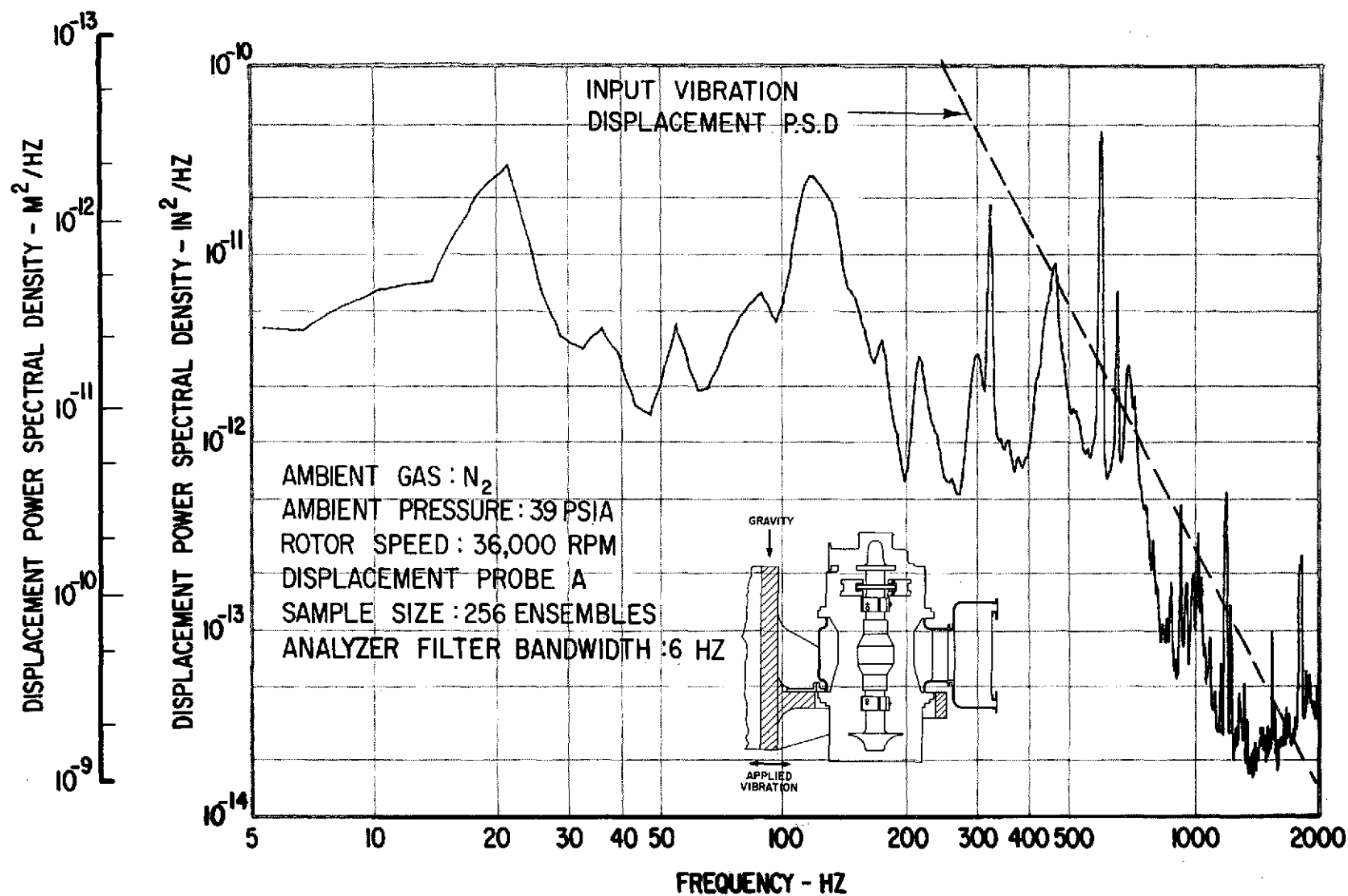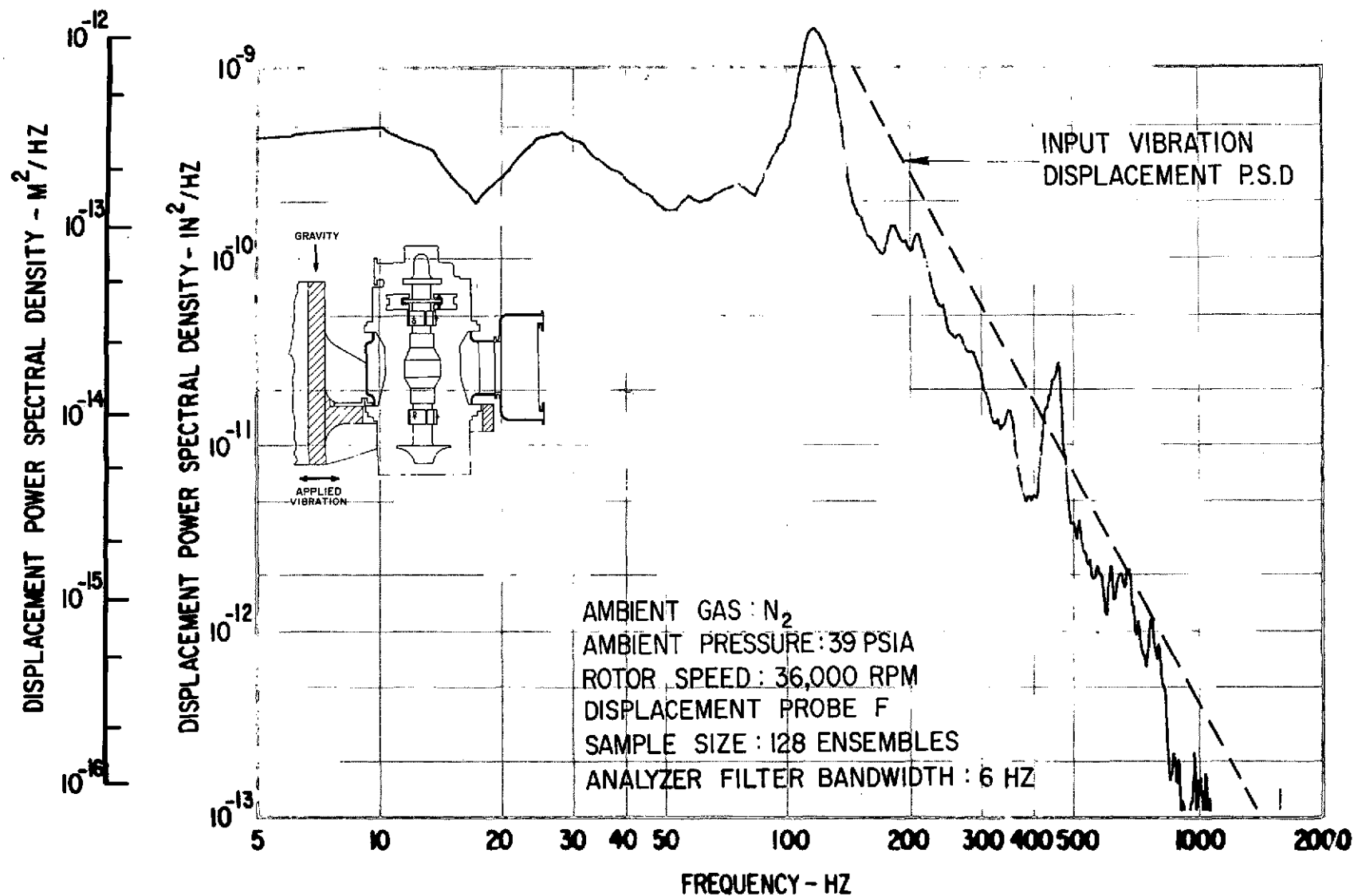Externally Pressurized)

Fig. 29   Frequency Distribution Of Pad-To-Shaft Pivot Film Thickness Variation For
Solid-Mounted Compressor Journal Bearing Pad With Journal Bearing Flexure
Dampers Under Externally-Imposed Shaped Random Vibrations (1.52 g rms
Input) According To NASA Spec 417-2-C-3.5 (Compressor Journal Bearing
Externally Pressurized)

Fig. 30   Frequency Distribution Of Pad-To-Shaft Pivot Film Thickness Variation For
Flex-Mounted Compressor Journal Bearing Pad With Journal Bearing Flexure
Dampers Under Externally-Imposed Shaped Random Vibrations (1.52 g rms
Input) According To NASA Spec 417-2-C-3.5 (Compressor Journal Bearing
Externally Pressurized)

MTI-16181

Fig. 31   Frequency Distribution Of Pad-To-Shaft Pivot Film Thickness Variation For
Solid-Mounted Compressor Journal Bearing Pad With Journal Bearing Flexure
Dampers Under Externally-Imposed Shaped Random Vibrations (1.52 g rms
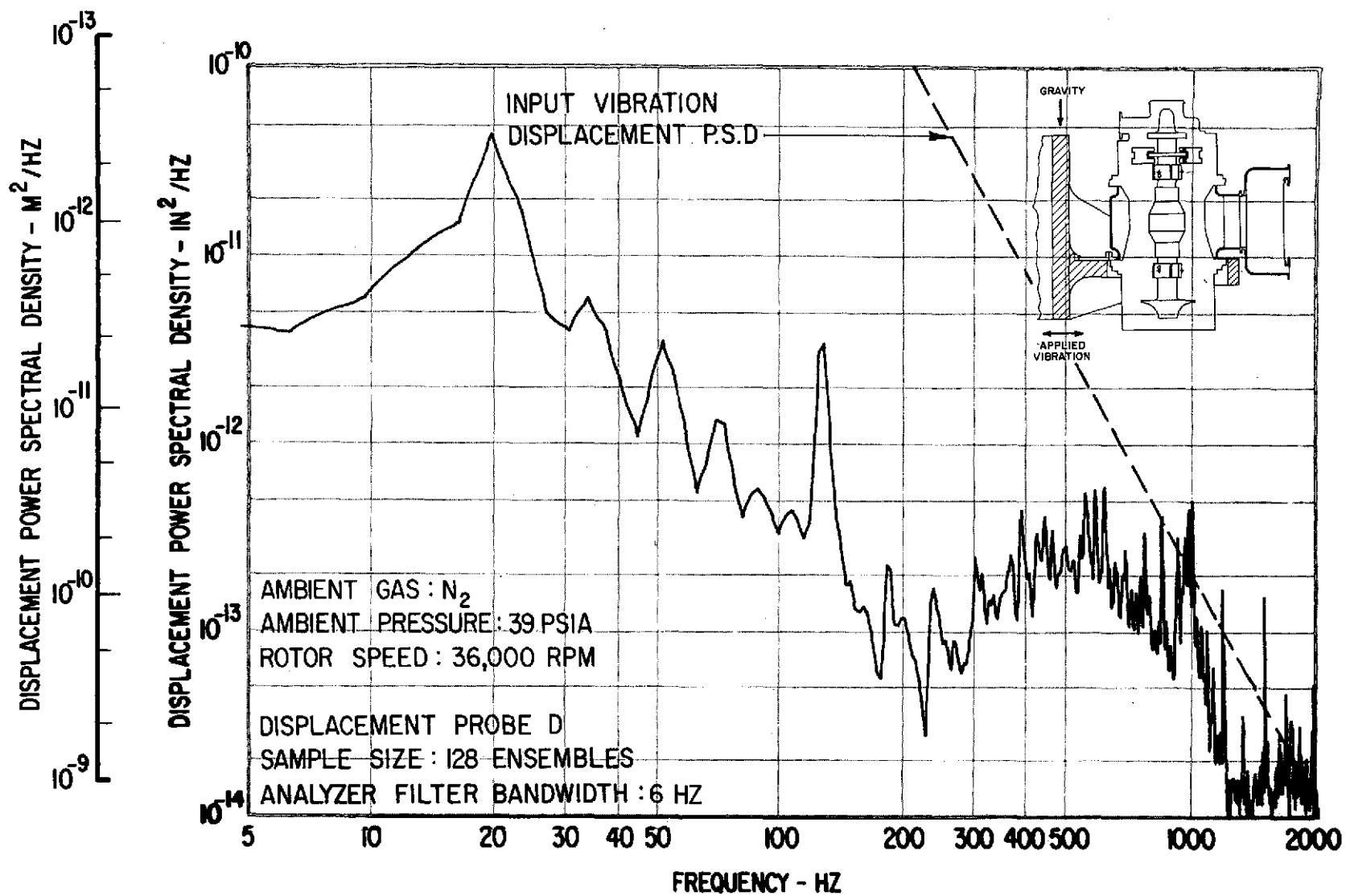Input) According To NASA Spec 417-2-C-3.5 (All Bearings Hydrodynamic)

Fig. 32   Frequency Distribution Of Pad-To-Shaft Pivot Film Thickness Variation For
Flex-Mounted Compressor Journal Bearing Pad With Journal Bearing Flexure
Dampers Under Externally-Imposed Shaped Random Vibrations (1.52 g rms
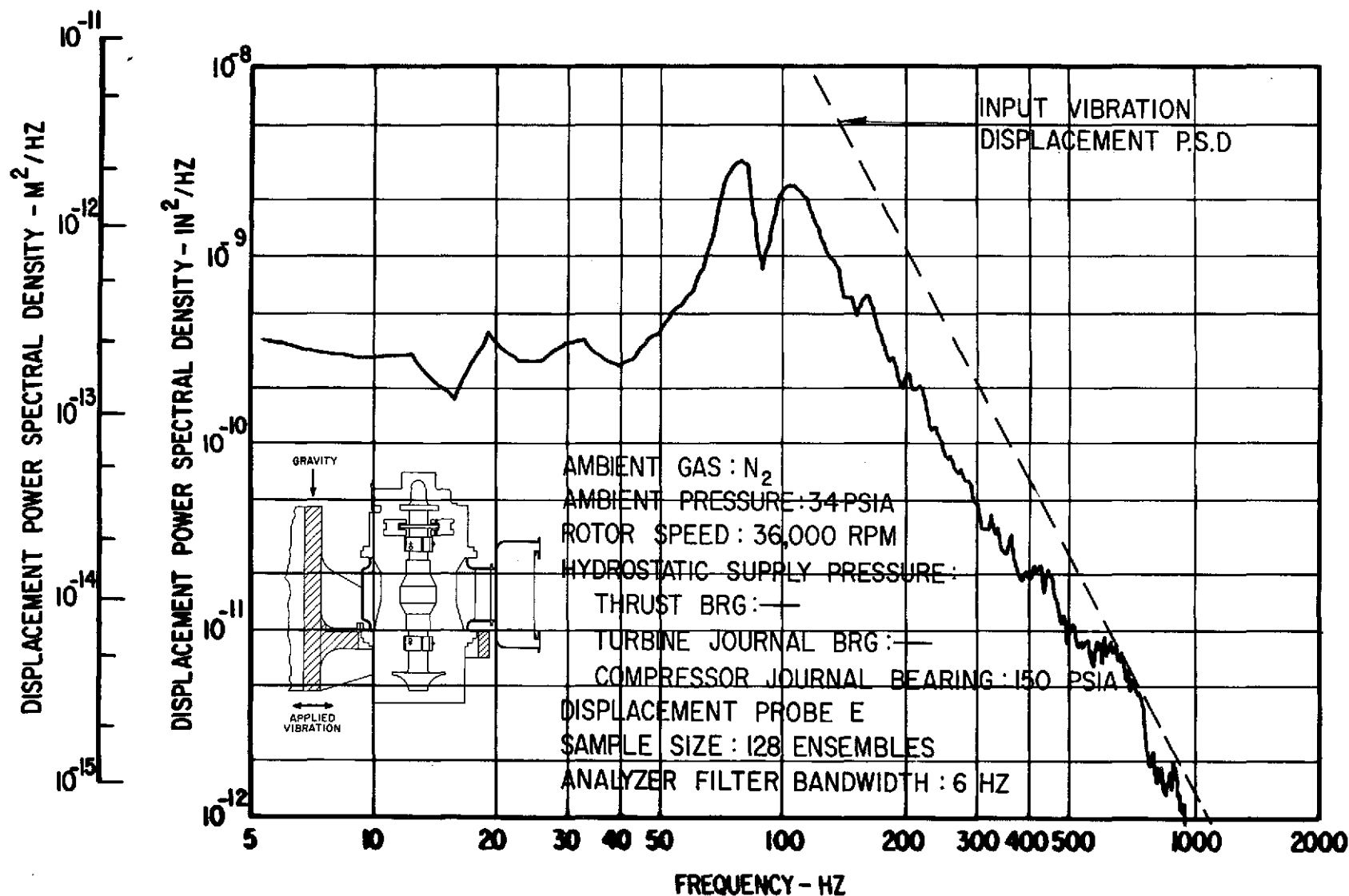Input) According To NASA Spec 417-2-C-3.5 (All Bearings Hydrodynamic)

Fig. 33   Frequency Distribution Of Pad-To-Shaft Pivot Film Thickness Variation For
Solid-Mounted Turbine Journal Bearing Pad With Journal Bearing Flexure
Dampers Under Externally-Imposed Shaped Random Vibrations (1.35 g rms
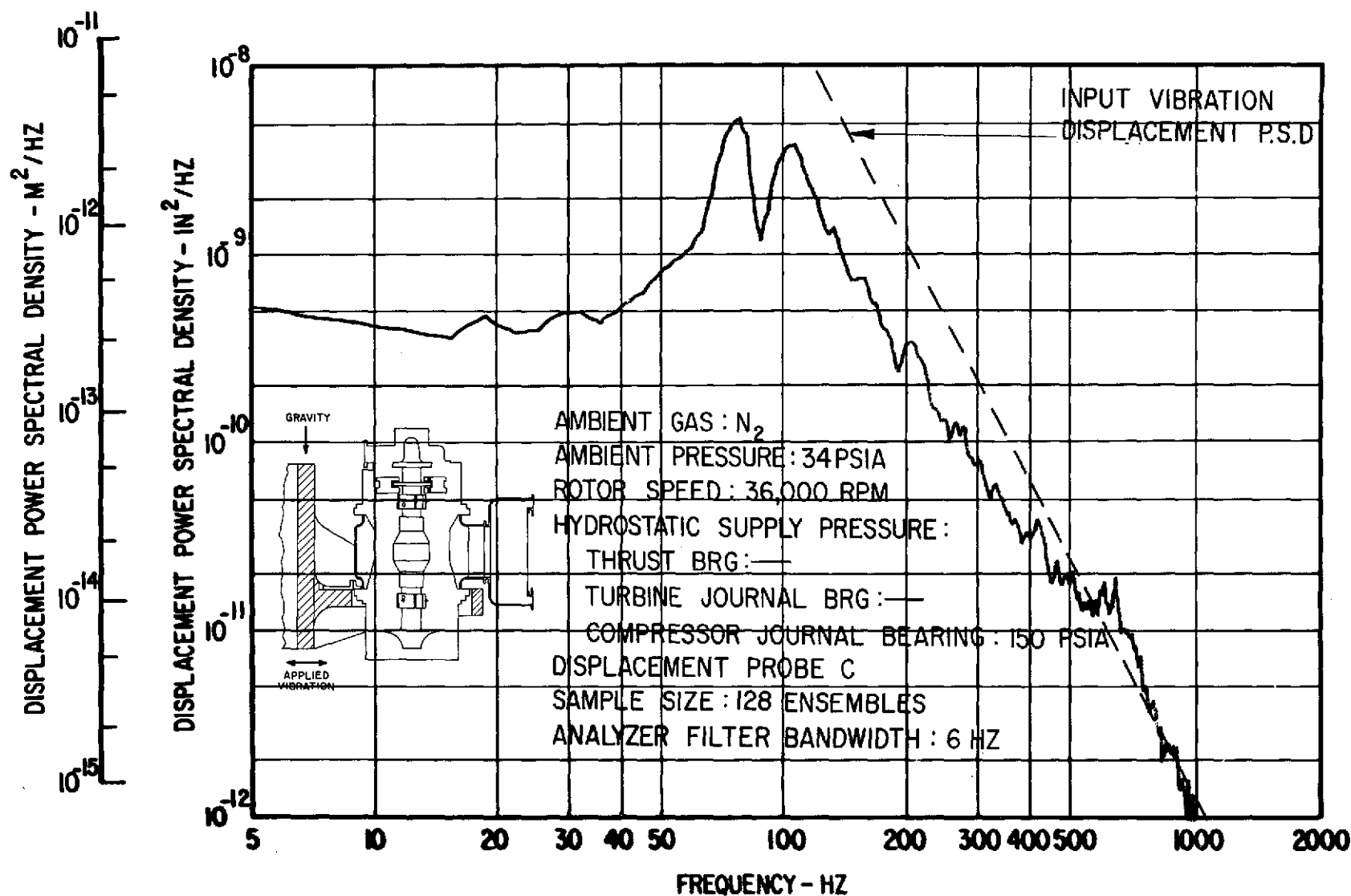Input) According To NASA Spec 417-2-C-3.5 (All Bearings Hydrodynamic)

Fig. 34   Frequency Distribution Of Pad-To-Shaft Pivot Film Thickness Variation For
Flex-Mounted Turbine Journal Bearing Pad With Journal Bearing Flexure
Dampers Under Externally-Imposed Shaped Random Vibrations (1.35 g rms
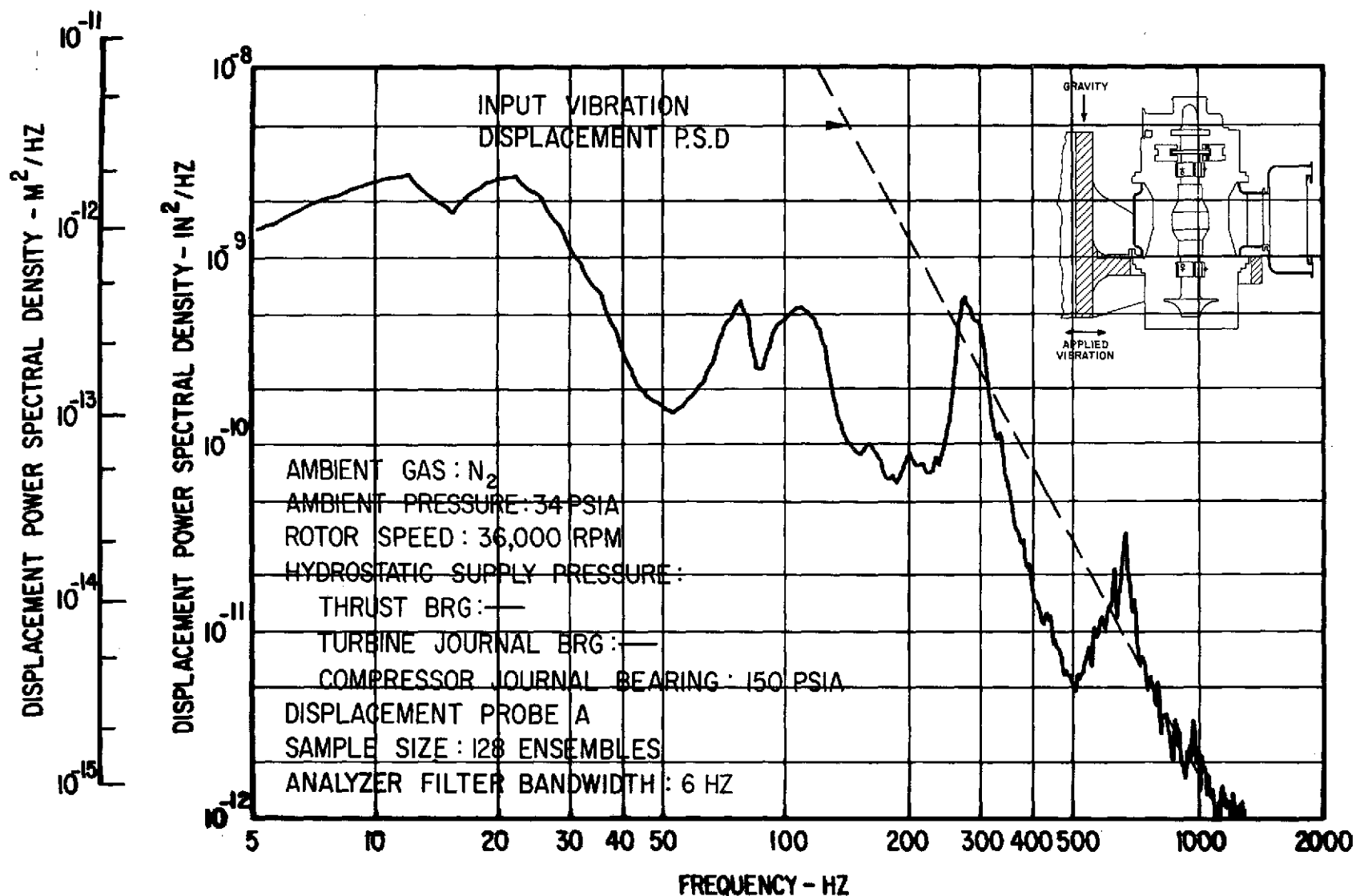Input) According To NASA Spec 417-2-C-3.5 (All Bearings Hydrodynamic)

Fig. 35   Frequency Distribution Of Pad-To-Shaft Pivot Film Thickness Variation For
Solid-Mounted Turbine Journal Bearing Pad With Journal Bearing Flexure
Dampers Under Externally-Imposed Shaped Random Vibrations (2.9 g rms
Input) According To NASA Spec 417-2-C-3.5

Fig. 36   Frequency Distribution Of Pad-To-Shaft Pivot Film Thickness Variation For
Solid-Mounted Compressor Journal Bearing Pad With Journal Bearing Flexure
Dampers Under Externally-Imposed Shaped Random Vibrations (2.9 g rms
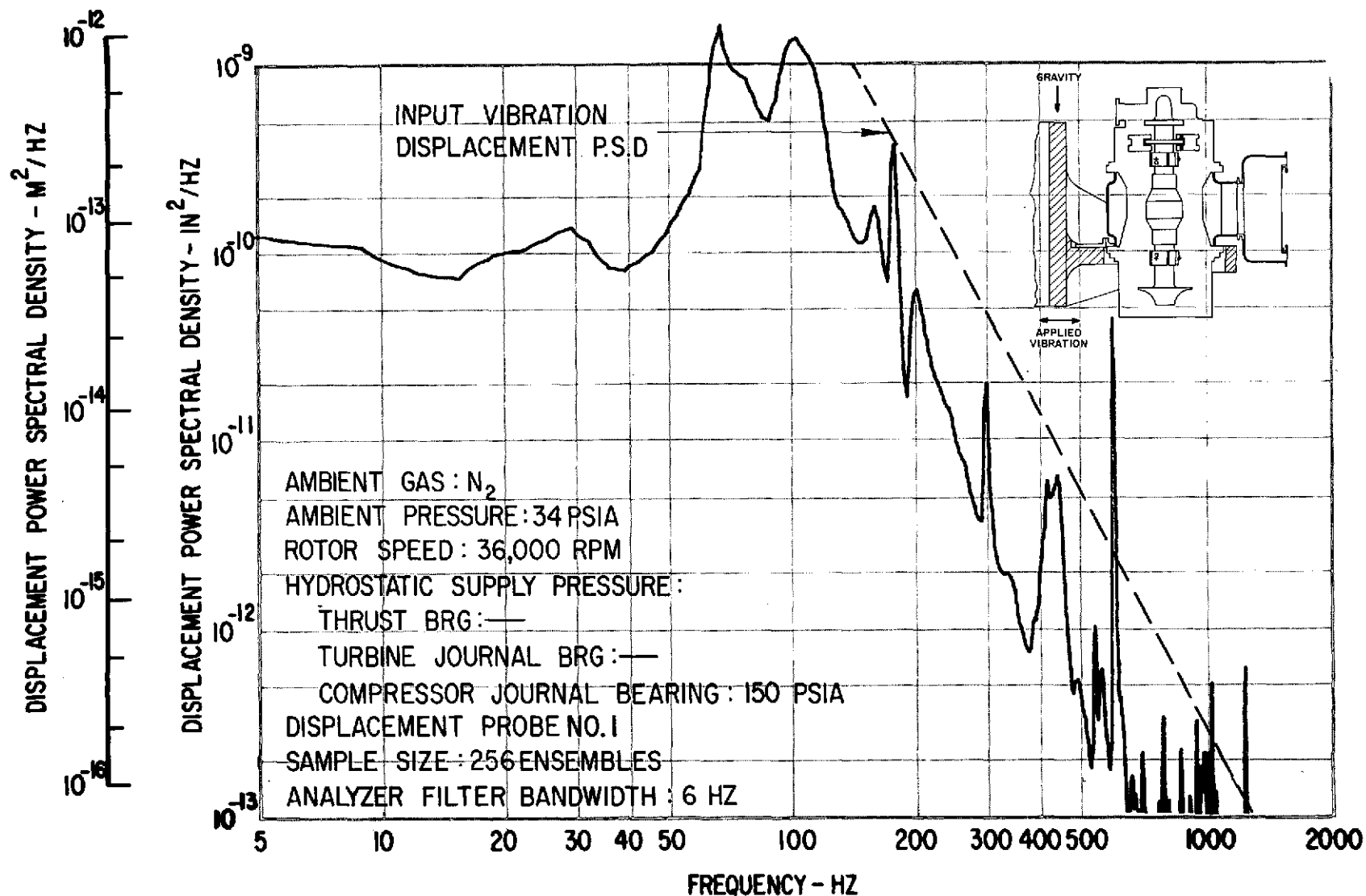Input) According To NASA Spec 417-2-C-3.5

MTI-16170

Fig. 37   Frequency Distribution Of Pad-To-Shaft Pivot Film Thickness Variation For
Flex-Mounted Compressor Journal Bearing Pad With Journal Bearing Flexure
Dampers Under Externally-Imposed Shaped Random Vibrations (2.9 g rms
Input) According To NASA Spec 417-2-C-3.5

MTI-16171

Fig. 38   Frequency Distribution Of Compressor Journal Rotor Amplitudes (Casing-To-Shaft) With Journal Bearing Flexure Dampers Under Externally-Imposed Shaped Random Vibrations (1.52 g rms Input) According To NASA Spec 417-2-C-3.5 (Compressor Journal Bearing Externally Pressurized)
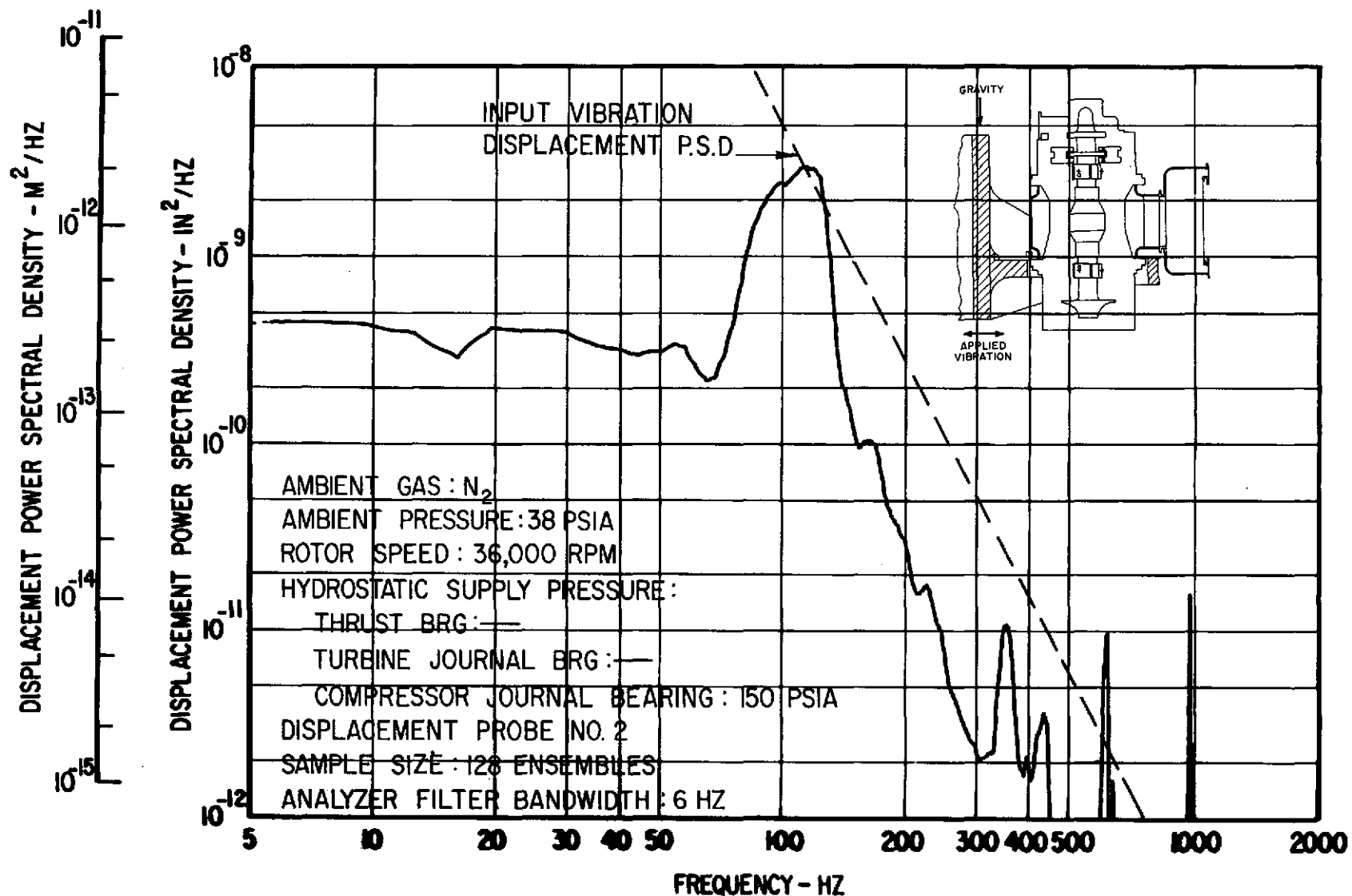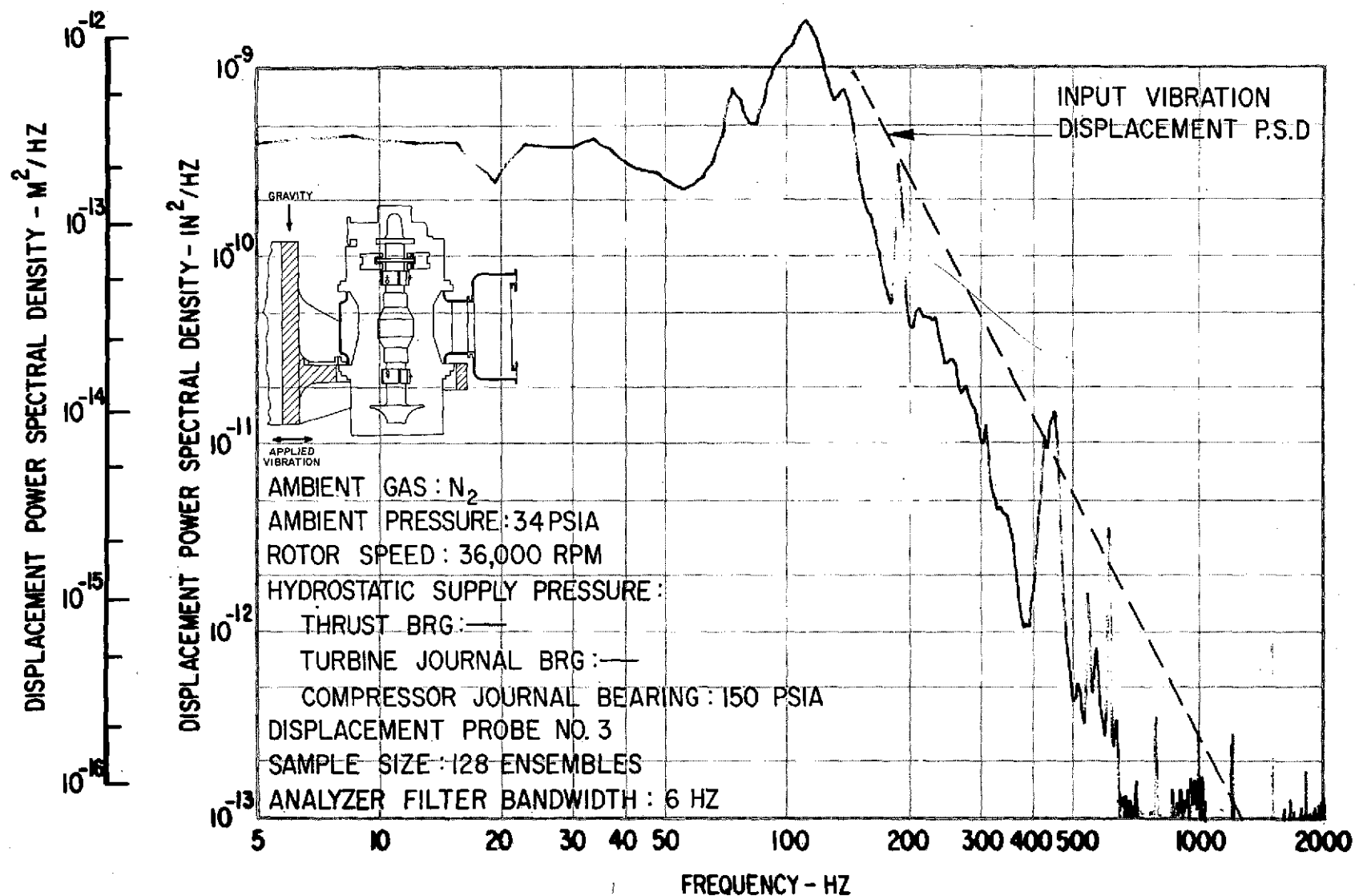
Fig. 39   Frequency Distribution Of Compressor Journal Rotor Amplitudes (Casing-To-Shaft) Without Journal Bearing Flexure Dampers Under Externally-Imposed Shaped Random Vibrations (1.52 g rms Input) According To NASA Spec 417-2-C-3.5 (Compressor Journal Bearing Externally Pressurized)

MTI-16172

Fig. 40   Frequency Distribution Of Turbine Journal Rotor Amplitudes (Casing-To-Shaft)
           With Journal Bearing Flexure Dampers Under Externally-Imposed Shaped Random
           Vibrations (1.52 g rms Input) According To NASA Spec 417-2-C-3.5 (Compressor
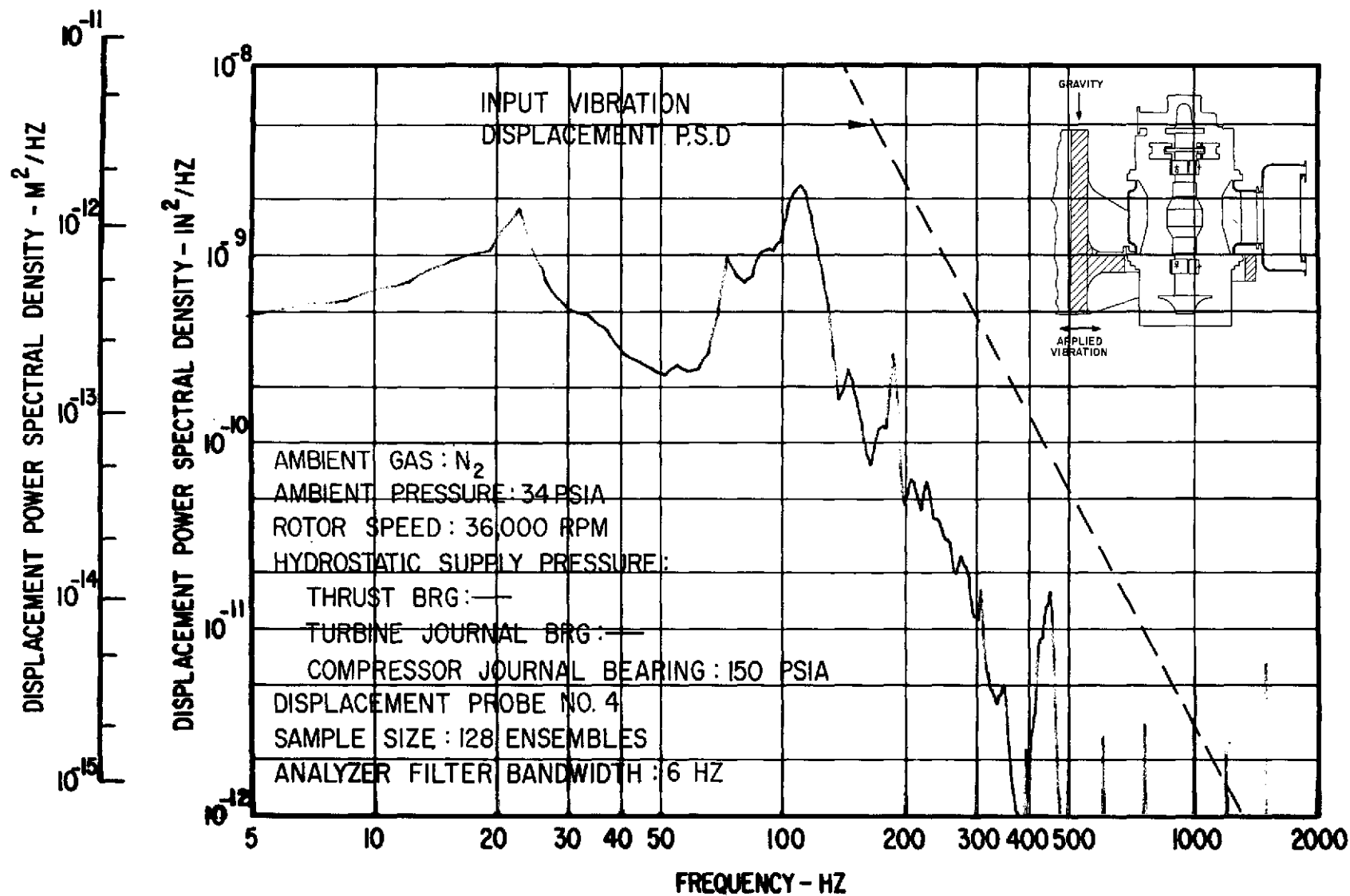   Journal Bearing Externally Pressurized)

MTI-16176

Fig. 41   Frequency Distribution Of Turbine Journal Rotor Amplitudes (Casing-To-Shaft)
With Journal Bearing Flexure Dampers Under Externally-Imposed Shaped Random
Vibrations (1.52 g rms Input) According To NASA Spec 417-2-C-3.5 (Compressor
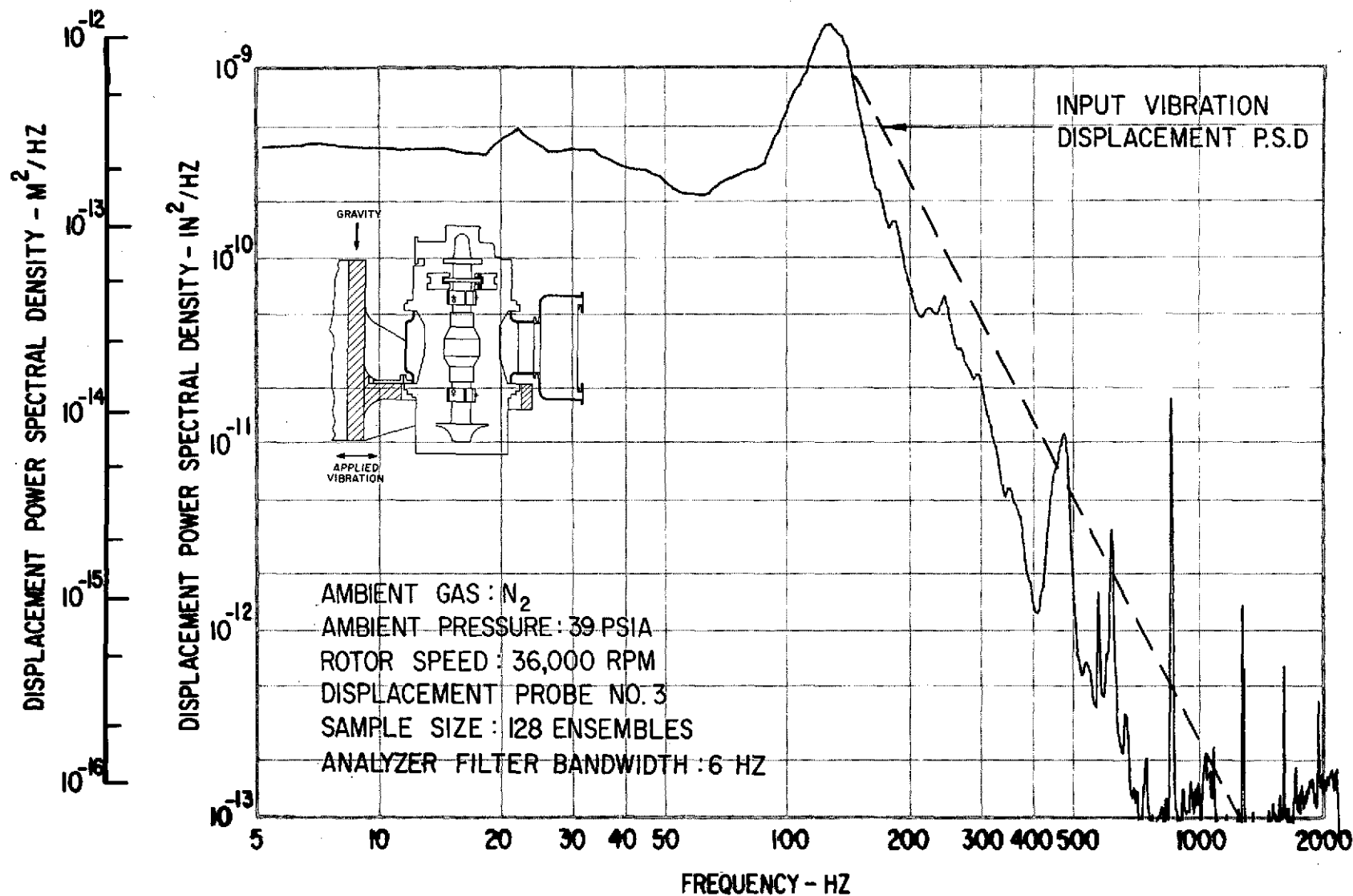Journal Bearing Externally Pressurized)

Fig. 42   Frequency Distribution Of Turbine Journal Rotor Amplitudes (Casing-To-Shaft)
With Journal Bearing Flexure Dampers Under Externally-Imposed Shaped Random
Vibrations (1.52 g rms Input) According To NASA Spec 417-2-C-3.5 (All
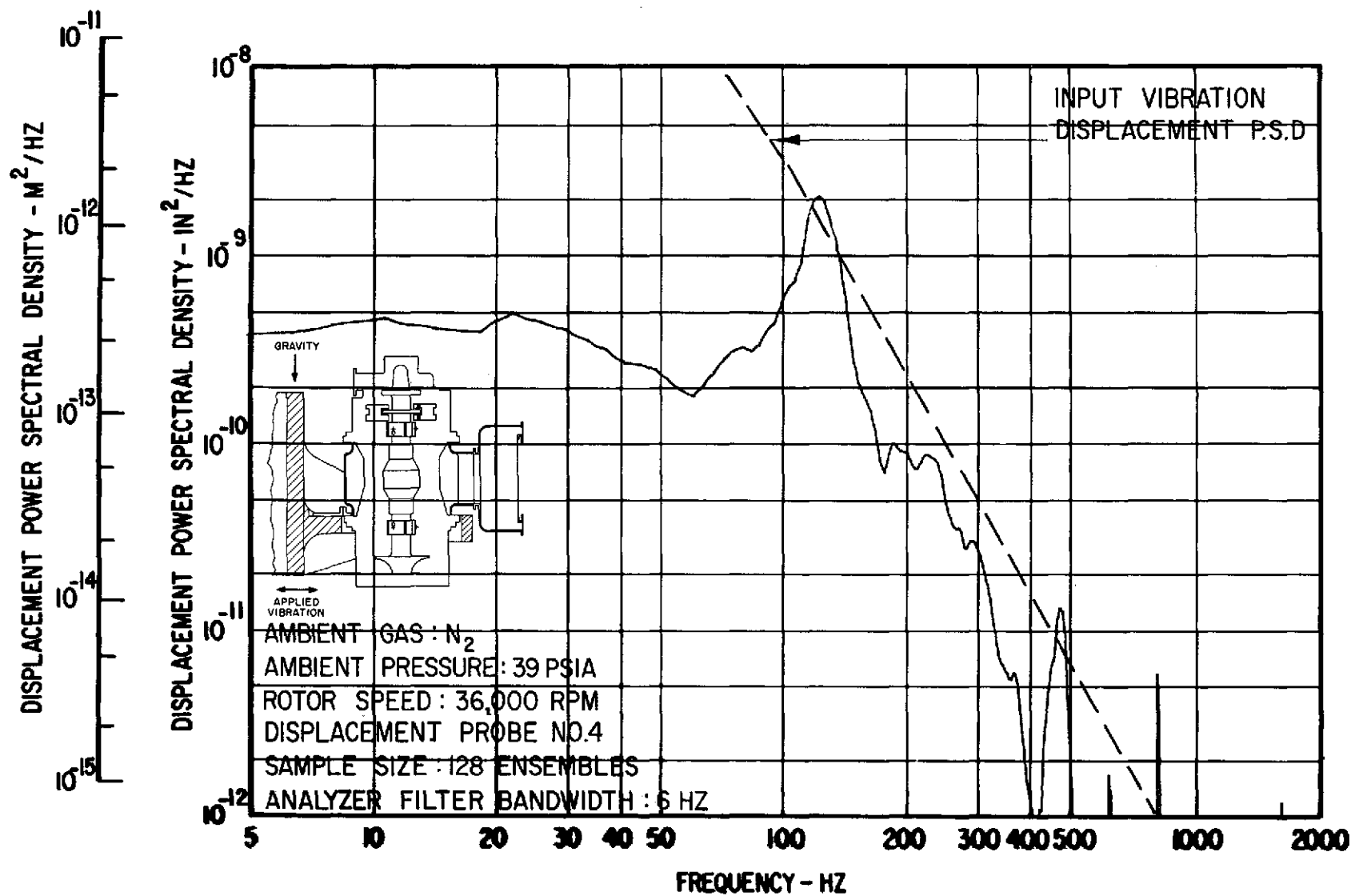Bearings Hydrodynamic)

Fig. 43   Frequency Distribution Of Turbine Journal Rotor Amplitudes (Casing-To-Shaft)
           With Journal Bearing Flexure Dampers Under Externally-Imposed Shaped Random
           Vibrations (1.52 g rms Input) According To NASA Spec 417-2-C-3.5 (All
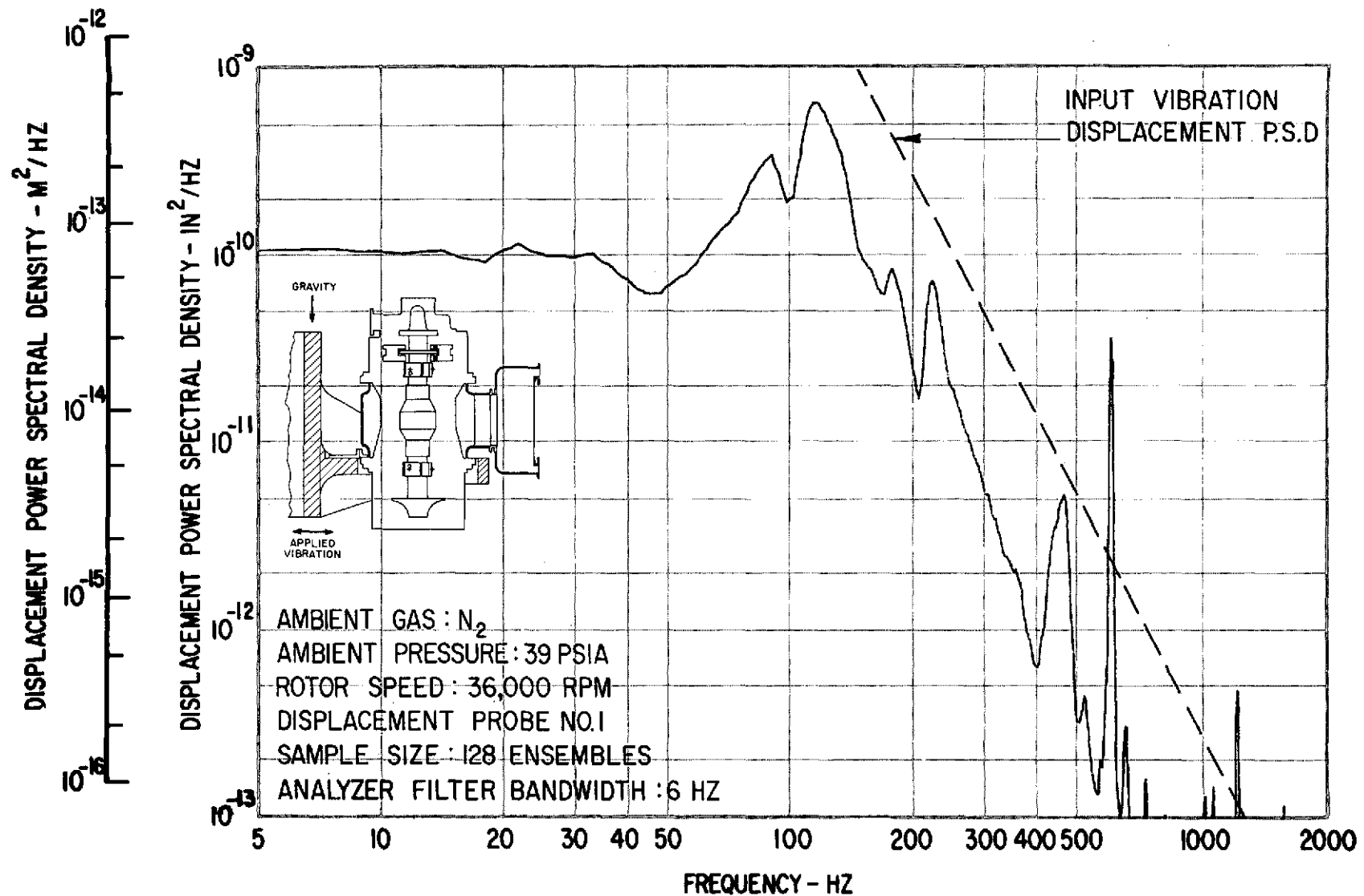   Bearings Hydrodynamic)

Fig. 44 Frequency Distribution Of Compressor Journal Rotor Amplitudes (Casing-To-Shaft) With Journal Bearing Flexure Dampers Under Externally-Imposed Shaped Random Vibrations (1.52 g rms Input) According To NASA Spec 417-2-C-3.5 (All Bearings Hydrodynamic)
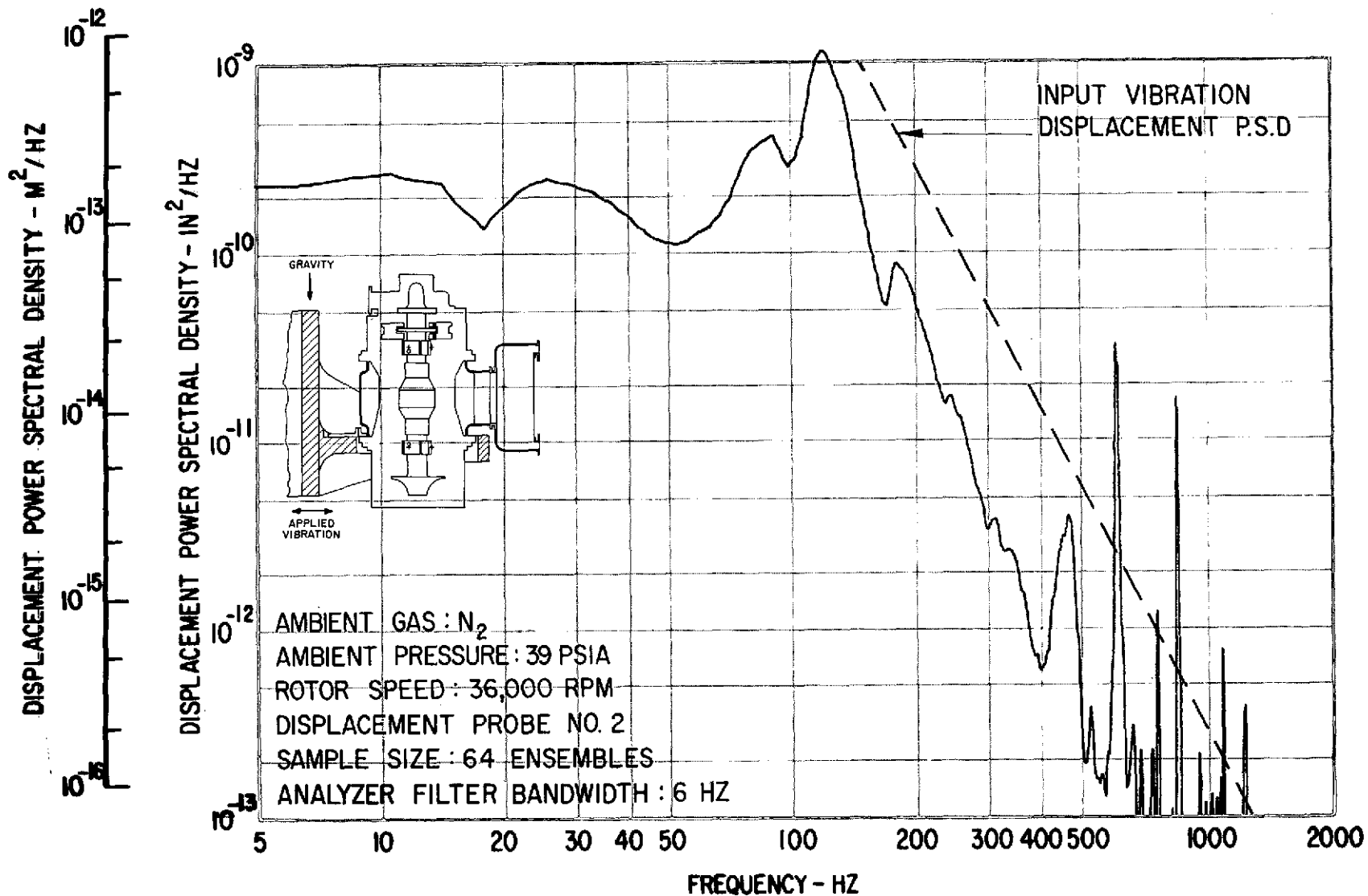
Fig. 45   Frequency Distribution Of Compressor Journal Rotor Amplitudes (Casing-To-Shaft) With Journal Bearing Flexure Dampers Under Externally-Imposed Shaped Random Vibrations (1.52 g rms Input) According To NASA Spec 417-2-C-3.5 (All Bearings Hydrodynamic)

DISTRIBUTION LIST

NASA-Lewis Research Center
21000 Brookpark Road
Cleveland, Ohio 44135
Attention: See List Below

G. Mervin Ault, MS 3-5
Robert E. English, MS 500-201
Donald Packe, MS 500-202
Del Drier, MS 21-4
William Wintucky, MS 500-202
Technology Utilization Office, MS 3-19
Report Control, MS 5-5
Library, MS 60-3
James H. Dunn, MS 500-202 (3 copies)
Gerald Boulanger, MS 500-206
Patent Counsel, MS 500-113

NASA Scientific and Technical Information Facility
Attention: Acquisitions Branch (10 copies)
P. O. Box 33
College Park, MD 20740

AiResearch Manufacturing Company
A Division of the Garrett Corporation
Attention: Mr. Anthony Pietsch
402 South 36th Street
Phoenix, AZ 85034